The density-matrix renormalization group

U. Schollwöck

RWTH Aachen University, D-52056 Aachen, Germany

(Published 26 April 2005)

The density-matrix renormalization group (DMRG) is a numerical algorithm for the efficient truncation of the Hilbert space of low-dimensional strongly correlated quantum systems based on a rather general decimation prescription. This algorithm has achieved unprecedented precision in the description of one-dimensional quantum systems. It has therefore quickly become the method of choice for numerical studies of such systems. Its applications to the calculation of static, dynamic, and thermodynamic quantities in these systems are reviewed here. The potential of DMRG applications in the fields of two-dimensional quantum systems, quantum chemistry, three-dimensional small grains, nuclear physics, equilibrium and nonequilibrium statistical physics, and time-dependent phenomena is also discussed. This review additionally considers the theoretical foundations of the method, examining its relationship to matrix-product states and the quantum information content of the density matrices generated by the DMRG.

CONTENTS

I. INTRODUCTION

Consider a crystalline solid; it consists of some 10^{26} or more atomic nuclei and electrons for objects on a human

scale. All nuclei and electrons are subject to the strong, long-range Coulomb interaction. While this system should *a priori* be described by the Schrödinger equation, its explicit solution is impossible to find. Yet, it has become clear over the decades that in many cases the physical properties of solids can be understood to a very good approximation in the framework of some effective one-body problem. This is a consequence of the very efficient interplay of nuclei and electrons in screening the Coulomb interaction, except on the very shortest length scales.

This comforting picture may break down as various effects invalidate the fundamental tenet of weak effective interactions, taking us into the field of strongly correlated quantum systems, in which the full electronic many-body problem has to be considered. Of the routes to strong correlation, let me mention just two, because it is at their meeting point that, from the point of view of physical phenomena, the density-matrix renormalization group (DMRG) has its origin.

On the one hand, for arbitrary interactions, the Fermi-liquid picture breaks down in one-dimensional solids and gives way to the Tomonaga-Luttinger liquid picture: essentially due to the small size of phase space, scattering processes for particles close to the Fermi energy become so important that the (fermionic) quasiparticle picture of Fermi-liquid theory is replaced by (bosonic) collective excitations.

On the other hand, for arbitrary dimensions, screening is typically so effective because of strong delocalization of valence electrons over the lattice. In transition metals and rare earths, however, the valence orbitals are inner d or f orbitals. Hence valence electrons are much more localized, though not immobile. There is now a strong energy penalty for placing two electrons in the same local valence orbital, and the motion of valence electrons becomes strongly correlated on the lattice.

To study strongly correlated systems, simplified *model Hamiltonians* have been designed that try to retain just the core ingredients needed to describe some physical phenomenon and methods for their treatment. Localization suggests the use of *tight-binding lattice models*, in which local orbitals on one site can take $N_{site}=4$ different states of up to two electrons ($|0\rangle, |\uparrow\rangle, |\downarrow\rangle, |\uparrow\downarrow\rangle$).

The simplest model Hamiltonian for just one valence orbital (band) with a kinetic-energy term (electron hopping between sites i and j with amplitude t_{ij}) and Coulomb repulsion is the on-site *Hubbard model* (Hubbard, 1963, 1964), in which just the leading on-site Coulomb repulsion U has been retained:

$$\hat{H}_{Hubbard} = -\sum_{\langle ij\rangle,\sigma} t_{ij}(c_{i\sigma}^\dagger c_{j\sigma} + \text{H.c.}) + U\sum_i n_{i\uparrow}n_{i\downarrow}. \qquad (1)$$

$\langle\rangle$ designates bonds. In the limit $U/t \gg 1$ double occupancy $|\uparrow\downarrow\rangle$ can be excluded, resulting in the $N_{site}=3$ state *t-J model*:

$$\hat{H}_{tJ} = -\sum_{\langle ij\rangle,\sigma} t_{ij}(c_{i\sigma}^\dagger c_{j\sigma} + \text{H.c.}) + \sum_{\langle ij\rangle} J_{ij}\left(\mathbf{S}_i \cdot \mathbf{S}_j - \frac{1}{4}n_i n_j\right),$$

$$(2)$$

in which the spin-spin interaction $J_{ij}=4t_{ij}^2/U$ is due to a second-order virtual hopping process possible only for electrons of opposite spin on sites i and j. At half-filling, the model simplifies even further to the spin-$\frac{1}{2}$ isotropic Heisenberg model,

$$\hat{H}_{Heisenberg} = \sum_{\langle ij\rangle} J_{ij}\mathbf{S}_i \cdot \mathbf{S}_j, \qquad (3)$$

placing collective (anti)ferromagnetism, which it describes, into the framework of strongly correlated systems. These and other model Hamiltonians have been modified in multiple ways.

In various fields of condensed-matter physics, such as high-temperature superconductivity, low-dimensional magnetism (spin chains and spin ladders), low-dimensional conductors, and polymer physics, theoretical research is focussing on the highly nontrivial properties of these seemingly simple models, which are believed to capture some of the essential physics. Recent progress in experiments on ultracold atomic gases (Greiner *et al.*, 2002) has allowed the preparation of strongly correlated bosonic systems in optical lattices with tunable interaction parameters, attracting many solid-state physicists to this field. On the conceptual side, important old and new questions are at the center of the physics of strongly correlated quantum systems, e.g., topological effects in quantum mechanics, the wide field of quantum phase transitions, and the search for exotic forms of order stabilized by quantum effects at low temperatures.

The typical absence of a dominant, exactly solvable contribution to the Hamiltonian, about which a perturbative expansion as in conventional many-body physics might be attempted, goes a long way towards explaining the inherent complexity of strongly correlated systems. This is why, apart from some exact solutions like those provided by the Bethe ansatz or certain toy models, most analytical approaches are quite uncontrolled in their reliability. While these approaches may yield important insight into the nature of the physical phenomena observed, it is ultimately up to numerical approaches to assess the validity of analytical approximations.

Standard methods in the field are the exact diagonalization of small systems, the various quantum Monte Carlo methods, and, less widely used, coupled-cluster methods and series expansion techniques. Since its introduction by White (1992), the density-matrix renormalization group has quickly achieved the status of a highly reliable, precise, and versatile numerical method in the field. Its main advantages are the ability to treat unusually large systems at high precision at or very close to zero temperature and the absence of the negative-sign problem that plagues the otherwise most powerful method, quantum Monte Carlo, making the latter of

limited use for frustrated spin or fermionic systems. A first striking illustration of DMRG precision was given by White and Huse (1993). Using modest numerical means to study the $S=1$ isotropic antiferromagnetic Heisenberg chain, they calculated the ground-state energy at almost machine precision, $E_0 = -1.401\,484\,0389\,71(4)J$, and the (Haldane) excitation gap as $\Delta = 0.410\,50(2)J$. The spin-spin correlation length was found to be $\xi = 6.03(2)$ lattice spacings. More examples of the versatility and precision that have made the reputation of the DMRG method will be found throughout the text. The major drawback of DMRG is that it displays its full force mainly for one-dimensional systems; nevertheless, interesting forays into higher dimensions have been made. By now, DMRG has, despite its complexity, become a standard tool of computational physics that many research groups in condensed-matter physics will want to have at hand. In the simulation of model Hamiltonians, it is part of a methodological triad consisting of exact diagonalization, quantum Monte Carlo, and DMRG.

Most DMRG applications still treat low-dimensional, strongly correlated model Hamiltonians, for which the method was originally developed. However, the core idea of DMRG, the construction of a renormalization-group flow in a space of suitably chosen density matrices, is quite general. In fact, another excellent way of conceptualizing DMRG is in the very general terms of quantum information theory. The versatility of the core idea has allowed the extension of DMRG applications to fields quite far from its origins, such as the physics of (three-dimensional) small grains, equilibrium and far-from-equilibrium problems in classical and quantum statistical mechanics, and the quantum chemistry of small to medium-sized molecules. Profound connections to exactly solvable models in statistical mechanics have emerged.

The aim of this review is to provide both the algorithmic foundations of DMRG and an overview of its main and by now quite diverse fields of applications.

I start with a discussion of the key algorithmic ideas needed to deal with the most conventional DMRG problem, the study of $T=0$ static properties of a one-dimensional quantum Hamiltonian (Sec. II). This includes standard improvements to the basic algorithm that should always be used to obtain a competitive DMRG application, a discussion of how to assess the numerical quality of DMRG output, and an overview of applications. Having read this first major section, the reader should be able to set up a standard DMRG with the major algorithmic design problems in mind.

I move on to a section on DMRG theory (Sec. III), discussing the properties of the quantum states generated by DMRG (matrix-product states) and the properties of the density matrices that are essential for its success; the section is closed by a reexamination of DMRG from a quantum information theory point of view. At least some superficial grasp of the key results of this section will be useful in the remainder of the review, while a more thorough reading might serve as a sum-

mary. All the sections that come after these key conceptual sections can then, to some degree, be read independently.

Among the various branches of applied DMRG, the applications to dynamical properties of quantum systems are presented first (Sec. IV). Next, I discuss attempts to use DMRG for systems with potentially large numbers of local degrees of freedom such as phononic models or Bose-Hubbard models (Sec. V).

Moving beyond the world of $T=0$ physics in one dimension, DMRG as applied to two-dimensional quantum Hamiltonians in real space with short-ranged interactions is introduced and various algorithmic variants are presented in Sec. VI.

Major progress has been made by abandoning the concept of an underlying real-space lattice, as various authors have developed DMRG variants for momentum space (Sec. VII.A), for small-molecule quantum chemistry (Sec. VII.B), and for mesoscopic small grains and nuclei (Sec. VII.C). All these fields are currently under very active development.

Early in the history of DMRG it was realized that its core renormalization idea might also be applied to the renormalization of transfer matrices that describe two-dimensional classical (Sec. VIII.A) or one-dimensional quantum systems (Sec. VIII.C) in equilibrium at finite temperature. Here, algorithmic details undergo major changes, such that this class of DMRG methods is often referred to as TMRG *(transfer-matrix renormalization group)*.

Yet another step can be taken by moving to physical systems that are out of equilibrium (Sec. IX). DMRG has been successfully applied to the steady states of non-equilibrium systems, leading to a non-Hermitian extension of the DMRG in which transition matrices replace Hamiltonians. Various methods for time-dependent problems are under development and have recently started to yield results unattainable by other numerical methods, not only at $T=0$, but also for finite temperature and in the presence of dissipation.

In this review, details of computer implementation have been excluded. Rather, I have tried to focus on details of algorithmic structure and their relation to the physical questions to be studied using DMRG and to give the reader some idea of the power and the limitations of the method. In the more standard fields of DMRG, I have not been (able to be) exhaustive even in listing applications. In the less established fields of DMRG, I have tried to be more comprehensive and to provide as much discussion of their details as possible, in order to make these fields better known and, hopefully, to stimulate thinking about further algorithmic progress. I have excluded, for lack of space, any extensive discussions of the analytical methods whose development has been stimulated by DMRG concepts. Last but not least, it should be mentioned that some of the topics of this review have been considered by other authors: White (1998) gives an introduction to the fundamentals of DMRG; a very detailed survey of DMRG as it was understood in late 1998 has been provided in a collection

of lectures and articles (Peschel, Hallberg, *et al.*, 1999), which also contains an account of DMRG history by White. More recently, the application of TMRG to quantum systems and two-dimensional DMRG has been reviewed by Shibata (2003). Hallberg (2003) gives a rather complete overview of DMRG applications. Dukelsky and Pittel (2004) focus on DMRG applications to finite Fermi systems such as small grains, small molecules, and nuclei.

A word on notation: All state spaces considered here can be factorized into local state spaces $\{|\sigma\rangle\}$ labeled by greek letters. DMRG forms blocks of lattice sites; I denote (basis) states $|m\rangle$ of such blocks by latin letters. These states depend on the size of the block; when necessary, I indicate the block length by subscripts $|m_\ell\rangle$. Correspondingly, $|\sigma_i\rangle$ is a local state on site i. Moreover, DMRG typically operates with two blocks and two sites, which are referred to as belonging to a "system" or "environment." Where this distinction matters, it is indicated by superscripts, $|m^S\rangle$ or $|\sigma^E\rangle$.

II. KEY ASPECTS OF DMRG

Historically, DMRG has its origin in the analysis by White and Noack (1992) of the failure of *real-space renormalization-group* (RSRG) methods to yield quantitatively acceptable results for the low-energy properties of quantum many-body problems. Most of the DMRG algorithm can be formulated in standard (real-space) renormalization-group (RG) language. Alternative points of view in terms of matrix product states and quantum information theory will be taken up later (Sec. III.A and Sec. III.C). Before moving on to the details, let me mention a debate that has been going on among DMRG practitioners on whether calling the DMRG algorithm a renormalization-group method is a misnomer. The answer depends on what one considers the essence of a renormalization-group (RG) method. If this essence is the systematic thinning out of degrees of freedom leading to effective Hamiltonians, DMRG is an RG method. However, it does not involve an ultraviolet or infrared energy cutoff in the degrees of freedom, which is at the heart of traditional RG methods and hence is often considered as part of the core concept.

A. Real-space renormalization of Hamiltonians

The set of concepts grouped under the heading of "renormalization" has proven extremely powerful in providing succinct descriptions of the collective behavior of systems of size L with a diverging number of degrees of freedom N_{site}^L. Starting from some microscopic Hamiltonian, degrees of freedom are iteratively integrated out and accounted for by modifying the original Hamiltonian. The new Hamiltonian will exhibit modified as well as new couplings, and renormalization-group approximations typically consist of physically motivated truncations of the set of couplings newly generated by the *a priori* exact elimination of degrees of freedom.

One obtains a simplified ("renormalized") effective Hamiltonian that should catch the essential physics of the system under study. The success of this approach rests on scale separation: for continuous phase transitions, the diverging correlation length sets a natural long-wavelength low-energy scale which dominates the physical properties, and fluctuations on shorter length scales may be integrated out and summed up into quantitative modifications of the long-wavelength behavior. In the Kondo problem, the width of the Kondo resonance sets an energy scale such that the exponentially decaying contributions of energy levels far from the resonance can be integrated out. This is the essence of the numerical renormalization group (Wilson, 1975).

Following up on the Kondo problem, it was hoped that thermodynamic-limit ground-state properties of other many-body problems such as the one-dimensional Hubbard or Heisenberg models might be treated similarly, with lattice sites replacing energy levels. However, results of real-space renormalization schemes turned out to be poor. While a precise analysis of this observation is hard for many-body problems, White and Noack (1992) identified the breakdown of the real-space renormalization group for the toy model of a single noninteracting particle hopping on a discrete one-dimensional lattice (the "particle in a box" problem). For a box of size L, the Hilbert space spanned by $\{|i\rangle\}$ is L dimensional; in state $|i\rangle$, the particle is on site i. The matrix elements of the Hamiltonian are band diagonal, $\langle i|\hat{H}|i\rangle = 2$; $\langle i|\hat{H}|i\pm 1\rangle = -1$ in some units. Consider now the following real-space renormalization-group procedure:

(1) Describe interactions on an initial sublattice ("block") A of length ℓ by a block Hamiltonian $\hat{H}_A$ acting on an M-dimensional Hilbert space.

(2) Form a compound block AA of length 2ℓ and the Hamiltonian $\hat{H}_{AA}$, consisting of two block Hamiltonians and interblock interactions. $\hat{H}_{AA}$ has dimension M^2.

(3) Diagonalize $\hat{H}_{AA}$ to find the M lowest-lying eigenstates.

(4) Project $\hat{H}_{AA}$ onto the truncated space spanned by the M lowest-lying eigenstates, $\hat{H}_{AA} \rightarrow \hat{H}_{AA}^{\text{tr}}$.

(5) Restart from step (2), with doubled block size: $2\ell \rightarrow \ell$, $AA \rightarrow A$, and $\hat{H}_{AA}^{\text{tr}} \rightarrow \hat{H}_A$, until the box size is reached.

The key point is that the decimation procedure of the Hilbert space is to take the lowest-lying eigenstates of the compound block AA. This amounts to the assumption that the ground state of the entire box will essentially be composed of energetically low-lying states living on smaller blocks. The outlined real-space renormalization procedure gives very poor results. The breakdown can best be understood visually (Fig. 1): assuming an already rather large block size, where dis-
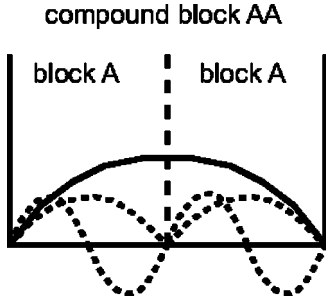
FIG. 1. Lowest-lying eigenstates of (dashed line) blocks A and (solid line) AA for the problem of a single particle in a box in the continuum limit.
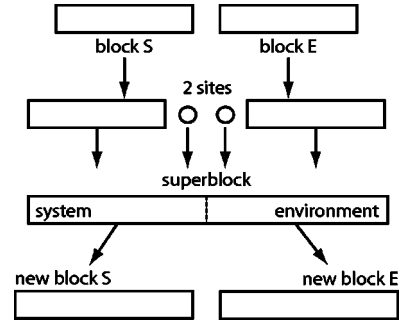

FIG. 2. System meets environment: Fundamental density-matrix renormalization-group (DMRG) construction of a superblock from two blocks and two single sites.

cretization can be neglected, the lowest-lying states of A all have nodes at the lattice ends, such that all product states of AA have nodes at the compound block center. The true ground state of AA has its maximum amplitude right there, such that it cannot be properly approximated by a restricted number of block states.

Merely considering isolated blocks imposes wrong boundary conditions, and White and Noack (1992) could obtain excellent results by combining Hilbert spaces from low-lying states of block A by assuming various combinations of fixed and free boundary conditions (i.e., enforcing a vanishing wave function or a vanishing wave-function derivative, respectively, at the boundaries). They also realized that combining various boundary conditions for a single particle would translate to accounting for fluctuations between blocks in the case of many interacting particles. Keeping this observation in mind, we now return to the original question of a many-body problem in the thermodynamic limit and formulate the following strategy: In order to analyze which states have to be retained for a finite-size block A, A has to be embedded in some environment, mimicking the thermodynamic-limit system in which A is ultimately embedded.

B. Density matrices and DMRG truncation

Consider, instead of the exponentially fast growth procedure outlined above, the following linear growth prescription (White, 1992): Assume that for a system (a *block* in DMRG language) of length ℓ we have an M^S-dimensional Hilbert space with states $\{|m_\ell^S\rangle\}$. The Hamiltonian $\hat{H}_\ell$ is given by matrix elements $\langle m_\ell^S|\hat{H}_\ell|\tilde{m}_\ell^S\rangle$. Similarly we know the matrix representations of local operators such as $\langle m_\ell^S|C_i|\tilde{m}_\ell^S\rangle$.

For linear growth, we now construct $\hat{H}_{\ell+1}$ in the product basis $\{|m_\ell^S\sigma\rangle\}\equiv\{|m_\ell^S\rangle|\sigma^S\rangle\}$, where $|\sigma^S\rangle$ are the N_{site} local states of a new site added.

The thermodynamic limit is now mimicked by embedding the system in an *environment* of the same size, assumed to have been constructed in analogy to the system. We thus arrive at a *superblock* of length $2\ell+2$ (Fig. 2), in which the arrangement chosen is typical, but not mandatory.

Because the final goal is the ground state in the thermodynamic limit, one studies the best approximation to it, the ground state of the superblock, obtained by numerical diagonalization:

$$|\psi\rangle = \sum_{m^S=1}^{M^S}\sum_{\sigma^S=1}^{N_{\text{site}}}\sum_{\sigma^E=1}^{N_{\text{site}}}\sum_{m^E=1}^{M^E}\psi_{m^S\sigma^S\sigma^Em^E}|m^S\sigma^S\rangle|m^E\sigma^E\rangle$$

$$= \sum_i^{N^S}\sum_j^{N^E}\psi_{ij}|i\rangle|j\rangle; \quad \langle\psi|\psi\rangle = 1, \tag{4}$$

where $\psi_{m^S\sigma^S\sigma^Em^E}=\langle m^S\sigma^S;\sigma^Em^E|\psi\rangle$. $\{|m^S\sigma^S\rangle\}\equiv\{|i\rangle\}$, and $\{|m^E\sigma^E\rangle\}\equiv\{|j\rangle\}$ are the orthonormal product bases of system and environment (subscripts have been dropped) with dimensions $N^S=M^SN_{\text{site}}$ and $N^E=M^EN_{\text{site}}$, respectively (for later generalizations, we allow $N^S\neq N^E$). Some truncation procedure from N^S to $M^S<N^S$ states must now be implemented. Let me present three lines of argument on the optimization of some quantum-mechanical quantity, all leading to the same truncation prescription focused on density-matrix properties. This is to highlight different aspects of the DMRG algorithm and to give confidence in the prescription found.

(1) *Optimization of expectation values (White, 1998):* If the superblock is in a pure state $|\psi\rangle$ as in Eq. (4), statistical physics describes the physical state of the system through a reduced density matrix $\hat{\rho}$,

$$\hat{\rho} = \text{Tr}_E|\psi\rangle\langle\psi|, \tag{5}$$

where the states of the environment have been traced out,

$$\langle i|\hat{\rho}|i'\rangle = \sum_j \psi_{ij}\psi_{i'j}^*. \tag{6}$$

$\hat{\rho}$ has N^S eigenvalues w_α and orthonormal eigenstates $\hat{\rho}|w_\alpha\rangle=w_\alpha|w_\alpha\rangle$, with $\Sigma_\alpha w_\alpha=1$ and $w_\alpha\geq 0$. We assume the states are ordered such that $w_1\geq w_2\geq w_3\geq\cdots$. The intuition that the ground state of the system is best described by retaining those M^S states with largest weight w_α in the density matrix can be formalized as follows. Consider some bounded operator $\hat{A}$ acting on the system, such as the energy

per lattice bond; $\|\hat{A}\| = \max_\phi |\langle\phi|\hat{A}|\phi\rangle/\langle\phi|\phi\rangle| \equiv c_A$. The expectation value of $\hat{A}$ is found to be, using Eqs. (4) and (6),

$$\langle\hat{A}\rangle = \langle\psi|\hat{A}|\psi\rangle/\langle\psi|\psi\rangle = \mathrm{Tr}_S\hat{\rho}\hat{A}. \tag{7}$$

Expressing Eq. (7) in the density-matrix eigenbasis, one finds

$$\langle\hat{A}\rangle = \sum_{\alpha=1}^{N^S} w_\alpha\langle w_\alpha|\hat{A}|w_\alpha\rangle. \tag{8}$$

Then, if we project the system state space down to the M^S dominant eigenvectors $|w_\alpha\rangle$ with the largest eigenvalues,

$$\langle\hat{A}\rangle_{\mathrm{approx}} = \sum_{\alpha=1}^{M^S} w_\alpha\langle w_\alpha|\hat{A}|w_\alpha\rangle, \tag{9}$$

and the error for $\langle\hat{A}\rangle$ is bounded by

$$|\langle\hat{A}\rangle_{\mathrm{approx}} - \langle\hat{A}\rangle| \le \left(\sum_{\alpha>M^S}^{N^S} w_\alpha\right)c_A \equiv \epsilon_\rho c_A. \tag{10}$$

This estimate holds in particular for energies. Several remarks are in order. Technically, I have neglected to trace the fate of the denominator in Eq. (7) upon projection; the ensuing correction of $(1 - \epsilon_\rho)^{-1}$ is of no relevance to the argument here, as $\epsilon_\rho \to 0$. The estimate could be tightened for any specific operator, since we know $\langle w_\alpha|\hat{A}|w_\alpha\rangle$, and a more efficient truncation procedure could be named. For arbitrary bounded operators acting on the system, the prescription to retain the state spanned by the M^S dominant eigenstates is optimal. For local quantities, such as energy, magnetization, or density, errors are of the order of the *truncated weight*

$$\epsilon_\rho = 1 - \sum_{\alpha=1}^{M^S} w_\alpha, \tag{11}$$

which emerges as the key estimate. Hence a fast decay of density-matrix eigenvalues w_α is essential for the performance of this truncation procedure. The *truncation error* of Eq. (10) is the total error only if the system had been embedded in the final and exactly described environment. Considering the iterative system and environment growth and their approximate representation at each step, we see that additional sources of an *environmental error* have to be considered. In practice therefore errors for observables calculated by DMRG are often much larger than the truncated weight, even after additional steps to eliminate environmental errors have been taken. Careful extrapolation of results in M^S (or ϵ_ρ) is therefore highly recommended, as will be discussed below.

(2) *Optimization of the wave function (White, 1992, 1993):* Quantum-mechanical objects are completely described by their wave function. It is thus a reasonable demand for a truncation procedure that the approximative wave function $|\tilde{\psi}\rangle$ in which the system space has been truncated to be spanned by only M^S orthonormal states $|\alpha\rangle = \sum_i u_{\alpha i}|i\rangle$,

$$|\tilde{\psi}\rangle = \sum_{\alpha=1}^{M^S}\sum_{j=1}^{N^E} a_{\alpha j}|\alpha\rangle|j\rangle, \tag{12}$$

minimize the distance in the quadratic norm

$$\||\psi\rangle - |\tilde{\psi}\rangle\|. \tag{13}$$

This problem finds a very compact solution in a singular-value decomposition, which was the original approach of White: Singular-value decomposition will be considered in a slightly different setting in the next section. The following is an alternative, more pedestrian approach. Assuming real coefficients for simplicity, one has to minimize

$$1 - 2\sum_{\alpha ij}\psi_{ij}a_{\alpha j}u_{\alpha i} + \sum_{\alpha j}a_{\alpha j}^2 \tag{14}$$

with respect to $a_{\alpha j}$ and $u_{\alpha i}$. For the solution to be stationary in $a_{\alpha j}$, we must have $\sum_i\psi_{ij}u_{\alpha i} = a_{\alpha j}$, finding that

$$1 - \sum_{\alpha ii'}u_{\alpha i}\rho_{ii'}u_{\alpha i'} \tag{15}$$

must be stationary for the global minimum of the distance (13), where we have introduced the density-matrix coefficients

$$\rho_{ii'} = \sum_j\psi_{ij}\psi_{i'j}. \tag{16}$$

Equation (15) is stationary, according to the Rayleigh-Ritz principle, for $|\alpha\rangle$ being the eigenvectors of the density matrix. Expressing Eq. (15) in the density-matrix eigenbasis, the global minimum is given by choosing $|\alpha\rangle$ to be the M^S eigenvectors $|w_\alpha\rangle$ to the largest eigenvalues w_α of the density matrix, as they are all non-negative, and the minimal distance squared is, using Eq. (11),

$$\||\psi\rangle - |\tilde{\psi}\rangle\|^2 = 1 - \sum_{\alpha=1}^{M^S} w_\alpha = \epsilon_\rho. \tag{17}$$

The truncation prescription now appears as a variational principle for the wave function.

(3) *Optimization of entanglement (Gaite, 2001, 2003; Galindo and Martín-Delgado, 2002; Osborne and Nielsen, 2002; Latorre et al., 2004):* Consider the superblock state $|\psi\rangle$ as in Eq. (4). The essential feature of a nonclassical state is its *entanglement*, the fact that it cannot be written as a simple product of one system and one environment state. Bipartite entanglement as relevant here can best be studied by representing $|\psi\rangle$ in its form after a *Schmidt decomposition* (Nielsen and Chuang, 2000): Assuming

without loss of generality $N^S \geq N^E$, consider the $(N^S \times N^E)$-dimensional matrix A with $A_{ij} = \psi_{ij}$. Singular-value decomposition guarantees $A = UDV^T$, where U is $(N^S \times N^E)$ dimensional with orthonormal columns, D is an $(N^E \times N^E)$-dimensional diagonal matrix with non-negative entries $D_{\alpha\alpha} = \sqrt{w_\alpha}$, and V^T is an $(N^E \times N^E)$-dimensional unitary matrix; $|\psi\rangle$ can be written as

$$|\psi\rangle = \sum_{i=1}^{N^S} \sum_{\alpha=1}^{N^E} \sum_{j=1}^{N^E} U_{i\alpha} \sqrt{w_\alpha} V_{\alpha j}^T |i\rangle|j\rangle$$

$$= \sum_{\alpha=1}^{N^E} \sqrt{w_\alpha} \left(\sum_{i=1}^{N^S} U_{i\alpha}|i\rangle \right) \left(\sum_{j=1}^{N^E} V_{j\alpha}|j\rangle \right). \quad (18)$$

The orthonormality properties of U and V^T ensure that $|w_\alpha^S\rangle = \sum_i U_{i\alpha}|i\rangle$ and $|w_\alpha^E\rangle = \sum_j V_{j\alpha}|j\rangle$ form orthonormal bases of system and environment, respectively, in which the Schmidt decomposition

$$|\psi\rangle = \sum_{\alpha=1}^{N_{\text{Schmidt}}} \sqrt{w_\alpha}|w_\alpha^S\rangle|w_\alpha^E\rangle \quad (19)$$

holds. $N^S N^E$ coefficients ψ_{ij} are reduced to $N_{\text{Schmidt}} \leq N^E$ nonzero coefficients $\sqrt{w_\alpha}$, $w_1 \geq w_2 \geq w_3 \geq \cdots$. Relaxing the assumption $N^S \geq N^E$, one has

$$N_{\text{Schmidt}} \leq \min(N^S, N^E). \quad (20)$$

The suggestive labeling of states and coefficients in Eq. (19) is motivated by the observation that upon tracing out environment or system the reduced density matrices for system and environment are found to be

$$\hat{\rho}_S = \sum_\alpha^{N_{\text{Schmidt}}} w_\alpha|w_\alpha^S\rangle\langle w_\alpha^S|; \quad \hat{\rho}_E = \sum_\alpha^{N_{\text{Schmidt}}} w_\alpha|w_\alpha^E\rangle\langle w_\alpha^E|. \quad (21)$$

Even if system and environment are different (Sec. II.D), both density matrices would have the same number of nonzero eigenvalues, bounded by the smaller of the dimensions of system and environment, and an identical eigenvalue spectrum. Quantum information theory now provides a measure of entanglement through the von Neumann entropy,

$$S_{\text{vN}} = -\operatorname{Tr} \hat{\rho} \ln_2 \hat{\rho} = -\sum_{\alpha=1}^{N_{\text{Schmidt}}} w_\alpha \ln_2 w_\alpha. \quad (22)$$

Hence our truncation procedure to M^S states preserves a maximum of system-environment entanglement if we retain the first M^S states $|w_\alpha\rangle$ for $\alpha = 1, \ldots, M^S$, as $-x \ln_2 x$ grows monotonically for $0 < x \leq 1/e$, which is larger than typical discarded eigenvalues. Let me add that this optimization statement holds strictly only for the unnormalized truncated state. Truncation leads to a wavefunction norm $\sqrt{1 - \epsilon_\rho}$ and enforces a new normalization, which changes the retained w_α and S_{vN}.

While one may easily construct density-matrix spectra for which upon normalization the truncated state produced by DMRG no longer maximizes entanglement, for typical density-matrix spectra the optimization statement still holds in practice.

C. Infinite-system DMRG

Collecting the results of the last two sections, the so-called *infinite-system DMRG algorithm* can now be formulated (White, 1992). Details of efficient implementation will be discussed in subsequent sections; here, we assume that we are looking for the ground state.

(1) Consider a lattice of some small size ℓ, forming the system block S. S lives on a Hilbert space of size M^S with states $\{|M_\ell^S\rangle\}$; the Hamiltonian $\hat{H}_\ell^S$ and the operators acting on the block are assumed to be known in this basis. At initialization, this may still be an exact basis of the block ($N_{\text{site}}^\ell \leq M^S$). Similarly, form an environment block E.

(2) Form a tentative new system block S′ from S and one added site (Fig. 2). S′ lives on a Hilbert space of size $N^S = M^S N_{\text{site}}$, with a basis of product states $\{|M_\ell^S \sigma\rangle\} \equiv \{|M_\ell^S\rangle|\sigma\rangle\}$. In principle, the Hamiltonian $\hat{H}_{\ell+1}^S$ acting on S′ can now be expressed in this basis (which will not be done explicitly for efficiency; see Sec. II.I). A new environment E′ is built from E in the same way.

(3) Build the superblock of length $2\ell + 2$ from S′ and E′. The Hilbert space is of size $N^S N^E$, and the matrix elements of the Hamiltonian $\hat{H}_{2\ell+2}$ could in principle be constructed explicitly, but this is avoided for efficiency reasons.

(4) Find by large sparse-matrix diagonalization of $\hat{H}_{2\ell+2}$ the ground state $|\psi\rangle$. This is the most time-consuming part of the algorithm (Sec. II.I).

(5) Form the reduced density matrix $\hat{\rho} = \operatorname{Tr}_E |\psi\rangle\langle\psi|$ as in Eq. (6) and determine its eigenbasis $|w_\alpha\rangle$ ordered by descending eigenvalues (weight) w_α. Form a new (reduced) basis for S′ by taking the M^S eigenstates with the largest weights. In the product basis of S′, their matrix elements are $\langle m_\ell^S \sigma | m_{\ell+1}^S\rangle$; taken as column vectors, they form an $N^S \times M^S$ rectangular matrix T. Proceed likewise for the environment.

(6) Carry out the reduced basis transformation $\hat{H}_{\ell+1}^{\text{tr}} = T^\dagger \hat{H}_{\ell+1} T$ onto the new M^S-state basis and take $\hat{H}_{\ell+1}^{\text{tr}} \to \hat{H}_{\ell+1}$ for the system. Do the same for the environment and restart with step (2) with block size $\ell + 1$ until some desired final length is reached. Operator representations also have to be updated (see Sec. II.G).
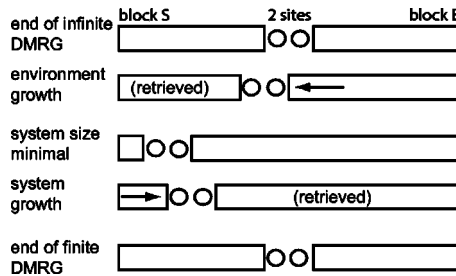
(7) Calculate desired ground-state properties (energies

FIG. 3. Finite-system DMRG algorithm: block growth and shrinkage.

FIG. 4. Currents on rung r of a t-J ladder induced by a source term on the left edge, after various sweeps of finite-system DMRG. From Schollwöck *et al.*, 2003.

and correlators) from $|\psi\rangle$; this step can also be carried out at each intermediate length.

If the Hamiltonian is reflection symmetric, one may consider system and environment to be identical. One is not restricted to choosing the ground state for $|\psi\rangle$; any state accessible by large sparse-matrix diagonalization of the superblock is allowed. Currently available algorithms for this diagonalization limit us, however, to the lowest-lying excitations (see Sec. II.I).

D. Infinite-system and finite-system DMRG

For many problems, infinite-system DMRG does not yield satisfactory answers: The idea of simulating the final system size cannot be implemented well by a small environment block in the early DMRG steps. DMRG is usually canonical, working at fixed particle numbers for a given system size (Sec. II.E). Electronic systems in which the particle number is growing during system growth to maintain particle density approximately constant are affected by a lack of "thermalization" of the particles injected during system growth; t-J models with a relatively small hole density or Hubbard models far from half-filling or with complicated filling factors are particularly affected. The strong physical effects of impurities or randomness in the Hamiltonian cannot be accounted for properly by infinite-system DMRG, as the total Hamiltonian is not yet known at intermediate steps. In systems with strong magnetic fields or close to a first-order transition one may be trapped in a metastable state favored for small system sizes, e.g., by edge effects.

Finite-system DMRG manages to eliminate these concerns to a very large degree and to reduce the error (almost) to the truncation error. The idea of the finite-system algorithm is to stop the infinite-system algorithm at some preselected superblock length L which is kept fixed. In subsequent DMRG steps (Fig. 3), one applies the steps of infinite-system DMRG, but instead of simultaneous growth of both blocks, growth of one block is accompanied by shrinkage of the other block. Reduced basis transformations are carried out only for the growing block. Let the environment block grow at the expense of the system block; to describe it, system blocks of all sizes and operators acting on this block, expressed in the basis of that block, must have been stored previously (at the infinite-system stage or previous applica-
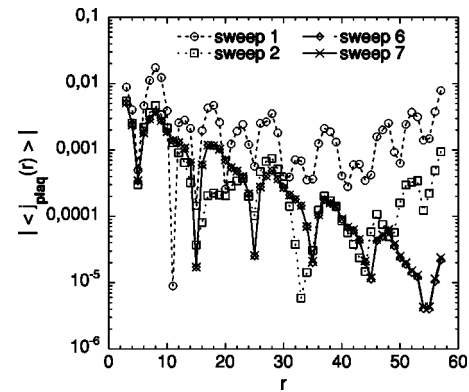
tions of finite-system DMRG). When the system block reaches some minimum size and becomes exact, growth direction is reversed. The system block now grows at the expense of the environment. All basis states are chosen while system and environment are embedded in the final system and in the knowledge of the full Hamiltonian. If the system is symmetric under reflection, blocks can be mirrored at equal size, otherwise the environment block is shrunk to some minimum and then regrown. A complete shrinkage and growth sequence for both blocks is called a *sweep*.

One sweep takes about two (if reflection symmetry holds) or four times the CPU time of the starting infinite-system DMRG calculation. For better performance, there is a simple, but powerful prediction algorithm (see Sec. II.I), which cuts down calculation times in finite-system DMRG by more than an order of magnitude. In fact, it will be seen that the speedup is larger the closer the current (ground) state is to the final, fully converged result. In practice, one therefore starts running the infinite-system DMRG with a rather small number of states M_0, increasing it while running through the sweeps to some final $M_{\text{final}} \gg M_0$. The resulting slowing down of DMRG will be offset by the increasing performance of the prediction algorithm. While there is no guarantee that finite-system DMRG is not trapped in some metastable state, it usually finds the best approximation to the ground state, and convergence is gauged by comparing results from sweep to sweep until they stabilize. This may take from a few to several dozen sweeps, with electronic problems at incommensurate fillings and random potential problems needing the most. In rare cases it has been observed that seemingly converged finite-system results are again suddenly improved after some further sweeps without visible effect have been carried out, showing a metastable trapping. It is therefore advisable to carry out additional sweeps and to judge DMRG convergence by carrying out runs for various M. Where possible, choosing a clever sequence of finite-system DMRG steps may greatly improve the wave function. This has been successfully attempted in

momentum-space DMRG (Sec. VII.A) and quantum-chemistry DMRG (Sec. VII.B).

To show the power of finite-system DMRG, consider the calculation of the plaquette currents induced on a *t-J* ladder by imposing a source current on one edge of the ladder (Schollwöck *et al.*, 2003). Figure 4 shows how the plaquette currents along the ladder evolve from sweep to sweep. While they are perfectly converged after six to eight sweeps, the final result, a modulated exponential decay, is far from what DMRG suggests after the first sweep, let alone in the infinite-system algorithm (not shown).

Despite the general reliability of the finite-system algorithm there might be (relatively rare) situations in which its results are misleading. It may, for example, be doubted whether competing or coexisting types of long-range order are well described by DMRG, as we shall see that it produces a very specific kind of wave function, the so-called matrix-product states (Sec. III.A). These states show either long-range order or, more typically, short-range correlations. In the case of competing forms of long-range order, the infinite-system algorithm might preselect one of them incorrectly, e.g., due to edge effects, and the finite-system algorithm would then be quite likely to fail to "tunnel" to the other, correct kind of long-range order due to the local nature of the improvements to the wave function. Perhaps such a problem is at the origin of the current disagreement between state-of-the-art DMRG (Jeckelmann, 2002b, 2003b; Zhang, 2004) and quantum Monte Carb results (Sandvik *et al.*, 2003, 2004) on the extent of a bond-ordered wave phase between a spin-density-wave phase and a charge-density-wave phase in the half-filled extended Hubbard model, but no consensus has as yet emerged.

E. Symmetries and good quantum numbers

A big advantage of DMRG is that the algorithm conserves a variety of, but not all, symmetries and good quantum numbers of the Hamiltonians. They may be exploited to reduce storage and computation time and to thin out Hilbert space by decomposing it into a sum of sectors. DMRG is optimal for studying the lowest-lying states of such sectors, and refining any such decomposition immediately gives access to more low-lying states. Hence the use of symmetries is standard practice in DMRG implementations. Symmetries used in DMRG fall into three categories, continuous Abelian, continuous non-Abelian, and discrete.

1. Continuous Abelian symmetries

The most frequently implemented symmetries in DMRG are the U(1) symmetries leading to total magnetization S_{tot}^z and total particle number N_{tot} as good (conserved) quantum numbers. If present for some Hamiltonian, all operators can be expressed in matrix form as dense blocks of nonzero matrix elements with all other matrix elements zero. These blocks can be labeled by good quantum numbers. In DMRG, reduced basis trans-

formations preserve these block structures if one fixes total magnetization and/or total particle number for the superblock. Assume that block and site states can at a given DMRG step be labeled by a good quantum number, say, particle number N. This is an essential prerequisite (cf. translational invariance leading to momentum conservation; see below). As the total number of particles is fixed, we have $N_{\text{tot}} = N_{m^S} + N_{\sigma^S} + N_{\sigma^E} + N_{m^E}$. Equation (6) implies that only matrix elements $\langle m^S \sigma^S | \hat{\rho} | \tilde{m}^S \tilde{\sigma}^S \rangle$ with $N_{m^S} + N_{\sigma^S} = N_{\tilde{m}^S} + N_{\tilde{\sigma}^S}$ can be nonzero. The density matrix thus has block structure, and its eigenvectors from which the next block's eigenbasis is formed can again be labeled by particle number $N_{m^S} + N_{\sigma^S}$. Thus, for all operators, only dense blocks of nonzero matrix elements have to be stored and considered. For superblock wave functions, a tensorial structure emerges as total particle number and/or magnetization dictate that only product states with compatible quantum numbers (i.e., adding up to the fixed total) may have nonzero coefficients.

The performance gains from implementing just the simple additive quantum numbers magnetization and particle number are impressive. Both in memory and CPU time significantly more than an order of magnitude will typically be gained.

2. Continuous non-Abelian symmetries

Non-Abelian symmetries that have been considered are the quantum group symmetry $\mathrm{SU}_q(2)$ (Sierra and Nishino, 1997), SU(2) spin symmetry (McCulloch and Gulacsi, 2000, 2001, 2002; Wada, 2000; Xiang *et al.*, 2001), and the charge SU(2) pseudospin symmetry (McCulloch and Gulacsi, 2002), which holds for the bipartite Hubbard model without field (Yang and Zhang, 1990): its generators are given by $I^+ = \Sigma_i (-1)^i c_{\uparrow i}^\dagger c_{\downarrow i}^\dagger$, $I^- = \Sigma_i (-1)^i c_{\downarrow i} c_{\uparrow i}$, and $I^z = \Sigma_i \frac{1}{2}(n_{\uparrow i} + n_{\downarrow i} - 1)$.

Implementation of non-Abelian symmetries is much more complicated than that of Abelian symmetries, the best-performing one (McCulloch and Gulacsi, 2002) building on Clebsch-Gordan transformations and the elimination of quantum numbers via the Wigner-Eckart theorem. It might be crucial for obtaining high-quality results in applications with problematically large truncated weight such as in two dimensions, where the truncated weight is cut by several orders of magnitude compared to implementations using only Abelian symmetries. The additional increase in performance is comparable to that due to use of U(1) symmetries over using no symmetries at all.

3. Discrete symmetries

I shall formulate these for a fermionic Hamiltonian of spin-$\frac{1}{2}$ particles.

(a) *Spin-flip symmetry*. If the Hamiltonian $\hat{H}$ is invariant under a general spin flip $\uparrow \leftrightarrow \downarrow$, one may introduce the spin-flip operator $\hat{P} = \Pi_i \hat{P}_i$, which is implemented locally on an electronic site as $\hat{P}_i |0\rangle = |0\rangle$,

$\hat{P}_i|\uparrow\rangle=|\downarrow\rangle$, $\hat{P}_i|\downarrow\rangle=|\uparrow\rangle$, $\hat{P}_i|\uparrow\downarrow\rangle=-|\uparrow\downarrow\rangle$ (fermionic sign). As $[\hat{H},\hat{P}]=0$, there are common eigenstates of $\hat{H}$ and $\hat{P}$ with $\hat{P}|\psi\rangle=\pm|\psi\rangle$.

(b) *Particle-hole symmetry*. If $\hat{H}$ is invariant under a particle-hole transformation, $[\hat{H},\hat{J}]=0$ for the particle-hole operator $\hat{J}=\Pi_i\hat{J}_i$, where the local operation is given by $\hat{J}_i|0\rangle=|\uparrow\downarrow\rangle$, $\hat{J}_i|\uparrow\rangle=(-1)^i|\downarrow\rangle$, $\hat{J}_i|\downarrow\rangle=(-1)^i|\uparrow\rangle$, $\hat{J}_i|\uparrow\downarrow\rangle=|0\rangle$, introducing a distinction between odd and even site sublattices, and eigenvalues $\hat{J}|\psi\rangle=\pm|\psi\rangle$.

(c) *Reflection symmetry (parity)*. In the case of reflection-symmetric Hamiltonians with open boundary conditions, parity is a good quantum number. The spatial reflection symmetry operator $\hat{C}_2$ acts globally. Its action on a DMRG product state is given by

$$\hat{C}_2|m^S\sigma^S\sigma^Em^E\rangle=(-1)^\eta|m^E\sigma^E\sigma^Sm^S\rangle \tag{23}$$

with a fermionic phase determined by $\eta=(N_{m^S}+N_{\sigma^S})(N_{m^E}+N_{\sigma^E})$. Again, eigenvalues are given by $\hat{C}_2|\psi\rangle=\pm|\psi\rangle$. Parity is not a good quantum number accessible to finite-system DMRG, except for the DMRG step with identical system and environment.

All three symmetries commute, and an arbitrary normalized wave function can be decomposed into eigenstates for any desired combination of eigenvalues ±1 by successively calculating

$$|\psi_\pm\rangle=\frac{1}{2}(|\psi\rangle\pm\hat{O}|\psi\rangle), \tag{24}$$

where $\hat{O}=\hat{P},\hat{J},\hat{C}_2$.

Parity may be easily implemented by starting the superblock diagonalization from a trial state (Sec. II.I) that has been made (anti)symmetric under reflection by Eq. (24). As $[\hat{H},\hat{C}_2]=0$, the final eigenstate will have the same reflection symmetry. Spin-flip and particle-hole symmetries may be implemented in the same fashion, provided $\hat{P}$ and $\hat{J}$ are generated by DMRG; as they are products of local operators, this can be done along the lines of Sec. II.G. Another way of implementing these two local symmetries is to realize that the argument given for magnetization and particle number as good density-matrix quantum numbers carries over to the spin-flip and particle-hole eigenvalues such that they can also be implemented as block labels.

4. Missing symmetries

Momentum is not a good quantum number in real-space DMRG, even if periodic boundary conditions (Sec. II.H) are used and translational invariance holds. This is because the allowed discrete momenta change during the growth process, and, more importantly, be-cause momentum does not exist as a good quantum number at the block level. Other DMRG variants with momentum as a good quantum number will be considered in Sec. VII.A.

F. Energies: Ground states and excitations

As a method working in a subspace of the full Hilbert space, DMRG is variational in energy. It provides upper bounds for energies $E(M)$ that improve monotonically with M, the number of basis states in the reduced Hilbert space. Two sources of errors have been identified, the environmental error due to inadequate environment blocks, which can be amended using the finite-system DMRG algorithm, and the truncation error. Assuming that the environmental error (which is hard to quantify theoretically) has been eliminated, i.e., finite-system DMRG has reached convergence after sufficient sweeping, the truncation error remains to be analyzed. Rerunning the calculation of a system of size L for various M, one observes for sufficiently large values of M that to a good approximation the error in energy per site scales linearly with the truncated weight,

$$[E(M)-E_{\text{exact}}]/L\propto\epsilon_\rho, \tag{25}$$

with a nonuniversal proportionality factor typically of order 1–10, sometimes more [this observation goes back to White and Huse (1993); Legeza and Fáth (1996) give a careful analysis]. As ϵ_ρ is often of order 10^{-10} or less, DMRG energies can thus be extrapolated using Eq. (25) quite reliably to the exact $M=\infty$ result, often almost at machine precision. The precision desired imposes the size of M, which for spin problems is typically in the lower hundreds, for electronic problems in the upper hundreds, and for two-dimensional and momentum-space problems in the lower thousands. As an example of DMRG precision, consider the results obtained for the ground-state energy per site of the $S=1$ antiferromagnetic Heisenberg chain in Table I.

Experiments relate to energy differences or relative ordering of levels. This raises the question of calculating excitations in DMRG. Excitations are easiest to calculate if they are the ground state in some other symmetry sector of the Hamiltonian and are thus algorithmically no different from true ground states. If, however, we are interested in some higher-lying state in a particular Hilbert space sector, DMRG restricts us to the lowest-lying such states because of the restrictions of large sparse-matrix diagonalizations (Sec. II.I). Excited states have to be "targeted" in the same way as the ground state. This means that they have to be calculated for the superblock at each iteration and to be represented optimally, i.e., reduced basis states have to be chosen such that the error in the approximation is minimized. It can be shown quite easily that this amounts to considering the eigenstates of the reduced density matrix

$$\hat{\rho}_S = \text{Tr}_E \sum_i \alpha_i |\psi_i\rangle\langle\psi_i|, \tag{26}$$

where the sum runs over all targeted states $|\psi_i\rangle$ (ground and a few excited states) and $\Sigma_i \alpha_i = 1$. There is no known optimal choice for the α_i, but it seems empirically to be most reasonable to weigh states roughly equally. To maintain a good overall description for all targeted states at a fixed M, typically fewer than five or so excited states are targeted. Best results are of course obtained by running DMRG for each energy level separately.

G. Operators and correlations

In general, we shall also be interested in evaluating static n-point correlators $\hat{O}^{(n)}_{i_1 \cdots i_n} = \hat{O}^{(1)}_{i_1} \cdots \hat{O}^{(1)}_{i_n}$ with respect to some eigenstate of the Hamiltonian. The most relevant cases are $n=1$ for density or local magnetization and $n=2$ for two-point density-density, spin-spin, or creation-annihilation correlators, $\langle n_i n_j \rangle$, $\langle S_i^+ S_j^- \rangle$, or $\langle c_i^\dagger c_j \rangle$.

Let us first consider the case $n=1$. The iterative growth strategy of DMRG imposes a natural three-step procedure of initializing, updating, and evaluating correlators.

(1) *Initialization.* $\hat{O}_i$ acts on site i. When site i is added to a block of length $\ell-1$, $\langle\sigma|\hat{O}_i|\tilde{\sigma}\rangle$ is evaluated. With $\{|m_\ell\rangle\}$ being the reduced basis of the new block incorporating site i and $\{|m_{\ell-1}\rangle\}$ that of the old block, one has

$$\langle m_\ell|\hat{O}_i|\tilde{m}_\ell\rangle = \sum_{m_{\ell-1}\sigma\tilde{\sigma}} \langle m_\ell|m_{\ell-1}\sigma\rangle\langle\sigma|\hat{O}_i|\tilde{\sigma}\rangle\langle m_{\ell-1}\tilde{\sigma}|\tilde{m}_\ell\rangle. \tag{27}$$

$\langle m_\ell|m_{\ell-1}\sigma\rangle$ is already known from the density-matrix eigenstates.

(2) *Update.* At each further DMRG step, an approximate basis transformation for the block containing the site in which $\hat{O}_i$ acts from $\{|m_\ell\rangle\}$ to $\{|m_{\ell+1}\rangle\}$ occurs. As $\hat{O}_i$ does not act on the new site, the operator transforms as

$$\langle m_{\ell+1}|\hat{O}|\tilde{m}_{\ell+1}\rangle = \sum_{m_\ell\tilde{m}_\ell\sigma} \langle m_{\ell+1}|m_\ell\sigma\rangle\langle m_\ell|\hat{O}|\tilde{m}_\ell\rangle$$
$$\times\langle\tilde{m}_\ell\sigma|\tilde{m}_{\ell+1}\rangle. \tag{28}$$

This expression is evaluated efficiently by splitting it into two $O(M^3)$ matrix-matrix multiplications.

(3) *Evaluation.* After the last DMRG step $\langle m^S\sigma^S\sigma^E m^E|\psi\rangle$ is known and $\langle\hat{O}_i\rangle$ reads, assuming $\hat{O}_i$ to act on some site in the system block,

$$\langle\psi|\hat{O}_i|\psi\rangle = \sum_{m^S\tilde{m}^S\sigma^S\sigma^E m^E} \langle\psi|m^S\sigma^S\sigma^E m^E\rangle\langle m^S|\hat{O}_i|\tilde{m}^S\rangle$$
$$\times \langle\tilde{m}^S\sigma^S\sigma^E m^E|\psi\rangle. \tag{29}$$

TABLE I. Ground-state energies per site E_0 of the $S=1$ isotropic antiferromagnetic Heisenberg chain for M block states kept and associated truncated weight $\epsilon_\rho(M)$. Adapted from White and Huse (1993).

M	$E_0(M)$	$\epsilon_\rho(M)$
36	-1.40148379810	5.61×10^{-8}
72	-1.40148403632	3.42×10^{-10}
110	-1.40148403887	1.27×10^{-11}
180	-1.401484038970	1.4×10^{-13}

In the case of two-point correlators, two cases have to be distinguished, whether the locations i and j of the contributing one-point operators act on different blocks or on the same block at the last step. This expression is again evaluated efficiently by splitting it into two $O(M^3)$ matrix-matrix multiplications.

If they act on different blocks, one follows through the procedure for one-point operators, yielding $\langle m^S|\hat{O}_i|\tilde{m}^S\rangle$ and $\langle m^E|\hat{O}_j|\tilde{m}^E\rangle$. The evaluation is done by the following modification of the one-point case:

$$\langle\psi|\hat{O}_i\hat{O}_j|\psi\rangle = \sum_{m^S\tilde{m}^S\sigma^S\sigma^E m^E\tilde{m}^E} \langle\psi|m^S\sigma^S\sigma^E m^E\rangle\langle m^S|\hat{O}_i|\tilde{m}^S\rangle$$
$$\times\langle m^E|\hat{O}_j|\tilde{m}^E\rangle\langle\tilde{m}^S\sigma^S\sigma^E\tilde{m}^E|\psi\rangle. \tag{30}$$

If they act on the same block, it is wrong to obtain $\langle m|\hat{O}_i\hat{O}_j|\tilde{m}\rangle$ through

$$\langle m|\hat{O}_i\hat{O}_j|\tilde{m}\rangle = \sum_{m'} \langle m|\hat{O}_i|m'\rangle\langle m'|\hat{O}_j|\tilde{m}\rangle \quad \text{(false)}, \tag{31}$$

where an approximate partition of unity has been inserted. This partition of unity is close to 1 to a very good approximation only when it is used to project the targeted wave function, for which it was constructed, but not in general.

Instead, such operators have to be built as a compound object at the moment when they live in a product Hilbert space, namely, when one of the operators acts on a block (of length $\ell-1$), the other on a single site that is being attached to the block. Then we know $\langle m_{\ell-1}|\hat{O}_i|\tilde{m}_{\ell-1}\rangle$ and $\langle\sigma|\hat{O}_j|\tilde{\sigma}\rangle$ and within the reduced bases of the block of length ℓ

$$\langle m_\ell|\hat{O}_i\hat{O}_j|\tilde{m}_\ell\rangle = \sum_{m_{\ell-1}\tilde{m}_{\ell-1}\sigma\tilde{\sigma}} \langle m_\ell|m_{\ell-1}\sigma\rangle\langle m_{\ell-1}|\hat{O}_i|\tilde{m}_{\ell-1}\rangle$$
$$\times \langle\sigma|\hat{O}_j|\tilde{\sigma}\rangle\langle\tilde{m}_{\ell-1}\tilde{\sigma}|\tilde{m}_\ell\rangle \tag{32}$$

is exact. Updating and final evaluation for compound operators proceed as for a one-point operator.

One-point operators show similar convergence behavior in M to that of local energy, but at reduced precision. While there is no exact variational principle for two-point correlations, derived correlation lengths are monotonically increasing in M, but always underestimated. The underestimation can actually be quite severe, of the

order of several percent, while the ground-state energy has already converged almost to machine precision.

As DMRG always generates wave functions with exponentially decaying correlations (Sec. III.A), power-law decays of correlations are problematic. Andersson *et al.* (1999) show that for free fermions the resulting correlation function mimics the correct power law on short-length scales increasing with M, but is purely exponential on larger scales. However, the derived correlation length diverges roughly as $M^{1.3}$, such that for $M \to \infty$ criticality is recovered.

H. Boundary conditions

From a physical point of view, periodic boundary conditions are normally highly preferable to the open boundary conditions used so far for studying bulk properties, as surface effects are eliminated and finite-size extrapolation works for much smaller system sizes. In particular, open boundaries introduce charge or magnetization oscillations not always easily distinguishable from true charge-density waves or dimerization [see White *et al.* (2002) for a thorough discussion on using bosonization to make the distinction].

However, it was observed early in the history of DMRG that ground-state energies for a given M are much less precise in the case of periodic boundary conditions than for open boundary conditions, with differences in the relative errors of up to several orders of magnitude. This is reflected in the spectrum of the reduced density matrix, which decays much more slowly (see Sec. III.B). However, it has been shown by Verstraete, Porras, and Cirac (2004) that this is an artifact of the conventional DMRG setup and that, at some algorithmic cost, essentially the same precision for a given M can be achieved for periodic as for open boundary conditions (Sec. III.A).

To implement periodic boundary conditions in the infinite-system DMRG algorithm, the block-site structure is typically changed as shown in Fig. 5; other setups however, are also feasible and used. For finite-system DMRG, the environment block grows at the expense of the system block, then the system block grows back, till the configuration of the end of the infinite-system algorithm is reached. This is repeated with changed roles (unless translational invariance allows identification of system and environment at equal size). A minor technical complication arises from the fact that blocks grow at both ends at various steps of the algorithm.

Beyond the usual advantages of periodic boundary conditions, combining results for periodic and antiperiodic boundary conditions allows the calculation of responses to boundary conditions such as spin stiffness, phase sensitivity (Schmitteckert and Eckern, 1996), or superfluid density (Rapsch *et al.*, 1999). Periodic and antiperiodic boundary conditions $c_{L+1}^\dagger = \pm c_1^\dagger$ are special cases of the general complex boundary condition $c_{L+1}^\dagger = e^{i\phi} c_1^\dagger$. Implementing the latter is a tedious but straightforward generalization of real-valued DMRG; memory

doubles, computation time quadruples. Numerical stability is assured because the density matrix remains Hermitian. This generalization has been used on a ring with interactions and impurities to determine the current $I(\phi)$, which is neither sawtoothlike nor sinusoidal (Meden and Schollwöck, 2003a), and thus to obtain the conductance of interacting nanowires (Meden and Schollwöck, 2003b). For open boundary conditions, complex-valued DMRG has been used to introduce infinitesimal current source terms for time-reversal symmetry breaking in electronic ladder structures (Schollwöck *et al.*, 2003).

I. Large sparse-matrix diagonalization

1. Algorithms

The key to DMRG performance is the efficient diagonalization of the large sparse-superblock Hamiltonian. All large sparse-matrix diagonalization algorithms iteratively calculate the desired eigenstate from some (random) starting state through successive costly matrix-vector multiplications. In DMRG, the two algorithms typically used are the Lanczos method (Cullum and Willoughby, 1985; Golub and van Loan, 1996) and the Jacobi-Davidson method (Sleijpen and van der Vorst, 1996). The pleasant feature of these algorithms is that for an $N \times N$-dimensional matrix it takes only a much smaller number $\tilde{N} \ll N$ of iterations, so that iterative approximations to eigenvalues converge very rapidly to the maximum and minimum eigenvalues of $\hat{H}$ at machine precision. With slightly more effort other eigenvalues at the edge of the spectrum can also be computed. Typical values for the number of iterations (matrix-vector multiplications) in DMRG calculations are of the order of 100.

2. Representation of the Hamiltonian

Naively, the superblock Hamiltonian is a $M^2 N_{\text{site}}^2$-dimensional matrix. As matrix-vector multiplications scale as (dimension)^2, DMRG would seem to be an algorithm of order $O(M^4)$. In reality, it is only $O(M^3)$, as typical tight-binding Hamiltonians act as sums over two-operator terms: Assuming nearest-neighbor interactions, the superblock Hamiltonian decomposes as

$$\hat{H} = \hat{H}_S + \hat{H}_{S\bullet} + \hat{H}_{\bullet\bullet} + \hat{H}_{\bullet E} + \hat{H}_E. \tag{33}$$

$\hat{H}_S$ and $\hat{H}_E$ contain all interactions within the system and environment blocks, respectively, and are hence of dimension M. Multiplying them to some state $|\psi\rangle$ is of order $M^3 N_{\text{site}}^2$. $\hat{H}_{S\bullet}$ and $\hat{H}_{\bullet E}$ contain interactions between blocks and the neighboring sites and hence are of dimension MN_{site}. Consider a typical interaction $S_\ell^+ S_{\ell+1}^-$, where ℓ is the last site of the block and $\ell+1$ a single site. Then
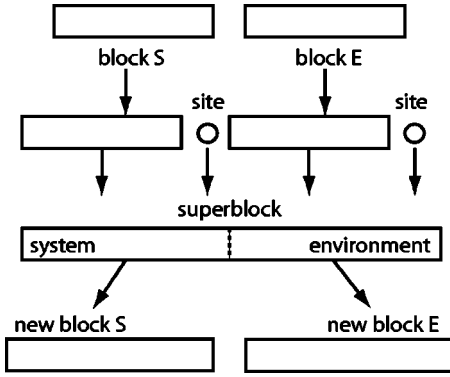
FIG. 5. Typical system and environment growth for periodic boundary conditions in the infinite-system algorithm.

$$\langle m^S\sigma^S|S_\ell^+ S_{\ell+1}^-|\tilde{m}^S\tilde{\sigma}^S\rangle = \langle m^S|S_\ell^+|\tilde{m}^S\rangle\langle\sigma^S|S_{\ell+1}^-|\tilde{\sigma}^S\rangle \qquad (34)$$

and multiplying this term to $|\psi\rangle$ is best carried out in a two-step sequence: the expression

$$\langle m\sigma\tau n|\phi\rangle = \sum_{m'\sigma'} \langle m\sigma|S^+S^-|m'\sigma'\rangle\langle m'\sigma'\tau n|\psi\rangle, \qquad (35)$$

which is of order $O(M^3 N_{site}^3)$ for the determination of all state coefficients, is decomposed as

$$\langle m'\sigma\tau n|\nu\rangle = \sum_{\sigma'} \langle\sigma|S^-|\sigma'\rangle\langle m'\sigma'\tau n|\psi\rangle, \qquad (36)$$

of order $O(M^2 N_{site}^3)$, and

$$\langle m\sigma\tau n|\phi\rangle = \sum_{m'} \langle m|S^+|m'\rangle\langle m'\sigma\tau n|\nu\rangle, \qquad (37)$$

of order $O(M^3 N_{site}^2)$, where an order of N_{site} is saved, important for large N_{site}. The Hamiltonian is never explicitly constructed. Such a decomposition is crucial when block-block interactions $\hat{H}_{SE}$ appear for longer-ranged interactions. Considering again S^+S^-, with S^- now acting on the environment block, factorization of the Hamiltonian again allows us to decompose the original term

$$\langle m\sigma\tau n|\phi\rangle = \sum_{m'n'} \langle mn|S^+S^-|m'n'\rangle\langle m'\sigma\tau n'|\psi\rangle, \qquad (38)$$

which is of inconveniently high-order $O(M^4 N_{site}^2)$ for the determination of all state coefficients, as

$$\langle m'\sigma\tau n|\nu\rangle = \sum_{n'} \langle n|S^-|n'\rangle\langle m'\sigma\tau n'|\psi\rangle, \qquad (39)$$

of order $O(M^3 N_{site}^2)$, and

$$\langle m\sigma\tau n|\psi\rangle = \sum_{m'} \langle m|S^+|m'\rangle\langle m'\sigma\tau n|\nu\rangle, \qquad (40)$$

of order $O(M^3 N_{site}^2)$, such that an order of M is saved and the algorithm is generally of order $O(M^3)$. This is essential for its performance.

3. Eigenstate prediction

Providing a good guess for the final eigenstate as starting state of the iterative diagonalization allows for arbitrary cutdowns in the number of iterations in the iterative diagonalization procedures.

For both the infinite-system and the finite-system DMRG it is possible to provide starting states that often have overlap ≈ 1 with the final state, leading to a dramatic reduction of iterations, often down to fewer than 10, speeding up the algorithm by about an order of magnitude.

In infinite-system DMRG, the physical system changes from step to step. It seems intuitive that for a very long system, the composition of the ground state from block and site states may only weakly depend on its length, such that the ground-state coefficients remain almost the same under system growth. One might therefore simply use the old ground state as a prediction state. This fails; while the absolute values of coefficients hardly change from step to step in long systems, the block basis states are fixed by the density-matrix diagonalization only up to the sign, such that the signs of the coefficients are effectively random. Various ways of fixing these random signs have been proposed (Schollwöck, 1998; Qin and Lou, 2001; Sun et al., 2002).

In the case of the finite-system DMRG, the physical system does not change from DMRG step to DMRG step, just the structure of the effective Hilbert space changes. White (1996b) has given a prescription for how to predict the ground state expressed in the block-site structure of the next DMRG step. If basis transformations were not incomplete, one could simply transform the ground state from one basis to the next to obtain a prediction state. The idea is to do this even though the transformation is incomplete. The state obtained turns out to be an often excellent approximation to the true ground state.

Let us assume that we have a system with open boundary conditions, with a current system block of length ℓ and an environment block of length $L-\ell-2$. The target state is known through $\langle m_\ell\sigma_{\ell+1}\sigma_{\ell+2}m_{L-\ell-2}|\psi\rangle$. Now assume that the system block is growing at the expense of the environment block, and we wish to predict the coefficients $\langle m_{\ell+1}\sigma_{\ell+2}\sigma_{\ell+3}m_{L-\ell-3}|\psi\rangle$, where in both DMRG steps $|\psi\rangle$ is describing the same quantum-mechanical state. As we also know $\langle m_\ell\sigma_{\ell+1}|m_{\ell+1}\rangle$ from the current DMRG iteration and $\langle m_{L-\ell-3}\sigma_{\ell+3}|m_{L-\ell-2}\rangle$ from some previous DMRG iteration, this allows us to carry out two incomplete basis transformations: First, we transform system block and site to the new system block, giving

$$\langle m_{\ell+1}\sigma_{\ell+2}m_{L-\ell-2}|\psi\rangle = \sum_{m_\ell\sigma_{\ell+1}} \langle m_{\ell+1}|m_\ell\sigma_{\ell+1}\rangle$$
$$\times\langle m_\ell\sigma_{\ell+1}\sigma_{\ell+2}m_{L-\ell-2}|\psi\rangle; \qquad (41)$$

second, we expand the current environment block into a product-state representation of a block with one site less and a site:

$$\langle m_{\ell+1}\sigma_{\ell+2}\sigma_{\ell+3}m_{L-\ell-3}|\psi\rangle = \sum_{m_{L-\ell-2}} \langle m_{L-\ell-3}\sigma_{\ell+3}|m_{L-\ell-2}\rangle$$
$$\times \langle m_{\ell+1}\sigma_{\ell+2}m_{L-\ell-2}|\psi\rangle. \quad (42)$$

The calculation involves two $O(M^3)$ matrix multiplications, and works independently of any assumptions for the underlying model. It relies on the fact that by construction our incomplete basis transformations are almost exact when applied to the target state(s).

J. Applications

In this section, I want to give a very brief overview of applications of standard DMRG, which will not be covered in more detail in later sections.

From the beginning, there has been a strong focus on one-dimensional Heisenberg models, in particular the $S=1$ case, in which the Haldane gap $\Delta=0.41052J$ was determined to five-digit precision by White and Huse (1993). Other authors have considered the equal-time structure factor (Sørensen and Affleck, 1994a, 1994b; Sieling *et al.*, 2000) and focused on topological order (Lou *et al.*, 2002, 2003; Qin *et al.*, 2003). There has been a particular emphasis on the study of the existence of free $S=\frac{1}{2}$ end spins in such chains (White and Huse, 1993; Batista *et al.*, 1998, 1999; Polizzi *et al.*, 1998; Hallberg *et al.*, 1999; Jannod *et al.*, 2000), in which the open boundary conditions of DMRG are very useful; for the study of bulk properties authors typically attach real $S=\frac{1}{2}$ end spins that bind to singlets with the effective ones, removing degeneracies due to boundary effects. Soon, studies were carried over to the $S=2$ Heisenberg chain, in which the first reliable determination of the gap $\Delta=0.085(5)$ and the correlation length $\xi\approx 50$ was provided by Schollwöck and Jolicœur (1995) and confirmed and enhanced in other works (Schollwöck, Golinelli, and Jolicœur, 1996; Schollwöck and Jolicœur, 1996; Qin, Wang, and Yu, 1997; Aschauer and Schollwöck, 1998; Wang *et al.*, 1999; Wada, 2000; Capone and Caprara, 2001). The behavior of Haldane (integer spin) chains in (staggered) magnetic fields was studied by Sørensen and Affleck (1993), Lou *et al.* (1999), Ercolessi *et al.* (2000), and Capone and Caprara (2001). In general, DMRG has been very useful in the study of plateaus in magnetization processes of spin chains (Tandon *et al.*, 1999; Citro *et al.*, 2000; Lou, Qin, Ng, *et al.*, 2000; Lou, Qin, and Su, 2000; Yamamoto *et al.*, 2000; Kawaguchi *et al.*, 2002; Silva-Valencia and Miranda, 2002; Hida, 2003).

The isotropic half-integer spin Heisenberg chains are critical. The logarithmic corrections to the power law of spin-spin correlations in the $S=\frac{1}{2}$ chain were first considered by Hallberg *et al.* (1995), later by Hikihara and Furusaki (1998), Tsai and Marston (2000), Shiroishi *et al.* (2001), and Boos *et al.* (2002). For the $S=\frac{3}{2}$ case, the central charge $c=1$ and again the logarithmic corrections

to the spin-spin correlations were determined by Hallberg *et al.* (1996). Quasiperiodic $S=\frac{1}{2}$ chains were considered by Hida (1999b, 2000) and the case of transverse fields by Hieida *et al.* (2001).

Bilinear-biquadratic $S=1$ spin chains have been extensively studied (Bursill *et al.*, 1994; Schollwöck, Jolicœur, and Garel, 1996; Sato, 1998) as well as the effect of Dzyaloshinskii-Moriya interactions (Zhao *et al.*, 2003).

Important, experimentally relevant generalizations of the Heisenberg model are obtained by adding frustrating interactions or dimerization, the latter modeling either static lattice distortions or phonons in the adiabatic limit. The ground-state phase diagrams of such systems have been extensively studied.[1] DMRG has been instrumental in the discovery and description of gapped and gapless chiral phases in frustrated spin chains (Kaburagi *et al.*, 1999; Hikihara, Kaburaga, *et al.*, 2000a; Hikihara, 2001, 2002; Hikihara *et al.*, 2001a, 2001b). Critical exponents for a supersymmetric spin chain were obtained by Senthil *et al.* (1999).

As a first step towards two dimensions and due to the many experimental realizations, spin ladders have been among the first DMRG applications going beyond simple Heisenberg chains, starting with White *et al.* (1994). In the meantime, DMRG has emerged as a standard tool for the study of spin ladders (White, 1996a; Legeza and Sólyom, 1997; Wang, 2000; Fath *et al.*, 2001; Hikihara and Furusaki, 2001; Trumper and Gazza, 2001; Zhu *et al.*, 2001; Wang *et al.*, 2002; Kawaguchi *et al.*, 2003). A focus of recent interest has been the effect of cyclic exchange interactions on spin ladders (Sakai and Hasegawa, 1999; Honda and Horiguchi, 2001; Nunner *et al.*, 2002; Hikihara *et al.*, 2003; Läuchli *et al.*, 2003).

Among other spin systems, ferrimagnets have been studied by Pati, Ramesha, and Sen (1997a, 1997b), Tonegawa *et al.* (1998), Hikihara, Tonegawa, *et al.* (2000), and Langari *et al.* (2000). One-dimensional toy models of the *kagomé* lattice have been investigated by Pati and Singh (1999), Waldtmann *et al.* (2000), and White and Singh (2000), whereas supersymmetric spin chains have been considered by Marston and Tsai (1999).

Spin-orbit chains with spin and pseudospin degrees of freedom are the large-U limit of the two-band Hubbard model at quarter filling and are hence an interesting and important generalization of the Heisenberg model. DMRG has allowed full clarification of the rich phase diagram (Pati *et al.*, 1998; Yamashita *et al.*, 1998, 2000a, 2000b; Itoi *et al.*, 2000; Pati and Singh, 2000).

DMRG in its finite-system version has also been very successful in the study of systems with impurities or randomness, in which the true ground state can be found

---

[1]Such studies include those of Bursill *et al.* (1995); Kolezhuk *et al.* (1996, 1997); Pati *et al.* (1996); White and Affleck (1996); Pati, Chitra, *et al.* (1997); Uhrig *et al.* (1999a, 1999b); Maeshima and Okunishi (2000); Itoi and Qin (2001); Kolezhuk and Schollwöck (2002).

with reasonable precision.[2] There has also been work on edges and impurities in Luttinger liquids (Qin *et al.*, 1996; Qin, Fabrizio, *et al.*, 1997; Bedürftig *et al.*, 1998; Schönhammer *et al.*, 2000).

The study of electronic models is somewhat more complicated because of the larger number of degrees of freedom and because of the fermionic sign. However, DMRG is free of the negative-sign problem of quantum Monte Carlo and hence the method of choice for one-dimensional electronic models. Hubbard chains[3] and Hubbard ladders[4] have been studied in the entire range of interactions as the precision of DMRG is found to depend only weakly on the interaction strength. The three-band Hubbard model has been considered by Jeckelmann *et al.* (1998) and Nishimoto, Jeckelmann, and Scalapino (2002). Similarly, authors have studied both the *t-J* model on chains (Chen and Moukouri, 1996; White and Scalapino, 1997b; Mutou *et al.*, 1998a; Doublet and Lepetit, 1999; Maurel *et al.*, 2001) and on ladders (Haywood *et al.*, 1995; White and Scalapino, 1997a, 1998c; Rommer *et al.*, 2000; Siller *et al.*, 2001, 2002).

The persistent current response to magnetic fluxes through rings has been studied by Byrnes *et al.* (2002) and Meden and Schollwöck (2003a); also it has been studied in view of possible quasiexact conductance calculations (Meden and Schollwöck, 2003b; Molina *et al.*, 2003).

Even before the advent of the Hubbard model, a very similar model, the Pariser-Parr-Pople model (Pariser and Parr, 1953; Pople, 1953), accommodating both dimerization effects and longer-range Coulomb interaction, had been invented in quantum chemistry to study conjugated polymer structures. DMRG has therefore been applied to polymers by many authors,[5] moving to more and more realistic models of molecules, such as polydiacaty-lene (Race *et al.* (2001, 2003), polyparaphenylene (Anusooya *et al.*, 1997; Barford *et al.*, 1998; Bursill and Barford, 2002), or polyenes (Bursill and Barford, 1999; Barford *et al.*, 2001; Zhang and George, 2001). Polymer phonons have also been considered in the nonadiabatic case (Barford, Bursill, and Lavrentiev, 2002). There is closely related work on the Peierls-Hubbard model (Pang and Liang, 1995; Jeckelmann, 1998; Otsuka, 1998; Anusooya *et al.*, 1999).

Since the early days of DMRG history (Yu and White, 1993) interest has also focused on the Kondo lattice, generic one-dimensional structures of itinerant electrons and localized magnetic moments, for both the one-channel[6] and two-channel cases (Moreno *et al.*, 2001). Anderson models have been studied by Guerrero and Yu (1995) and Guerrero and Noack (1996, 2001).

The bosonic version of the Hubbard model has been studied by Kühner and Monien (1998), Kühner *et al.* (2000), and Kollath *et al.* (2004), with emphasis on disorder effects by Rapsch *et al.* (1999). Sugihara (2004) has used DMRG to study a bosonic 1+1-dimensional field theory.

Going beyond one dimension, two-dimensional electron gases in a Landau level have been mapped to one-dimensional models suitable for DMRG (Shibata and Yoshioka, 2001, 2003; Bergholtz and Karlhede, 2003); DMRG was applied to molecular iron rings (Normand *et al.*, 2001) and has elucidated the lowest rotational band of the giant Keplerate molecule $Mo_{72}Fe_{30}$ (Exler and Schnack, 2003). More generic higher-dimensional applications will be discussed later.

Revisiting its origins, DMRG can also be used to provide high-accuracy solutions in one-particle quantum mechanics (Martín-Delgado *et al.*, 1999). As there is no entanglement in the one-particle wave function, the reduced basis transformation is formed from the M^S lowest-lying states of the superblock projected onto the system (after reorthonormalization). It has been applied to an asymptotically free model in two dimensions (Martín-Delgado and Sierra, 1999) and modified for up to three dimensions (Martín-Delgado *et al.*, 2001).

---

[2]Impurities have been studied by Schmitteckert and Eckern (1996), Wang and Mallwitz (1996), Martins *et al.* (1997), Mikeska *et al.* (1997), Zhang *et al.* (1997), Laukamp *et al.* (1998), Lou *et al.* (1998), Schmitteckert *et al.* (1998), Zhang, Igarashi, and Fulde (1998), Ng *et al.* (2000), whereas other authors have focused on random interactions or fields: Hida (1996, 1997a, 1997b, 1999a); Hikihara *et al.* (1999); Juozapavicius *et al.* (1999); Urba and Rosengren (2003).

[3]Studies include Sakamoto and Kubo (1996); Daul and Noack (1997, 1998, 2000); Lepetit and Pastor (1997); Zhang (1997); Aligia *et al.* (2000); Daul (2000); Daul and Scalapino (2000); Lepetit *et al.* (2000); Maurel and Lepetit (2000); Nishimoto *et al.* (2000); Aebischer *et al.* (2001); Jeckelmann (2002b).

[4]See, for example, Noack *et al.* (1994, 1995a, 1995b, 1997); Vojta *et al.* (1999, 2001); Bonca *et al.* (2000); Daul, Scalapino, and White (2000); Weihong *et al.* (2001); Hamacher *et al.* (2002); Marston *et al.* (2002); Scalapino *et al.* (2002); Schollwöck *et al.* (2003).

[5]These include Anusooya *et al.* (1997); Lepetit and Pastor (1997); Ramasesha *et al.* (1997, 2000); Shuai, Bredas, *et al.* (1997), Shuai, Pati, Bredas, *et al.* (1997); Shuai, Pati, Su, *et al.* (1997); Boman and Bursill (1998); Kuwabara *et al.* (1998); Shuai *et al.* (1998); Yaron *et al.* (1998); Bendazzoli *et al.* (1999); Barford and Bursill (2001); Barford, Bursill, and Smith (2002); Raghu *et al.* (2002).

III. DMRG THEORY

DMRG practitioners usually adopt a quite pragmatic approach when applying this tool to the study of some physical system. They consider the convergence of DMRG results upon tuning the standard DMRG control parameters, system size L, size of the reduced block Hilbert space M, and the number of finite-system sweeps, and judge DMRG results to be reliable or not. Beyond empiricism, in recent years a coherent theoreti-

---

[6]See the work of Carruzo and Yu (1996); Shibata, Nishino, *et al.* (1996), Shibata, Ueda, *et al.* (1996), Caprara and Rosengren (1997); Shibata, Sigrist, and Heeb (1997); Shibata, Tsvelik, and Ueda (1997); Shibata, Ueda, and Nishino (1997); Sikkema *et al.* (1997); Wang (1998); McCulloch *et al.* (1999); Watanabe *et al.* (1999); Garcia *et al.* (2000, 2002).

cal picture of the convergence properties and the algo-
rithmic nature of DMRG has emerged, and it is fair to
say that we now have good foundations of a DMRG
theory: DMRG generically produces a particular kind of
ansatz state, known in statistical physics as a matrix-
product state; if it well approximates the true state of the
system, DMRG will perform well. In fact, it turns out to
be rewarding to reformulate DMRG in terms of varia-
tional optimization within classes of matrix-product
states (Sec. III.A). In practice, DMRG performance is
best studied by considering the decay of the eigenvalue
spectrum of the reduced density matrix, which is fast for
one-dimensional gapped quantum systems, but generi-
cally slow for critical systems in one dimension and all
systems in higher dimensions (Sec. III.B). This renders
DMRG applications in such situations delicate at best.
A very coherent understanding of these properties is
now emerging in the framework of bipartite entangle-
ment measures in quantum information theory.

A. Matrix-product states

Like conventional RG methods, DMRG builds on
Hilbert-space decimation. There is, however, no Hamil-
tonian flow to some fixed point and no emergence of
relevant and irrelevant operators. Instead, there is a flow
to some fixed point in the space of the reduced density
matrices. As has been pointed out by various authors
(Östlund and Rommer, 1995; Martín-Delgado and Si-
erra, 1996; Rommer and Östlund, 1997; Dukelsky *et al.*,
1998; Takasaki *et al.*, 1999), this implies that DMRG
generates position-dependent matrix-product states
(Fannes *et al.*, 1989; Klümper *et al.*, 1993) as block states.
However, there are subtle but crucial differences be-
tween DMRG states and matrix-product states
(Takasaki *et al.*, 1999; Verstraete, Porras, and Cirac,
2004) that have important consequences regarding the
variational nature of DMRG.

1. Matrix-product states

These are simple generalizations of product states of
local states, which we take to be on a chain,

$$|\boldsymbol{\sigma}\rangle = |\sigma_1\rangle \otimes |\sigma_2\rangle \otimes \cdots \otimes |\sigma_L\rangle, \tag{43}$$

obtained by introducing linear operators $\hat{A}_i[\sigma_i]$ depend-
ing on the local state. These operators map from some
M-dimensional auxiliary state space spanned by an or-
thonormal basis $\{|\beta\rangle\}$ to another M-dimensional auxil-
iary state space spanned by $\{|\alpha\rangle\}$:

$$\hat{A}_i[\sigma_i] = \sum_{\alpha\beta} (A_i[\sigma_i])_{\alpha\beta} |\alpha\rangle\langle\beta|. \tag{44}$$

One may visualize the auxiliary state spaces to be lo-
cated on the bonds $(i, i+1)$ and $(i-1, i)$. The operators
are thus represented by $M \times M$ matrices $(A_i[\sigma_i])_{\alpha\beta}$; M
will be seen later to be the number of block states in
DMRG. We further demand for reasons explained be-
low that

$$\sum_{\sigma_i} \hat{A}_i[\sigma_i]\hat{A}_i^\dagger[\sigma_i] = \mathbb{I}. \tag{45}$$

A position-dependent unnormalized matrix-product
state for a one-dimensional system of size L is then
given by

$$|\psi\rangle = \sum_{\{\boldsymbol{\sigma}\}} \left(\langle\phi_L| \prod_{i=1}^{L} \hat{A}_i[\sigma_i] |\phi_R\rangle \right) |\boldsymbol{\sigma}\rangle, \tag{46}$$

in which $\langle\phi_L|$ and $|\phi_R\rangle$ are left and right boundary states
in the auxiliary state spaces located in the above visual-
ization to the left of the first and to the right of the last
site. They are used to obtain scalar coefficients. Position-
independent matrix-product states are obtained by mak-
ing Eq. (44) position independent, $\hat{A}_i[\sigma_i] \to \hat{A}[\sigma_i]$. For
simplicity, we shall consider only those in the following.
For periodic boundary conditions, boundary states are
replaced by tracing the matrix product:

$$|\psi\rangle = \sum_{\{\boldsymbol{\sigma}\}} \mathrm{Tr}\left[\prod_{i=1}^{L} \hat{A}_i[\sigma_i] \right] |\boldsymbol{\sigma}\rangle. \tag{47}$$

The best-known matrix-product state is the valence-
bond-solid ground state of the bilinear-biquadratic $S=1$
Affleck-Kennedy-Lieb-Tasaki Hamiltonian (Affleck *et
al.*, 1987, 1988), in which $M=2$.

2. Correlations in matrix-product states

Consider two local bosonic (for simplicity; see Ander-
sson *et al.*, 1999) operators $\hat{O}_j$ and $\hat{O}_{j+l}$, acting on sites j
and $j+l$, applied to the periodic boundary condition
matrix-product state of Eq. (47). The correlator $C(l)$
$= \langle\psi|\hat{O}_j\hat{O}_{j+l}|\psi\rangle / \langle\psi|\psi\rangle$ is then found, with $\mathrm{Tr}\, X\,\mathrm{Tr}\, Y$
$= \mathrm{Tr}(X \otimes Y)$ and $(ABC) \otimes (XYZ) = (A \otimes X)(B \otimes Y)(C \otimes Z)$, to be given by

$$C(l) = \frac{\mathrm{Tr}\, \bar{O}_j \bar{\mathbb{I}}^{l-1} \bar{O}_{j+l} \bar{\mathbb{I}}^{L-l-1}}{\mathrm{Tr}\, \bar{\mathbb{I}}^L}, \tag{48}$$

where we have used the following mapping (Rommer
and Östlund, 1997; Andersson *et al.*, 1999) from an op-
erator $\hat{O}$ acting on the local state space to an
M^2-dimensional operator $\bar{O}$ acting on products of auxil-
iary states $|\alpha\beta\rangle = |\alpha\rangle \otimes |\beta\rangle$:

$$\bar{O} = \sum_{\sigma\sigma'} \langle\sigma'|\hat{O}|\sigma\rangle \hat{A}^*[\sigma'] \otimes \hat{A}[\sigma]. \tag{49}$$

Note that $\hat{A}^*$ stands for $\hat{A}$ complex-conjugated only as
opposed to $\hat{A}^\dagger$. Evaluating Eq. (48) in the eigenbasis of
the mapped identity, $\bar{\mathbb{I}}$, we find that in the thermody-
namic limit $L \to \infty$

$$C(l) = \sum_{i=1}^{M^2} c_i \left(\frac{\lambda_i}{|\lambda_i|}\right)^l \exp(-l/\xi_i) \tag{50}$$

with $\xi_i = -1/\ln|\lambda_i|$. The λ_i are the eigenvalues of $\bar{\mathbb{I}}$, and the c_i depend on $\hat{O}$. This expression holds because, due to Eq. (45), $|\lambda_{i>1}| \leq 1$ and $\lambda_1 = 1$ for the eigenstate $\langle\alpha\beta|\lambda_1\rangle = \delta_{\alpha\beta}$. Equation (45) is thus seen to ensure normalizability of matrix-product states in the thermodynamic limit. Generally, all correlations in matrix-product states are either long ranged (if $c_i \neq 0$ for a $\lambda_i = 1$) or purely exponentially decaying. They are thus not suited for describing critical behavior in the thermodynamic limit. Even for gapped one-dimensional quantum systems their utility may seem limited, as the correlators $C(l)$ of these systems are generically of a two-dimensional classical Ornstein-Zernike form,

$$C(l) \sim \frac{e^{-l/\xi}}{\sqrt{l}}, \tag{51}$$

whereas exponential decay as in Eq. (50) is typical of one-dimensional classical Ornstein-Zernike forms. However, matrix-product states such as the Affleck-Kennedy-Lieb-Tasaki (AKLT) ground state arise as quantum disorder points in general Hamiltonian spaces as the quantum remnants of classical phase transitions in two-dimensional classical systems; these disorder points are characterized by dimensional reduction of their correlations and typically characterize the qualitative properties of subsets of the Hamiltonian space, which turns them into most useful toy models, as exemplified by the AKLT state (Schollwöck, Jolicœur, and Garel, 1996). Away from the disorder points, choosing increasingly large M as dimension of the ansatz matrices allows us to model the true correlation form as a superposition of exponentials for increasingly large l; even for power-law correlations, this modeling works for not too long distances.

3. DMRG and matrix-product states

To show that a DMRG calculation retaining M block states produces $M \times M$ matrix-product states, Östlund and Rommer (1995) considered the reduced basis transformation to obtain a block of size ℓ,

$$\langle m_{\ell-1}\sigma_\ell|m_\ell\rangle \equiv (A_\ell)_{m_\ell;m_{\ell-1}\sigma_\ell} \equiv (A_\ell[\sigma_\ell])_{m_\ell;m_{\ell-1}}, \tag{52}$$

such that

$$|m_\ell\rangle = \sum_{m_{\ell-1}\sigma_\ell} (A_\ell[\sigma_\ell])_{m_\ell;m_{\ell-1}}|m_{\ell-1}\rangle \otimes |\sigma_\ell\rangle. \tag{53}$$

The reduced-basis transformation matrices $A_\ell[\sigma_\ell]$ automatically obey Eq. (45), which here ensures that $\{|m_\ell\rangle\}$ is an orthonormal basis provided $\{|m_{\ell-1}\rangle\}$ is one as well. We may now use Eq. (53) for a backward recursion to express $|m_{\ell-1}\rangle$ via $|m_{\ell-2}\rangle$ and so forth. There is a (conceptually irrelevant) complication as the number of

block states for very short blocks is less than M. For simplicity, I assume that $N_{\text{site}}^{\tilde{N}} = M$ and stop the recursion at the shortest block of size $\tilde{N}$ that has M states, such that

$$|m_\ell\rangle = \sum_{m_{\tilde{N}}} \sum_{\sigma_{\tilde{N}+1},\ldots,\sigma_\ell} (A_\ell[\sigma_\ell]\cdots A_{\tilde{N}+1}[\sigma_{\tilde{N}+1}])_{m_\ell m_{\tilde{N}}}$$
$$\times |m_{\tilde{N}}\rangle \otimes |\sigma_{\tilde{N}+1}\cdots\sigma_\ell\rangle, \tag{54}$$

where we have boundary-site states $|m_{\tilde{N}}\rangle \equiv |\sigma_1\cdots\sigma_{\tilde{N}}\rangle$; hence

$$|m_\ell\rangle = \sum_{\sigma_1,\ldots,\sigma_\ell} (A_\ell[\sigma_\ell]\cdots A_{\tilde{N}+1}[\sigma_{\tilde{N}+1}])_{m_\ell,(\sigma_1\cdots\sigma_{\tilde{N}})}$$
$$\times |\sigma_1\cdots\sigma_\ell\rangle. \tag{55}$$

A comparison to Eq. (46) shows that DMRG generates position-dependent $M \times M$ matrix-product states as block states for a reduced Hilbert space of M states; the auxiliary state space to a local state space is given by the Hilbert space of the block to which the local site is the latest attachment. Combining Eqs. (4) and (55), we find that the superblock ground state of the full chain is the variational optimum in a space spanned by products of two local states and two matrix-product states,

$$|\psi\rangle = \sum_{m^S m^E} \sum_{\{\boldsymbol{\sigma}\}} \psi_{m^S\sigma_{L/2}\sigma_{L/2+1}m^E}$$
$$\times (A_{L/2-1}[\sigma_{L/2-1}]\cdots A_{\tilde{N}+1}[\sigma_{\tilde{N}+1}])_{m^S,(\sigma_1\cdots\sigma_{\tilde{N}})}$$
$$\times (A_{L/2+2}[\sigma_{L/2+2}]\cdots A_{L-\tilde{N}}[\sigma_{L-\tilde{N}}])_{m^E,(\sigma_{L+1-\tilde{N}}\cdots\sigma_L)}$$
$$\times |\sigma_1\cdots\sigma_L\rangle, \tag{56}$$

which I have written for the case of the two single sites at the chain center; an analogous form holds for all stages of the finite-system algorithm.

For gapped quantum systems we may assume that for blocks of length $\ell \gg \xi$ the reduced basis transformation becomes site independent, such that the ansatz matrix A generated by DMRG is essentially position independent in the bulk. At criticality, the finite-dimensional matrix-product state generated introduces some effective correlation length (growing with M). In fact, this has been verified numerically for free fermions at criticality, where the ansatz matrices for bulk sites converged exponentially fast to a position-independent ansatz matrix, but where this convergence slowed down with M (Andersson *et al.*, 1999).

The effect of the finite-system algorithm can be seen from Eq. (56) to be a sequence of local optimization steps of the wave function that have two effects: on the one hand, the variational coefficients $\psi_{m^S\sigma_S\sigma_E m^E}$ are optimized, and on the other, a new, improved ansatz matrix is obtained for the growing block, using the improved variational coefficients for a new reduced basis transformation.

In practical applications one observes that, even for translationally invariant systems with periodic boundary conditions and repeated applications of finite-system

sweeps, the position dependency of the matrix-product state does not go away completely as it strictly should, indicating room for further improvement. Dukelsky *et al.* (1998) and Takasaki *et al.* (1999) have pointed out and numerically demonstrated that finite-system DMRG (and TMRG; see Sec. VIII) results can be improved and better matrix-product states for translationally invariant Hamiltonians can be produced by switching, after convergence is reached, from the S••E scheme for the finite-system algorithm to an S•E scheme and carrying out some more sweeps. The rationale is that the variational ansatz of Eq. (56) generates (after the Schmidt decomposition and before truncation) ansatz matrices of dimension MN_{site} at the two local sites due to Eq. (20), whereas they are of dimension M at all other sites; this introduces a notable position dependence, deteriorating the overall wave function. In the new scheme, the new ansatz matrix, without truncation, also has dimension M [the dimension of the environment in Eq. (20)], so that the local state is not favored. The variational state now approaches its global optimum without further truncation, just improvements of the ansatz matrices.

The observation that DMRG produces variational states formed from products of local ansatz matrices has inspired the construction of variational ansatz states for the ground state of Hamiltonians (the recurrent variational approach; see Martín-Delgado and Sierra in Peschel, Hallberg, *et al.*, 1999) and the dominant eigenstate of transfer matrices (the tensor-product variational approach; Nishino *et al.*, 2000, 2001; Maeshima *et al.*, 2001; Gendiar and Nishino, 2002; Gendiar *et al.*, 2003).

Closer in spirit to the original DMRG concept is the *product wave-function renormalization group* (Nishino and Okunishi, 1995; Hieida *et al.*, 1997). This has been applied successfully to the magnetization process of spin chains in an external field where infinite-system DMRG is highly prone to metastable trapping (Sato and Akutsu, 1996; Hieida *et al.*, 1997, 2001; Okunishi *et al.*, 1999a) and to the restricted solid-on-solid model (Akutsu and Akutsu, 1998; Akutsu *et al.*, 2001a, 2001b). While in DMRG the focus is to determine for each iteration (superblock size) the wave function numerically as precisely as possible in order to derive the reduced basis transformation, the product wave-function renormalization group operates directly on the A matrices itself: at each iteration, one starts with an approximation to the wave function and local ansatz matrices related to it by a Schmidt decomposition. The wave function is then somewhat improved, by carrying out a few Lanczos steps at moderate effort, and again Schmidt decomposed. The transformation matrices thus obtained are used to transform (improve) the local ansatz matrices, which in turn are combined with the decomposition weights to define a wave function for the next larger superblock. The final result is reached when both the ansatz and transformation matrices become identical, as they should at the DMRG fixed point for reduced basis transformations.

4. Variational optimization in matrix-product states

If we compare Eq. (46) to Eq. (56), we see that the DMRG state differs from a true matrix-product state in its description of $|\psi\rangle$: The A matrices link auxiliary state spaces of a bond on the right of a site to those on the left for sites in the left block, but vice versa in the right block. This may be mended by a transposition. This done, one may write the prefactors of $|\sigma_1\cdots\sigma_L\rangle$ as a true product of matrices by rewriting $\psi_{mS_{\sigma_{L/2}}\sigma_{L/2+1}mE}$ as an $M\times M$ matrix $(\Psi[\sigma_{L/2}\sigma_{L/2+1}])_{mS;mE}$. The remaining anomaly is, as pointed out above, that the formal translational invariance of this state is broken by the indexing of Ψ by two sites, suggesting the modification of the S••E scheme for the finite-system algorithm to an S•E scheme as discussed above. However, as Verstraete, Porras, and Cirac (2004) have demonstrated, it is conceptually and algorithmically worthwhile to rephrase DMRG consistently in terms of matrix-product states right from the beginning, thereby also abandoning the block concept.

To this end, they introduce (with the exception of the first and last sites; see Fig. 6) two auxiliary state spaces of dimension M, a_ℓ to the left and b_ℓ to the right of site ℓ, such that on bond ℓ one has auxiliary state spaces b_ℓ and $a_{\ell+1}$. They now consider maps from $a_\ell\otimes b_\ell\rightarrow\mathcal{H}_\ell$ from the product of two auxiliary state spaces to the local state space, which can be written using matrices $(A_\ell[\sigma])_{\alpha\beta}$: $A_\ell=\Sigma_{\sigma_\ell}\Sigma_{\alpha_\ell\beta_\ell}(A_\ell[\sigma])_{\alpha\beta}|\sigma_\ell\rangle\langle\alpha_\ell\beta_\ell|$. The $|\alpha\rangle$ and $|\beta\rangle$ are states of the auxiliary state spaces. On the first and last site, the corresponding schemes map only from one auxiliary state space. These maps can now be used to generate a matrix-product state. To this purpose, Verstraete, Porras, and Cirac (2004) apply the string of maps $A_1\otimes A_2\otimes\cdots\otimes A_L$ to the product of maximally entangled states $|\phi_1\rangle|\phi_2\rangle\cdots|\phi_{L-1}\rangle$, in which $|\phi_i\rangle=\Sigma_{\beta_i=\alpha_{i+1}}|\beta_i\rangle|\alpha_{i+1}\rangle$. The maximal entanglement, in the language of matrix-product states, ensures that the prefactors of $|\sigma_1\cdots\sigma_L\rangle$ are given by products of $A[\sigma]$ matrices, hence this construction is a matrix-product state. Comparing this state to the representation of $|\psi\rangle$ in Eq. (56), one finds that the maps A are identical to the (possibly transposed) basis transformation matrices $A[\sigma]$, with the exception of the position of the single sites: in the S••E setup (bottom half of Fig. 6), there are no auxiliary state spaces between the two single sites, and one map corresponds to $\Psi[\sigma_\ell\sigma_{\ell+1}]$. In the S•E setup (top half of Fig. 6), this anomaly disappears and correctly normalized $A[\sigma_\ell]$ can be formed from $\Psi[\sigma_\ell]$.

The (finite-system) DMRG algorithm for the S•E setup can now be reformulated in this picture as follows: sweeping forward and backward through the chain, one keeps for site ℓ all A at other sites fixed and seeks the Ψ_ℓ that minimizes the total energy. From this, one determines A_ℓ and moves to the next site, seeking $\psi_{\ell+1}$, and so on, until all matrices have converged. In the final matrix-product state one evaluates correlators as in Eq. (48). It is important to note that in this setup there is no truncation error, as explained above in the language of

Schmidt decomposition. Shifting the active site therefore does not change the energy, and the next minimization can only decrease the energy (or keep it constant). This setup is therefore truly variational in the space of the states generated by the maps A and reaches a minimum of energy within that space (there is of course no guarantee of reaching the global minimum). By comparison, the setup S••E leads to a reduced basis transformation and always excludes two different auxiliary state spaces from the minimization procedure. It is hence not strictly variational.

In this setup the generalization to periodic boundary conditions is now easy. Additional auxiliary state spaces a_1 and b_L are introduced and maximally entangled as for all other bonds. There is now complete formal translational invariance of the ansatz (see Fig. 7). On this setup, one optimizes maps (matrices) A one by one, going forward and backward.

Verstraete, Porras, and Cirac (2004) have shown that, for a given M, they obtain roughly the same precision for periodic boundary conditions as for open boundary conditions. This compares extremely favorably with standard DMRG for periodic boundary conditions where (in the worst case) up to M^2 states are needed for the same precision.

B. Properties of DMRG density matrices

In order to gain a theoretical understanding of DMRG performance, we now take a look at the properties of the reduced density matrices and their truncation. Obviously, the ordered eigenvalue spectrum w_α of the reduced density matrix $\hat{\rho}$ should decay as quickly as possible to minimize the truncated weight $\epsilon_\rho = 1 - \Sigma_{\alpha=1}^{M} w_\alpha$ for optimal DMRG performance. This intuitively clear statement can be quantified: there are four major classes of density-matrix spectra, in descending order of DMRG performance.

(i)   Density-matrix spectra for $M \times M$ matrix-product states as exact eigenstates of quantum systems, with a finite fixed number of nonvanishing eigenvalues, leading to optimal DMRG performance.

(ii) Density-matrix spectra for non-matrix-product states of one-dimensional quantum systems with exponentially decaying correlations, and with leading exponential decay of w_α; spectra remaining essentially unchanged for system sizes in excess of the correlation length.

(iii) Density-matrix spectra for states of one-dimensional quantum systems at criticality, with a decay of w_α that slows down with increasing system size, leading to DMRG failure to obtain thermodynamic limit behavior.

(iv) Density-matrix spectra for states of two-dimensional quantum systems both at and away from criticality, in which the number of eigenvalues to be retained to keep a fixed truncation error

grows exponentially with system size, restricting DMRG to very small system sizes.

All scenarios translate to classical systems of one additional dimension, due to the standard quantum-classical mapping from d- to $(d+1)$-dimensional systems.

1. DMRG applied to matrix-product states

A state $|\tilde{\psi}\rangle$ of the matrix-product form of Eq. (46) with dimension $\tilde{M}$ can be written as

$$|\tilde{\psi}\rangle = \sum_{\alpha=1}^{\tilde{M}} |\tilde{\psi}_\alpha^S\rangle|\tilde{\psi}_\alpha^E\rangle \rightarrow |\psi\rangle = \sum_{\alpha=1}^{\tilde{M}} \sqrt{w_\alpha}|\psi_\alpha^S\rangle|\psi_\alpha^E\rangle, \qquad (57)$$

where we have arbitrarily cut the chain into (left) system and (right) environment with

$$|\tilde{\psi}_\alpha^S\rangle = \sum_{\{\boldsymbol{\sigma}^S\}} \langle\phi_S|\prod_{i\in S} A[\sigma_i]|\alpha\rangle|\boldsymbol{\sigma}^S\rangle, \qquad (58)$$

and similarly $|\tilde{\psi}_\alpha^E\rangle$; $|\psi\rangle$, $|\psi_\alpha^S\rangle$, and $|\psi_\alpha^E\rangle$ are the corresponding normalized states. An appropriate treatment of boundary sites is tacitly implied [cf. the discussion before Eq. (55)]. Then the density matrix $\hat{\rho}_S = \Sigma_{\alpha=1}^{\tilde{M}} w_\alpha |\psi_\alpha^S\rangle\langle\psi_\alpha^S|$ and has a finite spectrum of $\tilde{M}$ nonvanishing eigenvalues. The truncated weight will thus be zero if we choose $M > \tilde{M}$ for DMRG, as DMRG generates these states [see Eq. (55)].

In such cases, DMRG may be expected to become an exact method up to small numerical inaccuracies. This has been observed recurrently; Kaulke and Peschel (in Peschel, Hallberg, *et al.*, 1999) provide an excellent example, the non-Hermitian q-symmetric Heisenberg model with an additional boundary term. This Hamiltonian is known to have matrix-product ground states of varying complexity (i.e., matrix sizes $\tilde{M}$) for particular choices of parameters (see also Alcaraz *et al.*, 1994). Monitoring the eigenvalue spectrum of the DMRG density matrix for a sufficiently long system, Kaulke and Peschel found that indeed it collapses at these particular values: all eigenvalues but the $\tilde{M}$ largest vanish at these points (Fig. 8). Similarly, a class of two-dimensional quantum Hamiltonians with exact matrix-product ground states has been studied using DMRG by Hieida *et al.* (1999).

2. DMRG applied to generic gapped one-dimensional systems

It is quite easy to observe numerically that for gapped one-dimensional quantum systems the eigenvalue spectrum of the density matrices decays essentially exponentially such that the truncated weight can be reduced exponentially fast by increasing M, which is the hallmark of DMRG success. Moreover, the eigenvalue spectrum converges to some thermodynamic-limit form.

Peschel, Kaulke, and Legeza (1999) have confirmed these numerical observations by studying exact density-matrix spectra that may be calculated for the one-
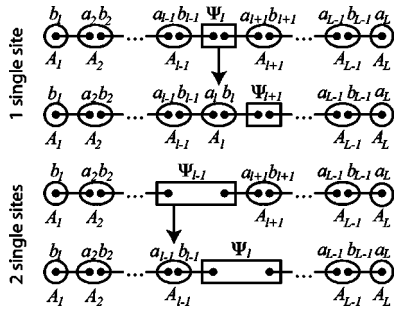
FIG. 6. Pictorial representation of S•E (above) and S••E (below) DMRG schemes for open boundary conditions as introduced by Verstraete, Porras, and Cirac, 2004. Paired dots represent auxiliary state spaces linked to a local state space. Straight lines symbolize maximal entanglement, ellipses and rectangles map to local state spaces as detailed in the text. Note the special role of the boundary sites. Adapted from Verstraete, Porras, and Cirac, 2004.

dimensional Ising model in a transverse field and the *XXZ* Heisenberg chain in its antiferromagnetic gapped regime, using a corner transfer-matrix method (Baxter, 1982).

In those cases, the eigenvalues of $\hat{\rho}$ are given, up to a global normalization, as

$$w \propto \exp\left(-\sum_{j=0}^{\infty} \epsilon_j n_j\right) \tag{59}$$

with fermionic occupation numbers $n_j = 0,1$ and an essentially linear energy spectrum ϵ_j: these are typically some integer multiple of a fundamental scale ϵ. The density-matrix eigenvalue spectrum shows clear exponential decay only for large eigenvalues due to the increasing degree of degeneracy of the eigenvalue spectrum, as the number of possible partitions of ϵn into $\epsilon_j n_j$ grows. DMRG density matrices perfectly reproduce this behavior (Fig. 9). Combining such exactly known corner transfer-matrix spectra with results from the theory of partitions, Okunishi *et al.* (1999b) derived the asymptotic form

$$w_\alpha \sim \exp(-\text{const} \times \ln^2 \alpha) \tag{60}$$

for the αth eigenvalue (see also Chan *et al.*, 2002).

These observations imply that for a desired truncated weight the number of states to be kept remains finite even in the thermodynamic limit and that the truncated weight decays exponentially fast in M, with some price to be paid due to the increasing degree of degeneracy occurring for large M.

3. DMRG applied to one-dimensional systems at criticality

Numerically, one observes at criticality that the eigenvalue spectrum decays dramatically slower and that for increasing system size this phenomenon tends to aggravate (Chung and Peschel, 2001), with errors in, e.g.,

ground-state energies increasing by several orders of magnitude compared to gapped systems (Legeza and Fáth, 1996).

Hence the double question arises of the decay of the eigenvalue spectrum for the density matrix of a given system size and the size dependency of this result. Chung and Peschel (2001) have shown for generic Hamiltonians quadratic in fermionic operators that the density-matrix spectrum is once again of the form of Eq. (59), but the energies ϵ_j are now no longer given by a simple relationship linear in j. Instead, they show much slower, curved growth, that slows down with system size. Translating this into actual eigenvalues of the density matrix, they show less than exponential decay, slowing down with system size. This implies that for one-dimensional quantum systems at criticality numerical convergence for a fixed system size will no longer be exponentially fast in M. Maintaining a desired truncated weight in the thermodynamic limit implies a diverging number M of states to be kept.

4. DMRG in two-dimensional quantum systems

Due to the large interest in two-dimensional quantum systems, we now turn to the question of DMRG convergence in gapped and critical systems. In the early days of DMRG, Liang and Pang (1994) observed numerically that to maintain a given precision, an exponentially growing number of states $M \sim \alpha^L$, $\alpha > 1$, had to be kept for system sizes $L \times L$. However, reliable information from numerics is very difficult to obtain here, due to the very small system sizes in actual calculations. Chung and Peschel (2000) have studied a (gapped) system of interacting harmonic oscillators, in which the density matrix can be written as the bosonic equivalent of Eq. (59), with eigenvalues, again up to a normalization,

$$w \propto \exp\left(-\sum_{j=0}^{\infty} \epsilon_j b_j^\dagger b_j\right). \tag{61}$$

Considering strip systems of size $L \times N$ with $N \leqslant L$, numerical evaluations have shown that

$$\epsilon_j \sim \text{const} \times j/N, \tag{62}$$

hence the eigenvalue decay slows down exponentially with inverse system size. This $1/N$ behavior can be understood by considering the spectrum of N chains without interchain interaction, which is given by the spectrum of the single chain with N-fold degeneracy introduced. Interaction will lift this degeneracy, but will not fundamentally change the slowdown this imposes on the decay of the density-matrix spectrum [see also du Croo de Jongh and van Leeuwen (1998) for the generic argument]. Taking bosonic combinatorics into account, one finds

$$w_\alpha \sim \exp[-(\text{const}/N)\ln^2 \alpha], \tag{63}$$

which is a consistent extension of Eq. (60). For a system of size 10×10, typical truncation errors of 10^{-5} for $M = 100$, 10^{-7} for $M = 500$, and 10^{-8} for $M = 1000$ have been
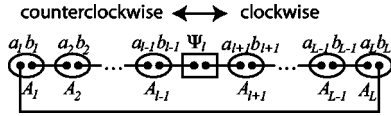
FIG. 7. Periodic boundary condition setup used in the algorithm of Verstraete, Porras, and Cirac (2004). Labeling as in previous figure. Adapted from Verstraete, Porras, and Cirac, 2004.

reported (see Fig. 10), reflecting the very slow convergence of DMRG in this case.

For a critical system, the noninteracting fermion model may be used once again as a model system (Chung and Peschel, 2001). For $M=2000$ states, for this simple model, the resulting truncation error is 5×10^{-2} for systems of size 12×12, 5×10^{-1} for 16×16, and 10^{-1} for size 20×20. Here, DMRG is clearly at its limits.

5. DMRG precision for periodic boundary conditions

While for periodic boundary conditions the overall properties of DMRG density matrices are the same as those of their open-boundary-condition counterparts, their spectra have been observed numerically to decay much more slowly. Away from criticality, this is due to some (usually only approximate) additional factor-of-2 degeneracy of the eigenvalues. This can be explained by studying the amplitudes of density-matrix eigenstates. Chung and Peschel (2000) have demonstrated in their noncritical harmonic-oscillator model that the density-matrix eigenstates associated with high eigenvalue weight are strongly located close to the boundary between system and environment (Fig. 11). Hence, in a periodic system, in which there are two boundary points, there are for the high-weight eigenvalues two essentially identical sets of eigenstates localized at the left and right boundary, respectively, leading to the approximate double degeneracy of high-weight eigenvalues. At criticality, no such simple argument holds, but DMRG is similarly affected by a slower decay of spectra.

In a recent study, Verstraete, Porras, and Cirac (2004) have shown that this strong deterioration of DMRG is essentially due to its particular setup for simulating periodic boundary conditions, and have provided a new formulation of the algorithm which produces results of the same quality as for open boundary conditions for the same number of states kept, at the cost of losing matrix sparseness (see Sec. III.A).

C. DMRG and quantum information theory—A new perspective

As understood in the early phases of DMRG development (White, 1992; White and Noack, 1992), the reason for the success of the method is that no system is considered in isolation, but embedded in a larger entity. In fact, as discussed in Sec. II.B, DMRG truncation can be understood in the language of quantum information
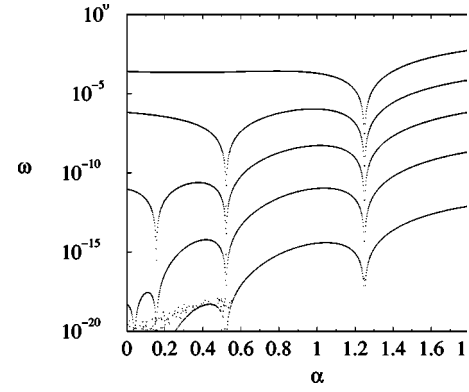

FIG. 8. Largest density-matrix eigenvalues vs a tuning parameter α in a $q=1/4$-symmetric Heisenberg chain. Largest eigenvalue ≈ 1 invisible on logarithmic scale; eigenvalue collapse indicates pure matrix-product states of small finite dimension. From Kaulke and Peschel in Peschel, Hallberg, et al., 1999. Reprinted with permission.

theory as preserving the maximum entanglement between system and environment as measured by the von Neumann entropy of entanglement,

$$S = - \text{Tr } \hat{\rho} \ln_2 \hat{\rho} = - \sum_\alpha w_\alpha \ln_2 w_\alpha, \quad (64)$$

in an M-dimensional block state space.

Latorre et al. (2004) have calculated the entropy of entanglement S_L for systems of length L embedded in infinite (an)isotropic XY chains and for systems embedded in finite, periodic Heisenberg chains of length N, both with and without external field. Both models show critical and noncritical behavior depending on anisotropy and field strength. In the limit $N \to \infty$, $S_L \leq L$, which is obtained by observing that entropy is maximal if all 2^L states are equally occupied with amplitude 2^{-L}. They find that $S_L \to \infty$ for $L \to \infty$ at criticality, but saturates as $S_L \to S_L^*$ for $L \approx \xi$ in the noncritical regime. At criticality, however, S_L grows far less than permitted by $S_L \leq L$, but obeys logarithmic behavior,

$$S_L = k \log_2 L + \text{const.} \quad (65)$$

The constant k is found to be given by $k=1/6$ for the anisotropic XY model at the critical field $H_c=1$ and by $k=1/3$ for the isotropic XY model at $H_c=1$ as well as the isotropic Heisenberg model for $H \leq H_c=1$ (for an isotropic XY model in field $H < H_c$, see Fig. 12). Away from criticality, the saturation value S_L^* decreases with decreasing correlation length ξ (Fig. 13).

One-dimensional quantum spin chains at criticality are described by conformally invariant $(1+1)$-dimensional field theories. In fact, Eq. (65) can be linked (Gaite, 2003; Latorre et al., 2004) to the geometric entropy (Callan and Wilczek, 1994) of such field theories,
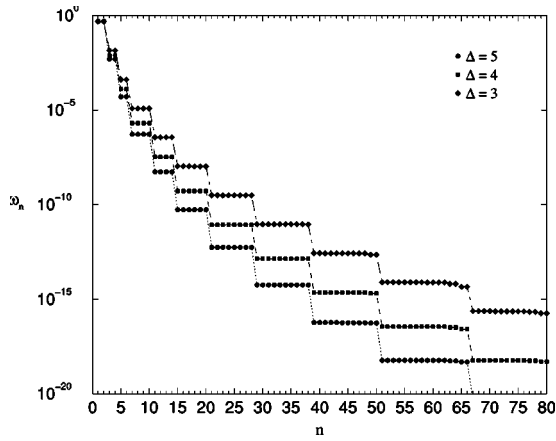
FIG. 9. Density-matrix eigenvalues w_n vs eigenvalue number n for a gapped XXY Heisenberg chain of $L=98$ and three values of anisotropy $\Delta > \Delta_c=1$. Degeneracies are as predicted analytically. From Peschel, Kaulke, and Legeza, 1999. Reprinted with permission.

$$S_L^{\text{geo}} = \frac{c + \bar{c}}{6} \log_2 L, \qquad (66)$$

where c ($\bar{c}$) are the central charges, if one observes that for the anisotropic XY model $c=\bar{c}=1/2$ and for the Heisenberg model and isotropic XY model $c=\bar{c}=1$.

Geometric entropy arguments for $(d+1)$-dimensional field theories use a bipartition of d-dimensional space by a $(d-1)$-dimensional hypersurface, which is shared by system S and environment E. By the Schmidt decomposition, S and E share the same reduced density-matrix spectrum, hence entanglement entropy, which is now argued to reside essentially on the shared hypersurface (cf. the locus of highest-weight density-matrix eigenstates in Fig. 11; see also Gaite, 2001). Taking the thermodynamic (infrared) limit, we find that entropy scales as the hypersurface area,

$$S_L \propto \left(\frac{L}{\lambda} \right)^{d-1}, \qquad (67)$$

where λ is some ultraviolet cutoff which in condensed-matter physics we may fix at some lattice spacing. Introducing a gap (mass), an essentially infrared property, into this field theory does not modify this behavior generated on ultraviolet scales on the hypersurface. In $d=1$, a more careful argument shows that there is a (subleading) logarithmic correction as given above at criticality or a correction saturating at some L away from criticality.

S_L is the number of qubits corresponding to the entanglement information. To code this information in DMRG, one needs a system Hilbert space of size $M \geq 2^{S_L}$; in fact, numerical results indicate that M and 2^{S_L} are—to a good approximation—proportional. Taking the linear dimensions of total space and embedded system to $N, L \to \infty$, quantum information theory hence provides us with a unified picture of DMRG perfor-

mance, which is in perfect agreement with the observations obtained by studying density-matrix spectra:

(i) In one-dimensional quantum systems away from criticality, DMRG yields very precise results for the thermodynamic limit for some finite number of states kept, $M \sim 2^{S_L^*}$, which grows with the correlation length.

(ii) In one-dimensional quantum systems at criticality, the number of states that has to be kept will diverge as

$$M(L) \sim L^k, \qquad (68)$$

with k from Eq. (65). This explains the failure of DMRG for critical one-dimensional systems as $L \to \infty$. As k is small, this statement has to be qualified; DMRG still works for rather large finite systems.

(iii) In higher-dimensional quantum systems, the number of states to be kept will diverge as

$$M(L) \sim 2^{L^{d-1}}, \qquad (69)$$

rendering the understanding of thermodynamic-limit behavior by conventional DMRG quite impossible; information is beyond retrieval just as in a black hole—whose entropy scales with its surface, as the entanglement entropy would in a three-dimensional DMRG application. In any case, even for higher-dimensional systems, DMRG may be a very useful method as long as system size is kept resolutely finite, as it is in nuclear physics or quantum chemistry applications. Recent proposals (Verstraete and Cirac, 2004) also show that it is possible to formulate generalized DMRG ansatz states in such a way that entropy shows correct size dependency in two-dimensional systems (see Sec. VI).

Legeza *et al.* (2003a) have carried the analysis of DMRG state selection using entanglement entropy even further, arguing that the acceptable truncated weight—not identical to, but closely related to the entropy of entanglement, which emerges as the key quantity—should be kept fixed during DMRG runs, determining how many states M have to be retained at each iteration. This dynamical block state selection has already been applied in various contexts (Legeza and Sólyom, 2003; Legeza *et al.*, 2003b). More recently, Legeza and Sólyom (2004) have tightened the relationship between quantum information theory and DMRG state selection by proposing a further refinement of state selection. M is now chosen variably to keep loss of quantum information below some acceptable threshold. They argue that this loss is given as

$$\chi(\mathcal{E}) \equiv S(\hat{\rho}) - p_{typ} S(\hat{\rho}_{typ}) - (1 - p_{typ}) S(\hat{\rho}_{atyp}). \qquad (70)$$

Here, $\hat{\rho} = p_{typ} \hat{\rho}_{typ} + (1 - p_{typ}) \hat{\rho}_{atyp}$. For a given M, $\hat{\rho}_{typ}$ is formed from the M dominant eigenstates of $\hat{\rho}$, $\hat{\rho}_{atyp}$ from the remaining ones, with $1 - p_{typ}$ being the trun-
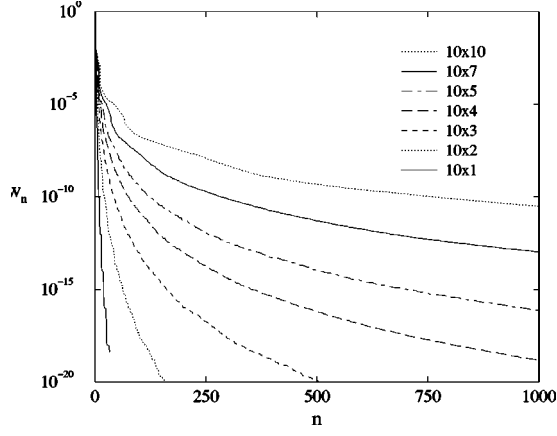
FIG. 10. Density-matrix eigenvalues w_n for rectangular two-dimensional gapped systems of interacting harmonic oscillators. The leftmost curve corresponds to the one-dimensional case. From Chung and Peschel, 2000. Reprinted with permission.

cated weight and $\hat{\rho}_{typ,atyp}$ scaled to have trace one. Legeza and Sólyom (2004) report a very clear linear relationship between DMRG errors and $\chi(\mathcal{E})$.

IV. ZERO-TEMPERATURE DYNAMICS

As we have seen, DMRG is an excellent method for calculating ground states and selected excited eigenstates at almost machine precision. On the other hand, the targeting of specific states suggests that DMRG is not suitable for calculating dynamical properties of strongly correlated systems even at $T=0$, as the time evolution of general excited states will explore large parts of the Hilbert space. Closer inspection has revealed, however, that the relevant parts of Hilbert space can be properly addressed by DMRG. For some operator $\hat{A}$, one may define a (time-dependent) Green's function at $T=0$ in the Heisenberg picture by

$$iG_A(t'-t) = \langle 0|\hat{A}^{\dagger}(t')\hat{A}(t)|0\rangle \tag{71}$$

with $t' \geq t$ for a time-independent Hamiltonian $\hat{H}$. Going to frequency range, the Green's function reads

$$G_A(\omega+i\eta) = \langle 0|\hat{A}^{\dagger}\frac{1}{E_0+\omega+i\eta-\hat{H}}\hat{A}|0\rangle, \tag{72}$$

where η is some positive number to be taken to zero at the end. We may also use the spectral or Lehmann representation of correlations in the eigenbasis of $\hat{H}$,

$$C_A(\omega) = \sum_n |\langle n|\hat{A}|0\rangle|^2 \delta(\omega+E_0-E_n). \tag{73}$$

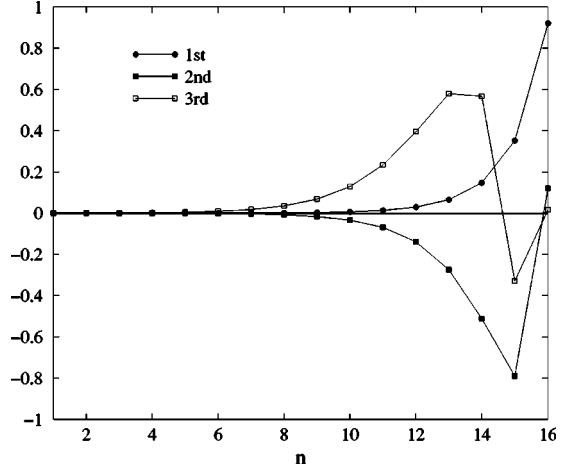This frequency-dependent correlation function is related to $G_A(\omega+i\eta)$ as

FIG. 11. Amplitudes of highest-weight single-particle eigenstates of the left-block density matrix for a one-dimensional open chain of $L=32$ interacting harmonic oscillators. From Chung and Peschel, 2000. Reprinted with permission.

$$C_A(\omega) = \lim_{\eta \to 0^+} -\frac{1}{\pi}\text{Im}\, G_A(\omega+i\eta). \tag{74}$$

In the following, I shall also use $G_A(\omega)$ and $C_A(\omega+i\eta)$ where the limit $\eta \to 0^+$ will be assumed to have been taken in the former and omitted in the latter case. The role of η in DMRG calculations is threefold: First, it ensures causality in Eq. (72). Second, it introduces a finite lifetime $\tau \propto 1/\eta$ to excitations, such that on finite systems they can be prevented from traveling to the open boundaries where their reflection would induce spurious effects. Third, η provides a Lorentzian broadening of $C_A(\omega)$,

$$C_A(\omega+i\eta) = \frac{1}{\pi}\int d\omega' C_A(\omega')\frac{\eta}{(\omega-\omega')^2+\eta^2}, \tag{75}$$

which serves either to broaden the numerically obtained discrete spectrum of finite systems into some thermodynamic-limit behavior or to broaden analytical results for C_A for comparison to numerical spectra in which $\eta>0$.

Most DMRG approaches to dynamical correlations center on the evaluation of Eq. (72). The first, which I refer to as Lanczos vector dynamics, was pioneered by Hallberg (1995) and calculates highly time-efficient, but comparatively rough approximations to dynamical quantities, adopting the Balseiro-Gagliano method to DMRG. The second approach, which is referred to as the correction vector method (Ramasesha *et al.*, 1997; Kühner and White, 1999), is yet another, older scheme adapted to DMRG, one much more precise, but numerically much more expensive. A third approach, called dynamical DMRG, has been proposed by Jeckelmann (2002a); while on the surface it is only a minor reformulation of the correction vector method, it will be seen to be much more precise.

Very recently, dynamical correlations as in Eq. (71) have also been calculated directly in real time using
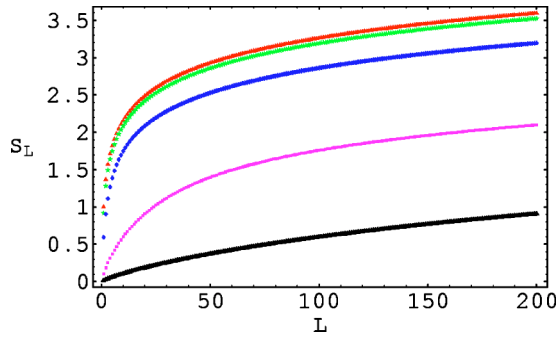
FIG. 12. (Color in online edition) Diverging von Neumann entropy S_L vs block length L for a critical isotropic XY chain in external fields $H < H_c$. Increasing field strengths suppress entropy. From Latorre *et al.*, 2004. Reprinted with permission.

time-dependent DMRG with adaptive Hilbert spaces (Vidal, 2003, 2004; Daley *et al.*, 2004; White and Feiguin, 2004), as will be discussed in Sec. IX.C. These may then be Fourier transformed to a frequency representation. As time-dependent DMRG is best suited for short times (i.e., high frequencies), and the methods discussed in this section are typically best for low frequencies, this alternative approach may be very attractive to cover wider frequency ranges.

All approaches share the need for precision control and the elimination of finite-system and/or boundary effects. Beyond DMRG-specific checks of convergence, precision may be checked by comparisons to independently obtained equal-time correlations using the following sum rules:

$$\int_{-\infty}^{\infty} d\omega\, C_A(\omega) = \langle 0|\hat{A}^\dagger \hat{A}|0\rangle, \tag{76}$$

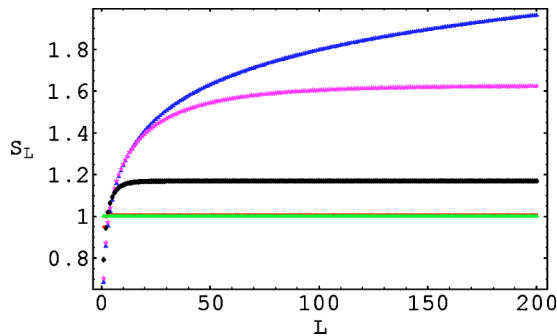$$\int_{-\infty}^{\infty} d\omega\, \omega C_A(\omega) = \langle 0|\hat{A}^\dagger[\hat{H},\hat{A}]|0\rangle, \tag{77}$$

FIG. 13. (Color in online edition) Saturating density-matrix entropy S_L vs block length L for an Ising chain in a transverse field $H \leqslant H_c$. Saturation entropy grows with $H \to H_c$; divergence is recovered at criticality (top curve). From Latorre *et al.*, 2004. Reprinted with permission.

$$\int_{-\infty}^{\infty} d\omega\, \omega^2 C_A(\omega) = \langle 0|[\hat{A}^\dagger,\hat{H}][\hat{H},\hat{A}]|0\rangle, \tag{78}$$

where the first equation holds for $\eta \geqslant 0$ and the latter two only as $\eta \to 0$. As DMRG is much more precise for equal-time than dynamical correlations, comparisons are made to DMRG results which for the purpose may be considered exact. Finite-size effects due to boundary conditions can be treated in various ways. They can be excluded completely by the use of periodic boundary conditions at the price of much lower DMRG precision (Hallberg, 1995). In cases where open boundary conditions are preferred, two situations should be distinguished. If $\hat{A}$ acts locally, such as in the calculation of an optical conductivity, one may exploit the fact that finite η exponentially suppresses excitations (Jeckelmann, 2002a). As they travel at some speed c through the system, a thermodynamic limit $L \to \infty$, $\eta \to 0$ with $\eta = c/L$ may be taken consistently. For the calculation of dynamical structure functions like those obtained in elastic neutron scattering, $\hat{A}$ is a spatially delocalized Fourier transform, and another approach must be taken. The open boundaries introduce both genuine edge effects and a hard cut to the wave functions of excited states in real space, leading to a large spread in momentum space. To limit bandwidth in momentum space, filtering is necessary. The filtering function should be narrow in momentum space and broad in real space, while simultaneously strictly excluding edge sites. Kühner and White (1999) have introduced the so-called Parzen filter F_P,

$$F_P(x) = \begin{cases} 1 - 6|x|^2 + 6|x|^3, & 0 \leqslant |x| \leqslant 1/2 \\ 2(1-|x|)^3, & 1/2 \leqslant |x| \leqslant 1, \end{cases} \tag{79}$$

where $x = i/L_P \in [-1,1]$, the relative site position in the filter for a total filter width $2L_P$. In momentum space F_P has a wave-vector uncertainty $\Delta q = 2\sqrt{3}/L_P$, which scales as L^{-1} if one scales L_P with system size L. For finite-size extrapolations it has to be ensured that filter size does not introduce a new size dependency. This can be ensured by introducing a Parzen-filter prefactor given by $\sqrt{140\pi/151L_P}$.

A. Continued-fraction dynamics

The technique of *continued-fraction dynamics* was first exploited by Gagliano and Balseiro (1987) in the framework of exact ground-state diagonalization. Obviously, the calculation of Green's functions as in Eq. (72) involves the inversion of $\hat{H}$ (or more precisely, $E_0 + \omega + i\eta - \hat{H}$), a typically very large sparse Hermitian matrix. This inversion is carried out in two, at least formally, exact steps. First, an iterative basis transformation taking $\hat{H}$ to a tridiagonal form is carried out. Second, this tridiagonal matrix is then inverted, allowing the evaluation of Eq. (72).

Let us call the diagonal elements of $\hat{H}$ in the tridiagonal form a_n and the subdiagonal elements b_n^2. The coefficients a_n, b_n^2 are obtained as the Schmidt-Gram coefficients in the generation of a Krylov subspace of unnormalized states starting from some arbitrary state, which we take to be the excited state $\hat{A}|0\rangle$:

$$|f_{n+1}\rangle = \hat{H}|f_n\rangle - a_n|f_n\rangle - b_n^2|f_{n-1}\rangle, \qquad (80)$$

with

$$|f_0\rangle = \hat{A}|0\rangle, \qquad (81)$$

$$a_n = \frac{\langle f_n|\hat{H}|f_n\rangle}{\langle f_n|f_n\rangle}, \qquad (82)$$

$$b_n^2 = \frac{\langle f_{n-1}|\hat{H}|f_n\rangle}{\langle f_{n-1}|f_{n-1}\rangle} = \frac{\langle f_n|f_n\rangle}{\langle f_{n-1}|f_{n-1}\rangle}. \qquad (83)$$

The global orthogonality of the states $|f_n\rangle$ (at least in formal mathematics) and the tridiagonality of the new representation (i.e., $\langle f_i|\hat{H}|f_j\rangle = 0$ for $|i-j| > 1$) follow by induction. It can then be shown quite easily by an expansion of determinants that the inversion of $E_0 + \omega + i\eta - \hat{H}$ leads to a continued fraction such that the Green's function G_A reads

$$G_A(z) = \cfrac{\langle 0|\hat{A}^\dagger \hat{A}|0\rangle}{z - a_0 - \cfrac{b_1^2}{z - a_1 - \cfrac{b_2^2}{z - \cdots}}}, \qquad (84)$$

where $z = E_0 + \omega + i\eta$. This expression can now be evaluated numerically, giving access to dynamical correlations.

In practice, several limitations occur. The iterative generation of the coefficients a_n, b_n^2 is equivalent to a Lanczos diagonalization of $\hat{H}$ with starting vector $\hat{A}|0\rangle$. Typically, the convergence of the lowest eigenvalue of the transformed tridiagonal Hamiltonian to the ground-state eigenvalue of $\hat{H}$ will have happened after $n \sim O(10^2)$ iteration steps for standard model Hamiltonians. Lanczos convergence is, however, accompanied by numerical loss of global orthogonality, which computationally is ensured only locally, invalidating the inversion procedure. The generation of coefficients has to be stopped before that. Kühner and White (1999) have proposed monitoring, for normalized vectors, $\langle f_0|f_n\rangle > \epsilon$ as a termination criterion. The precision of this approach therefore depends on whether the continued fraction has sufficiently converged at termination. With $\hat{A}|0\rangle$ as the starting vector, convergence will be fast if $\hat{A}|0\rangle$ is a long-lived excitation (close to an eigenstate) such as would be the case if the excitation were part of an excitation band; this will typically not be the case if it is part of an excitation continuum.

It should also be mentioned that, beyond the above complications also arising for exact diagonalization with an exact $\hat{H}$, additional approximations are introduced in DMRG, as the Hamiltonian itself is of course not exact.

Instead of evaluating the continued fraction of Eq. (84), one may also exploit the fact that, upon normalization of the Lanczos vectors $|f_n\rangle$ and accompanying rescaling of a_n and b_n^2, the Hamiltonian is iteratively transformed into a tridiagonal form in a new approximate orthonormal basis. When one transforms the basis $\{|f_n\rangle\}$ by a diagonalization of the tridiagonal Hamiltonian matrix to the approximate energy eigenbasis of $\hat{H}, \{|n\rangle\}$ with eigenenergies E_n, the Green's function can be written within this approximation as

$$G_A(\omega + i\eta) = \sum_n \langle 0|\hat{A}^\dagger|n\rangle\langle n|\frac{1}{E_0 + \omega + i\eta - E_n}|n\rangle$$
$$\times \langle n|\hat{A}|0\rangle, \qquad (85)$$

where the sum runs over all approximate eigenstates. The dynamical correlation function is then given by

$$C_A(\omega + i\eta) = \frac{\eta}{\pi}\sum_n \frac{|\langle n|\hat{A}|0\rangle|^2}{(E_0 + \omega - E_n)^2 + \eta^2}, \qquad (86)$$

where the matrix elements in the numerator are simply the $|f_0\rangle$ expansion coefficients of the approximate eigenstates $|n\rangle$.

For a given effective Hilbert-space dimension M, optimal precision within these constraints can be obtained by targeting not only the ground state, but also a selected number of states of the Krylov sequence. While a first approach is to take arbitrarily the first n states generated (say, five to ten) at equal weight, the approximate eigenbasis formulation gives direct access to the relative importance of the vectors. The importance of a Lanczos vector $|f_n\rangle$ is given by, writing $|A\rangle = \hat{A}|0\rangle$,

$$\lambda_n = \sum_m |\langle A|m\rangle|^2 |\langle m|f_n\rangle|^2, \qquad (87)$$

which assesses the contribution the vector makes to an approximative eigenstate $|m\rangle$, weighted by that eigenstate's contribution to the Green's function. The density matrix may then be constructed from the ground state and a number of Lanczos vectors weighted according to Eq. (87). The weight distribution indicates the applicability of the Lanczos vector approach: for the spin-1 Heisenberg chain at $q = \pi$, where there is a one-magnon band at $\omega = \Delta = 0.41J$, three target states carry 98.9% of total weight, whereas for the spin-1/2 Heisenberg chain at $q = \pi$ with a two-spinon continuum for $0 \leqslant \omega \leqslant \pi J$, the first three target states carry only 28.0%, indicating severe problems with precision (Kühner and White, 1999).

There is currently no precise rule for resolving the dilemma of targeting as many states as possible while retaining sufficient precision in the description of each single one.

As an example of the excellent performance of this method, one may consider the isotropic spin-1 Heisenberg chain, for which the single-magnon line is shown in Fig. 14. Exact diagonalization, quantum Monte Carlo, and DMRG are in excellent agreement, with the exception of the region $q \to 0$, where the single-magnon band forms only the bottom of a magnon continuum. Here Lanczos vector dynamics do not correctly reproduce the 2Δ gap at $q = 0$, which is much better resolved by quantum Monte Carlo.

The intuition that excitation continua are badly approximated by a sum over some $O(10^2)$ effective excited states is further corroborated by considering the spectral weight function $S^+(q = \pi, \omega)$ [use $A = S^+$ in Eq. (74)] for a spin-1/2 Heisenberg antiferromagnet. As shown in Fig. 15, Lanczos vector dynamics roughly capture the right spectral weight, including the $1/\omega$ divergence, as can be seen from the essentially exact correction vector curve, but no convergent behavior can be observed upon an increase of the number of targeted vectors. The very fast Lanczos vector method is thus certainly useful for getting a quick overview of spectra, but is not suited to detailed quantitative calculations of excitation continua, only excitation bands. Nevertheless, this method has been applied successfully to the $S = \frac{1}{2}$ antiferromagnetic Heisenberg chain (Hallberg, 1995), the spin-boson model (Nishiyama, 1999), the Holstein model (Zhang *et al.*, 1999), and spin-orbital chains in external fields (Yu and Haas, 2000). Okunishi *et al.* (2001) have used it to extract spin chain dispersion relations. Garcia *et al.* (2004) have used continued-fraction techniques to provide a self-consistent impurity solver for dynamical mean-field calculations (Metzner and Vollhardt, 1989; Georges *et al.*, 1996).

B. Correction vector dynamics

Even before the advent of DMRG, another way of obtaining more precise spectral functions had been proposed by Soos and Ramasesha (1989); it was first applied using DMRG by Ramasesha *et al.* (1997) and Kühner and White (1999). After preselection of a fixed frequency ω one may introduce a *correction vector*:

$$|c(\omega + i\eta)\rangle = \frac{1}{E_0 + \omega + i\eta - \hat{H}} \hat{A}|0\rangle, \qquad (88)$$

which, if known, allows for trivial calculation of the Green's function and hence the spectral function at this particular frequency:

$$G_A(\omega + i\eta) = \langle A|c(\omega + i\eta)\rangle. \qquad (89)$$

The correction vector itself is obtained by solving the large sparse linear equation system given by

$$(E_0 + \omega + i\eta - \hat{H})|c(\omega + i\eta)\rangle = \hat{A}|0\rangle. \qquad (90)$$

To actually solve this non-Hermitian equation system, the current procedure is to split the correction vector into real and imaginary parts, to solve the Hermitian

equation for the imaginary part, and exploit the relationship to the real part:

$$[(E_0 + \omega - \hat{H})^2 + \eta^2]\mathrm{Im}|c(\omega + i\eta)\rangle = -\eta\hat{A}|0\rangle \qquad (91)$$

$$\mathrm{Re}|c(\omega + i\eta)\rangle = \frac{\hat{H} - E_0 - \omega}{\eta}\mathrm{Im}|c(\omega + i\eta)\rangle. \qquad (92)$$

The standard method for solving a large sparse linear equation system is the conjugate-gradient method (Golub and van Loan, 1996), which effectively generates a Krylov space, as does the Lanczos algorithm. The main implementation work in this method is to provide $\hat{H}^2\mathrm{Im}|c\rangle$. Two remarks are in order. The reduced basis representation of $\hat{H}^2$ is obtained by squaring the effective Hamiltonian generated by DMRG. This approximation is found to work extremely well as long as both real and imaginary parts of the correction vector are included as target vectors. While the real part is not needed for the evaluation of spectral functions, $(E_0 + \omega - \hat{H})\mathrm{Im}|c\rangle \sim \mathrm{Re}|c\rangle$ due to Eq. (92); and targeting $\mathrm{Re}|c\rangle$ ensures minimal truncation errors in $\hat{H}\,\mathrm{Im}|c\rangle$. The fundamental drawback of using a squared Hamiltonian is that, for all iterative eigenvalue or equation solvers, the speed of convergence is determined by the matrix condition number, which drastically deteriorates by the squaring of a matrix. Many schemes are available to improve the convergence of conjugate-gradient methods, usually based on providing the solution to some related but trivial equation system, such as that formed from the diagonal elements of the large sparse matrix (Golub and van Loan, 1996).

In the simplest form of the correction vector method, the density matrix is formed from targeting four states, $|0\rangle$, $\hat{A}|0\rangle$, $\mathrm{Im}|c(\omega + i\eta)\rangle$, and $\mathrm{Re}|c(\omega + i\eta)\rangle$.

As has been shown by Kühner and White (1999), it is not necessary to calculate a very dense set of correction vectors in ω space to obtain the spectral function for an entire frequency interval. Assuming that the finite convergence factor η ensures a good description of an entire range of energies of width $\approx \eta$ by the correction vector, they applied the Lanczos vector method as detailed in the last section to $\hat{A}|0\rangle$, using the effective Hamiltonian obtained by also targeting the correction vector, to obtain the spectral function in some interval around their anchor value for ω. Comparing the results for some ω obtained by starting from neighboring anchoring frequencies allows for excellent convergence checks (Fig. 16). In fact, they found that the best results were obtained for a two-correction-vector approach in which two correction vectors were calculated and targeted for two frequencies ω_1, $\omega_2 = \omega_1 + \Delta\omega$ and the spectral function obtained for the interval $[\omega_1, \omega_2]$. This method was, for example, able to provide a high-precision result for the spinon continuum in the $S = 1/2$ Heisenberg chain where standard Lanczos dynamics fails (Fig. 15).

Reducing the broadening factor η, it is also possible to resolve finite-system peaks in the spectral function, ob-

taining to some approximation both location and weight of the Green's-function poles.

The correction vector method has been applied to determine the nonlinear optical coefficients of Hubbard chains and derived models by Pati *et al.* (1999); Kühner *et al.* (2000) have extracted the ac conductivity of the Bose-Hubbard model with nearest-neighbor interactions. Raas *et al.* (2004) have used it to study the dynamic correlations of single-impurity Anderson models and were able to resolve sharp dominant resonances at high energies, using optimized algorithms for the matrix inversion needed to obtain the correction vector.

C. Dynamical DMRG

A further important refinement of DMRG dynamics is obtained by a reformulation of the correction vector method in terms of a minimization principle, which has been called "dynamical DMRG" (Jeckelmann, 2002a). While the fundamental approach remains unchanged, the large sparse equation system is replaced by a minimization of the functional

$$W_{A,\eta}(\omega,\psi) = \langle\psi|(E_0 + \omega - \hat{H})^2 + \eta^2|\psi\rangle + \eta\langle A|\psi\rangle$$
$$+ \eta\langle\psi|A\rangle. \tag{93}$$

At the minimum, the minimizing state is

$$|\psi_{\min}\rangle = \text{Im}|c(\omega + i\eta)\rangle. \tag{94}$$

Even more importantly, the value of the functional itself is

$$W_{A,\eta}(\omega,\psi) = -\pi\eta C_A(\omega + i\eta), \tag{95}$$

such that for the calculation of the spectral function it is not necessary to explicitly use the correction vector. The huge advantage is that if the correction vector is known to some precision ϵ (which will be essentially identical for the equation solver and the minimizer), the value of the functional itself is, by general properties of variational methods, known to the much higher precision ϵ^2. Hence the DMRG algorithm is essentially implemented as in the correction vector method, with the same target vectors, until they converge under sweeping, but with the minimization of $W_{A,\eta}(\omega,\psi)$ replacing the sparse equation solver. Results that are obtained for a sequence of ω_i may then be extended to other ω by suitable interpolation (Jeckelmann, 2002a), also exploiting first derivatives of spectral functions that are numerically accessible at the anchor points.

For dynamical quantities, there are no strict statements on convergence. However, convergence for large M seems to be monotonic, with C_A typically underestimated.

The high-quality numerical data obtained from dynamical DMRG in fact allow for an extrapolation to the thermodynamic limit. As pointed out by Jeckelmann (2002a), the double limit
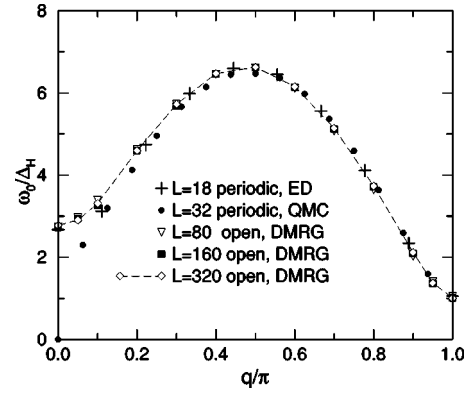

FIG. 14. Single-magnon line of the $S=1$ Heisenberg antiferromagnet from exact diagonalization, quantum Monte Carlo, and DMRG for various system sizes and boundary conditions. From Kühner and White, 1999. Reprinted with permission.

$$C_A(\omega) = \lim_{\eta\to 0}\lim_{L\to\infty} C_A(L;\omega + i\eta), \tag{96}$$

where limits may not be interchanged and which is very hard to take numerically, may be taken as a single limit,

$$C_A(\omega) = \lim_{\eta(L)\to 0} C_A[L;\omega + i\eta(L)], \tag{97}$$

provided that $\eta(L)\to 0$ as $L\to\infty$ is chosen such that the finiteness of the system is not visible for the chosen $\eta(L)$ and it thus seems to be in the thermodynamic limit from a level-spacing perspective. This implies that $\eta(L) > \delta\omega(L)$, the maximum level spacing of the finite system around energy ω. For a typical tight-binding Hamiltonian such as the Hubbard model, one finds

$$\eta(L) \gtrsim \frac{c}{L}, \tag{98}$$

where c is the bandwidth (and, in such Hamiltonians, also a measure of propagation velocity). The key argument is now that if $\eta(L)$ is chosen according to that prescription, the scaling of numerical results broadened by $\eta(L)$ is the same as for some thermodynamic-limit form known or conjectured analytically subject to Lorentzian broadening using the same η. From Lorentzian broadening of model spectra one can then show that a local δ peak in an otherwise continuous spectrum with weight C^0 scales as $C^0/\pi\eta(L)$, and that a power-law divergence $(\omega-\omega_0)^{-\alpha}$ at a band edge is signaled by a scaling as $\eta(L)^{-\alpha}$. More model spectra are discussed by Jeckelmann (2002a).

Dynamical DMRG has been extensively used to study the spectrum and the optical conductivity of the extended Hubbard model (Jeckelmann *et al.*, 2000; Essler *et al.*, 2001; Jeckelmann, 2003a; Kim *et al.*, 2004). The optical conductivity may be calculated as

$$\sigma_1(\omega) = -\frac{1}{L\omega}\lim_{\eta\to 0}\text{Im}\, G_J(\omega + i\eta), \tag{99}$$

with the current operator $\hat{J} = -ie\Sigma_{i\sigma}t_i(c^\dagger_{\sigma,i}c_{\sigma,i+1} - c^\dagger_{\sigma,i+1}c_{\sigma,i})$. Another possibility is to use
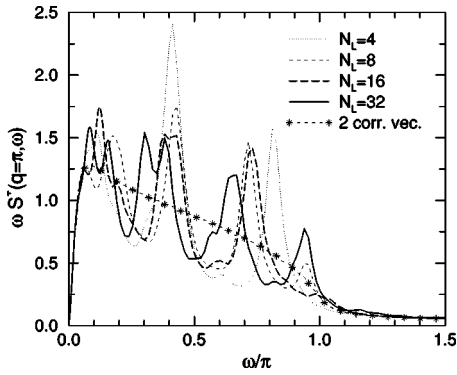
FIG. 15. Spectral weight $S^+(q=\pi,\omega)$ of the $S=1/2$ Heisenberg antiferromagnet from Lanczos vector and correction vector DMRG. N_L indicates the number of target states; $M=256$. Note that spectral weight times ω is shown. From Kühner and White, 1999. Reprinted with permission.

$$\sigma_1(\omega) = -\frac{1}{L\omega}\lim_{\eta\to 0}\mathrm{Im}[(\omega+i\eta)G_D(\omega+i\eta)], \qquad (100)$$

with the dipole operator $\hat{D}=-e\Sigma_i(n_i-1)$.

In the noninteracting limit $U=0$, the optical conductivity is nonvanishing in a band $2|\Delta|<\omega<4t$ with square-root edge divergences. Dynamical DMRG quantitatively reproduces all features of the exact solution, including the divergence. It is even possible to extract the degree of the singularity. Moving to the strongly interacting case $U\gg t$, one expects two continuous bands due to the dimerization at $2|\Delta|\leqslant|\omega-U|\leqslant4t$ and the Hubbard resonance at $\omega=U$. Figure 17, which compares to analytical solutions, shows both that the bands are reproduced with excellent quality (up to broadening at the edges) and that the δ singularity is measured with extremely high precision. Similarly, very precise spectral functions for the Hubbard model away from half-filling have been obtained (Benthien *et al.*, 2004). Nishimoto and Jeckelmann (2004) have shown that dynamical DMRG may also be applied to impurity problems, such as the flat-band single-impurity Anderson model, upon suitable discretization of the band. Recently, Nishimoto *et al.* (2004) have extended this to a precise calculation of the Green's function of a single-impurity Anderson model with arbitrary band, thereby providing a high-quality self-consistent impurity solver needed for dynamical mean-field calculations (Metzner and Vollhardt, 1989; Georges *et al.*, 1996).

V. BOSONS AND DMRG: MANY LOCAL DEGREES OF FREEDOM

So far, our discussion of DMRG applications has been largely restricted to quantum spin and electronic systems, which are characterized by a fixed, usually small number of degrees of freedom per site. As algorithmic performance relies heavily on N_{site} small [formally $O(N_{\mathrm{site}}^3)$, in practice rather $O(N_{\mathrm{site}}^2)$], one may wonder whether DMRG is applicable to bosonic degrees of free-

dom with $N_{\mathrm{site}}=\infty$. Such bosonic degrees of freedom occur, for example, in the Bose-Hubbard model,

$$\hat{H}_{BH} = -t\sum_i b_{i+1}^\dagger b_i + b_i^\dagger b_{i+1} + \frac{U}{2}\sum_i n_i(n_i-1), \qquad (101)$$

which has come to the forefront of research due to the realization of a tunable quantum phase transition from a Mott insulating to a superfluid phase in ultracold bosonic atomic gases in optical lattices (Greiner *et al.*, 2002). Another model of interest is the Holstein model, in which electrons (also spinless fermions or *XY* spins) couple to local (quantum) phonons that react dynamically and are not *a priori* in some adiabatic limit,

$$\hat{H}_{\mathrm{Hol}} = -t\sum_i c_{\sigma,i+1}^\dagger c_{\sigma,i} + c_{\sigma,i}^\dagger c_{\sigma,i+1} - \gamma\sum_i (b_i^\dagger + b_i)(n_i-1)$$
$$+ \omega\sum_i (b_i^\dagger b_i + 1/2). \qquad (102)$$

It models electrons in a vibrating lattice and opens the way to polaron physics. Yet another model is the spin-boson model, which models the dissipative coupling of a two-state system to a thermal reservoir given by bosonic oscillators:

$$\hat{H}_{SB} = -\frac{\Delta}{2}\sigma^x + \sum_i \omega_i b_i^\dagger b_i + \frac{\sigma^z}{2}\sum_i f_i(b_i^\dagger + b_i). \qquad (103)$$

A. Moderate number of degrees of freedom

The simplest conceptual approach is to arbitrarily truncate the local-state space to some N_{max} for the bosonic degrees of freedom and to check for DMRG convergence both in M and in N_{max}. This approach has been very successful in the context of the Bose-Hubbard model in which the on-site Coulomb repulsion U suppresses large occupation numbers. It has been used for the standard Bose-Hubbard model (Kühner and Monien, 1998; Kühner *et al.*, 2000), with a random potential (Rapsch *et al.*, 1999), in a parabolic potential due to a magnetic trap for cold atoms (Kollath *et al.*, 2004), and with non-Hermitian hopping and a pinning impurity to model superconductor flux lines (Hofstetter *et al.*, 2004). Typically, allowing for about three to five times the average occupation is sufficient as N_{max}. Similarly, the physics of the fluctuation of confined membranes (Nishiyama, 2002a, 2002b, 2003) and quantum strings (Nishiyama, 2001) necessitates the introduction of a larger number of local vibrational states. Other applications that are more problematic have been to phonons, both with (Caron and Moukouri, 1996; Maurel and Lepetit, 2000; Maurel *et al.*, 2001) and without (Caron and Moukouri, 1997) coupling to magnetic or fermionic degrees of freedom. While they are believed to be reliable in giving a generic impression of physical phenomena, for more precise studies more advanced techniques are necessary (compare the results of Caron and Moukouri, 1996 and of Bursill, 1999).
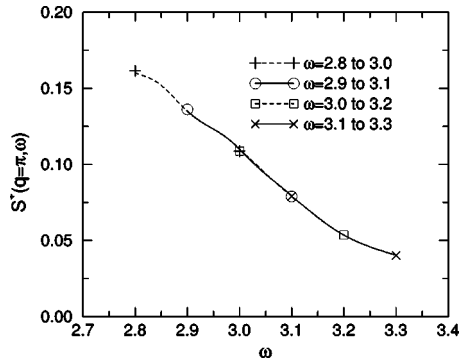
FIG. 16. Spectral weight of the $S=1/2$ Heisenberg antiferromagnet from correction vector DMRG. $M=256$ states kept. Spectral weights have been calculated for ω intervals starting from various anchoring frequencies for the correction vector. From Kühner and White, 1999. Reprinted with permission.

B. Large number of degrees of freedom

Essentially three approaches have been taken to reduce the large, possibly divergent number of states per site to a small number manageable by DMRG.

Bursill (1999) has proposed a so-called *four-block approach* that is particularly suited to periodic boundary conditions and is a mixture of Wilson numerical renormalization group and DMRG ideas. Starting from four initial blocks of size 1 with M states (this may be a relatively large number of electronic and phononic degrees of freedom) forming a ring, one solves for the ground state of that M^4-state problem; density matrices are then formed to project out two blocks and form a new block of double size with M^2 states, which are truncated down to M using the density-matrix information. From four of these blocks, a new four-block ring is built, leading to a doubling of system size at every step. Calculations may be simplified beyond the usual time-saving techniques by reducing the number of M^4 product states to some smaller number of states for which the product of their weights in the density matrices is in excess of some very small ϵ, of the order of 10^{-25} to 10^{-10}. Translation operators applied to the resulting ground state of the four blocks on the ring allow the explicit construction of specific momentum eigenstates, in particular for $k=0$ and $k=\pi$. For both an XY-spin (Bursill, 1999) and isotropic-spin (Bursill *et al.*, 1999) variety of the Holstein model, this method allows one to trace out very precisely a Kosterlitz-Thouless phase transition from a quasi-long-ranged antiferromagnet for small spin-phonon coupling to a dimerized, gapped phase. As Kosterlitz-Thouless phase transitions exhibit an exponentially slow opening of the gap (Okamoto and Nomura, 1992), the exact localization of the transition by analyzing the gap is problematic. It is rather convenient to apply the level-spectroscopy technique (Nomura and Okamoto, 1994), which locates the phase transition by a small-system finite-size extrapolation of the crossing points g^* of the lowest-lying excitation of different symmetries, including $k=0$ and $k=\pi$ states that are easily accessible in the four-block approach. It was found that, in the neighborhood of the phase transition, roughly 30 phonon states were sufficient to obtain converged results. A similar scenario for the Kosterlitz-Thouless transition was obtained for spinless fermions in the Holstein model (Bursill *et al.*, 1998).

An approach more in the spirit of DMRG, the so-called *local state reduction*, was introduced by Zhang, Jeckelmann, and White (1998). While it can also be combined with exact diagonalization, I want to formulate it in a DMRG setup. Assuming a chain with fermionic and a small number of bosonic degrees of freedom on each site, one of the sites is chosen as the "big site" to which a further number of bare bosonic degrees of freedom is added. Within a DMRG calculation, a density matrix is formed for the big site to truncate the number of degrees of freedom down to some fixed number of optimal degrees of freedom. This procedure is repeated throughout the lattice in the finite-system algorithm, sweeping for convergence and for the addition of further bosonic degrees of freedom. The standard prediction algorithm makes the calculation quite fast. Physical quantities are then extracted within the optimal phononic state space. As can be seen from Fig. 18, merely keeping two or three optimal states, in which high-lying bare states have non-negligible weight, may be as efficient as keeping of the order of a hundred bare states. This approach has allowed the demonstration of the strong effect of quantum lattice fluctuations in trans-polyacetylene (Barford, Bursill, and Lavrentiev, 2002). Combined with Lanczos-vector dynamics, very precise dynamical susceptibilities have been extracted for spin-boson models (Nishiyama, 1999). Extensions of the method are offered by Friedman (2000) and Fehske (2000).

Jeckelmann and White (1998) have devised a further approach in which 2^n bosonic degrees of freedom are embodied by n *fermionic pseudosites*: writing the number of the bosonic degree of freedom as a binary number, the degree of freedom is encoded by empty and full fermionic pseudosites as dictated by the binary number. All operators on the bosonic degrees of freedom can now be translated into (rather complicated) operators on the fermionic pseudosites. Finite-system DMRG is then applied to the resulting Hamiltonian. Jeckelmann and co-workers have been able to study polaronic self-trapping of electrons in the Holstein model for up to 128 phonon states and have located very precisely the metal-insulator transition in this model (Jeckelmann *et al.*, 1999).

VI. TWO-DIMENSIONAL QUANTUM SYSTEMS

Since the spectacular discovery of high-T_c superconductivity related to CuO_2 planes, there has been a strong focus on two-dimensional quantum systems. Early on, it was suggested that the Hubbard model or the t-J model away from half-filling might be simple yet powerful enough to capture essential features of high-T_c superconductivity. The analytical study of these quantum systems is plagued by problems similar to the one-
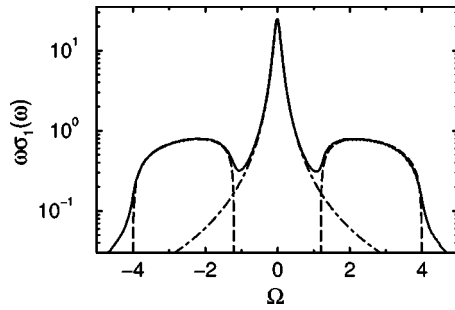
FIG. 17. Optical conductivity for a Peierls-Hubbard model in the $U \gg t$ limit, $L=128$, $\eta=0.1$, $\Omega=\omega-U$: solid line, dynamical DMRG; dot-dashed line, broadened exact δ contribution; dashed line, unbroadened thermodynamic-limit bands. Note log-linear scale. From Jeckelmann, 2002a. Reprinted with permission.

dimensional case, as in many effective field theories $d=2$ is the lower critical dimension and few exact results are available. Numerically, exact diagonalization methods are even more restricted in two dimensions, and quantum Monte Carlo is difficult to use for fermionic models away from half filling due to the negative-sign problem. Can DMRG help?

The first step in any two-dimensional application of DMRG is to identify blocks and sites in order to apply the strategies devised in the one-dimensional case. Assuming nearest-neighbor interactions on a square lattice, one might organize columns of sites into one supersite such that blocks are built from supersites, sweeping through the system horizontally. While this approach maintains short-ranged interactions, it must fail for any two-dimensional strip of appreciable width L as the number of states per supersite grows exponentially as N_{site}^L and is only useful for narrow ladder systems.

The standard approach [Noack, White, and Scalapino in Landau *et al.* (1994), Liang and Pang (1994), White (1996b)], known as the *multichain approach*, is to define a suitable one-dimensional path over all sites of the two-dimensional lattice, such as the configuration shown in Fig. 19.

One may now apply standard one-dimensional finite-system DMRG at the price of long-ranged interactions of range $2L$ both within and between blocks, as indicated in Fig. 19. An inherent difficulty is the preparation of blocks and operators for application of the finite-system algorithm, as there is no precursor infinite-system DMRG run in some sequence of smaller systems possible in this setup. Few compositions of smaller blocks in this scheme resemble the final system at all. While Liang and Pang (1994) have simply switched off all non-nearest-neighbor interactions in the mapped one-dimensional system and applied standard infinite-system DMRG in order to switch on all interactions in finite-system runs, one can also grow blocks in a standard infinite-system DMRG run, where some very short, exactly solvable system is used as environment such that the entire superblock remains treatable. This and similar warmup procedures will generate starting states for

finite-system DMRG far from anything physically realistic. As finite-system DMRG provides only sequential local updates to that state, there is no guarantee that the system will not get trapped in some local minimum state. That such trappings do exist is seen from frequent observations that seemingly converged systems may, after many further sweeps, suddenly experience major "ground-state" energy drops into some new (possible) ground state.

White and co-workers have followed the approach of exploiting local trappings by theorizing ahead of using DMRG on possible ground-state types using other analytical or numerical techniques and of forcing these types of states onto the system by the application of suitable local magnetic fields and chemical potentials. These external fields are then switched off and the convergence behavior of the competing proposed states under finite-system DMRG observed. This procedure generates a set of states, each of which corresponds to a local energy minimum. The associated physical properties may be measured and compared (see White and Scalapino, 1998a and White and Scalapino, 2000 for a discussion). In the multichain approach, the two-dimensional Heisenberg model (White, 1996b), the two-dimensional t-J model (White and Scalapino, 1998a, 1998b, 2000; Kampf *et al.*, 2001; Chernychev *et al.*, 2003) with particular emphasis on stripe formation, and the six-leg ladder Hubbard model (White and Scalapino, 2003) have been studied.

Among competing setups (du Croo de Jongh and van Leeuwen, 1998; Henelius, 1999; Farnell, 2003; Moukouri and Caron, 2003), Xiang *et al.* (2001) have set up a two-dimensional algorithm that uses a true DMRG calculation all along and builds $L \times L$ systems from previously generated $(L-1) \times (L-1)$ systems while keeping the lattice structure intact. It can be applied to all lattices that can be arranged to be square with suitable interactions. For example, a triangular lattice is a square lattice with additional next-nearest-neighbor interactions along one diagonal in each square.

A one-dimensional path is organized as shown in Fig. 20, where the pair of free sites may be zipped through the square along the path using the standard finite-system algorithm, yielding arbitrary block sizes. In particular, one may obtain triangular upper or lower blocks as shown in Fig. 21. Combining these blocks from a $(L-1) \times (L-1)$ system and adding two free sites at the corners, one arrives at an $L \times L$ system. Here, the upper left free site can be zipped to be a neighbor of the lower-right free site, as it sits next to active block ends (i.e., the ends where new sites are added). The pair of free sites can now be zipped through the system to yield the desired triangular blocks for the step $L \rightarrow L+1$.

This approach systematically yields lower energies than the multichain approach for both two-dimensional square and triangular $S=1/2$ Heisenberg models with the exception of very small systems. Even for a relatively modest number of states kept ($M=300$), Xiang *et al.* (2001) report thermodynamic-limit extrapolations in good agreement with large-scale quantum Monte Carlo

simulations: For the square lattice, they find E_∞ $=-0.3346$ versus a quantum Monte Carlo result E_∞ $=-0.334\,719(3)$ (Sandvik, 1997). The potential of this approach seems far from exploited at the moment.

So far, I have been tacitly assuming that interactions are of the same order along both spatial directions. Experimentally, a relatively frequent situation is that one-dimensional quantum systems are weakly coupled along a second axis. At high enough temperatures this interaction will washed out, but at sufficiently low temperatures there will be a crossover from one- to two-dimensional behavior. Such systems may be studied by attempting a precise one-dimensional description and introducing the weak interchain interaction on the mean field or some other perturbative level. Moukouri and Caron (2003) and Moukouri (2004) have used DMRG in a similar spirit by solving a one-dimensional system using standard DMRG with M states and determining the M' lowest-lying states for the superblock. Chain lengths are chosen such that the lowest-lying excitation of the finite chain is down to the order of the interchain coupling. These states are taken to be the states of a "site," and are combined to a new effective Hamiltonian, which is once again treated using DMRG. Results for weakly coupled spin chains are in good agreement with quantum Monte Carlo results; however, M' is currently severely limited to several tens.

A severe limitation on two-dimensional DMRG is provided by the exponential growth of M with L for a preselected truncated weight or ground-state precision (Sec. III.B). For frustrated and fermionic systems beyond the very small exact diagonalization range (6×6 for $S=1/2$ spins), DMRG may yet be the method of choice as quantum Monte Carlo suffers from the negative-sign problem and even medium-sized fermionic systems of size, say, 12×12 sites would be most useful; in models with non-Abelian symmetries, the implementation of the associated good quantum numbers has been shown to reduce drastically the truncation error for a given number of states (McCulloch and Gulacsi, 2000, 2001, 2002; McCulloch *et al.*, 2001).

Very recently, Verstraete and Cirac (2004) have proposed a new approach to two-dimensional quantum systems combining a generalization of their matrix-product formulation of DMRG (Verstraete, Porras, and Cirac, 2004) and imaginary-time evolution (Verstraete, Garcia-Ripoll, and Cirac, 2004), discussed in Sec. III.A and Sec. IX.C. One-dimensional matrix-product states are formed from matrix products of $M\times M$ matrices $(A[\sigma])_{\alpha\beta}$, with M-dimensional auxiliary state spaces on the bond to the left and right of each site. The two-dimensional generalization for a square lattice is given by the contraction of tensors $(A[\sigma])_{\alpha\beta\gamma\delta}$ with M-dimensional auxiliary state spaces on the four adjacent bonds. Finite-temperature and ground states are calculated by imaginary-time evolution of a totally mixed state along the lines of Verstraete, Garcia-Ripoll, and Cirac (2004). As tensorial contractions lead (in contrast to the case of the ansatz matrices $A[\sigma]$ appearing in
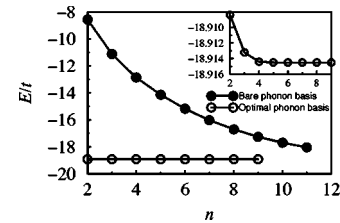

FIG. 18. Optimal vs bare phonon states: ground-state energy convergence for a four-site Holstein model at half-filling vs number of (optimal, bare) phonon states kept. From Zhang, Jeckelmann, and White, 1998.

one dimension) to a proliferation of indices on resulting tensors, a suitable truncation scheme is needed, as described by Verstraete and Cirac (2004).

An appealing feature of this approach is that the entropy of entanglement for a cut through a system of size $L\times L$ will scale, for fixed M, linearly in system size, as it should generically. The errors in energy seem to decrease exponentially in M. M is currently very small (up to 5), as the algorithm scales badly in M; however, as M variational parameters are available on each bond, even a small M corresponds to large variational spaces. At the time of writing, it is too early to assess the potential of this new approach; however, current results and the conceptual clarity of this approach make it seem very promising.

VII. BEYOND REAL-SPACE LATTICES: MOMENTUM-SPACE DMRG, QUANTUM CHEMISTRY, SMALL GRAINS, AND NUCLEAR PHYSICS

In this section, I shall consider three groups of DMRG applications that seem to have very little in common at first sight: the study of translationally invariant low-dimensional models in momentum space, high-precision quantum chemistry calculations for small molecules, and studies of small grains and nuclei. However, from a DMRG point of view, all share fundamental properties. Let me first discuss momentum-space DMRG, move on to quantum chemistry, and finish by considering small grains and nuclear physics.

A. Momentum-space DMRG

Real-space DMRG precision dramatically deteriorates when applied to long-ranged interactions or hoppings. Moreover, momentum is not accessible as a good quantum number in real-space DMRG. Momentum-space DMRG, on the other hand, makes momentum a good quantum number, works naturally with periodic boundary conditions, and allows trivial manipulation of the single-particle dispersion relation. Momentum-space DMRG has already yielded highly satisfying dispersion relations and momentum distributions in excellent agreement with analytical results (Nishimoto, Jeckelmann, *et al.*, 2002).
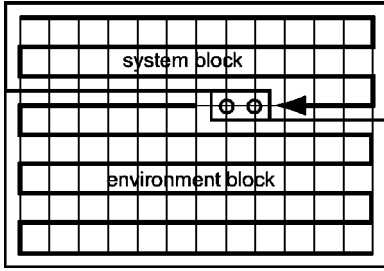
FIG. 19. Standard reorganization of a two-dimensional lattice as a zigzag one-dimensional chain with long-ranged interactions for DMRG treatment. Typical blocks during a finite-system DMRG application are shown.
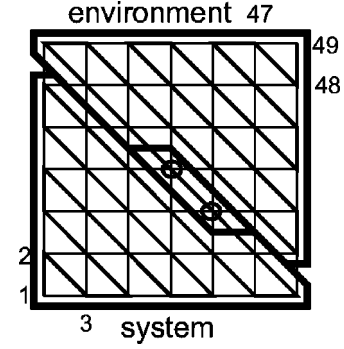

FIG. 20. Diagonal reorganization of a two-dimensional lattice as used by Xiang *et al.* (2001). Typical blocks during a finite-system DMRG application are shown.

Consider for definiteness a Hubbard model with local interaction U, but long-ranged hopping t_{ij},

$$\hat{H}_{LR} = \sum_{ij\sigma} t_{ij} c^{\dagger}_{\sigma,i} c_{\sigma,j} + U \sum_i n_{i\uparrow} n_{i\downarrow} \tag{104}$$

in arbitrary dimensions; site i is localized at $\mathbf{r}_i$ and $t_{ij} = t(\mathbf{r}_i - \mathbf{r}_j)$. With L lattice sites, Fourier transformations

$$c^{\dagger}_{\sigma,\mathbf{k}} = \frac{1}{\sqrt{L}} \sum_j e^{i\mathbf{k}\cdot\mathbf{r}_j} c^{\dagger}_{\sigma,j} \tag{105}$$

yield the band structure

$$\epsilon(\mathbf{k}) = \sum_{\mathbf{r}} e^{-i\mathbf{k}\cdot\mathbf{r}} t(\mathbf{r}) \tag{106}$$

and the Hamiltonian

$$\hat{H} = \sum_{\mathbf{k},\sigma} \epsilon(\mathbf{k}) c^{\dagger}_{\sigma,\mathbf{k}} c_{\sigma,\mathbf{k}} + \frac{U}{L} \sum_{\mathbf{k}_1,\mathbf{k}_2,\mathbf{k}_3} c^{\dagger}_{\uparrow\mathbf{k}_1} c^{\dagger}_{\downarrow\mathbf{k}_2} c_{\downarrow\mathbf{k}_3} c_{\uparrow\mathbf{k}_1+\mathbf{k}_2-\mathbf{k}_3}. \tag{107}$$

The reciprocal lattice points $\mathbf{k}$ are now taken to be "sites." Note that L is not the linear size of the lattice, but is taken to be the total lattice size (because of the typical DMRG mapping to one dimension).

The key idea (Xiang, 1996) is to arrange these sites into a one-dimensional chain with long-ranged interactions that is treated by the real-space finite-system DMRG (Nishimoto, Jeckelmann, *et al.*, 2002; Legeza *et al.*, 2003a). In addition to the conventional good quantum numbers, states will also be classified by total momentum, which allows a further substantial segmentation of Hilbert space (by a factor of order L). Hence for the same number of states kept, momentum-space DMRG is much faster than real-space DMRG.

To obtain an efficient implementation, several issues have to be addressed.

(i)   In momentum space there is a huge proliferation of interaction terms of $O(L^3)$ that have to be generated, stored, and applied to wave functions efficiently.

(ii)   For an application of the finite-system DMRG algorithm, we need to provide blocks and operators living on these blocks for all block sizes. In real space, they are naturally generated during the

infinite-system stage of the algorithm. In momentum space, another warmup procedure must be found.

(iii) On a one-dimensional lattice with short-ranged interactions it is natural to group sites as they are arranged in real space. In momentum space with long-ranged interactions, there is no obvious site sequence, even in the one-dimensional case. Does the arrangement affect convergence properties? Is there an optimal arrangement?

Let us discuss these points in the following.

(i)   *DMRG operator representation for general two-body-interaction Hamiltonians*. In principle we should like to use DMRG to treat the generic Hamiltonian

$$\hat{H}_{\text{two-body}} = \sum_{ij} T_{ij} c^{\dagger}_i c_j + \sum_{ijkl} V_{ijkl} c^{\dagger}_i c^{\dagger}_j c_k c_l, \tag{108}$$

where T_{ij} encodes kinetic energy and one-body potentials and V_{ijkl} a generic two-body (Coulomb) interaction; for simplicity, we assume spin to be contained in the orbital indices. In the worst-case scenario, all V_{ijkl} are different, although symmetries and model properties may yield decisive simplifications. In momentum space, for example, $V_{ijkl} \neq 0$ for one l only once ijk is fixed due to momentum conservation.

As for operators living on the same block,

$$\langle m | c^{\dagger}_i c_j | \tilde{m} \rangle \neq \sum_{m'} \langle m | c^{\dagger}_i | m' \rangle \langle m' | c_j | \tilde{m} \rangle, \tag{109}$$

all operator pairings have to be stored separately. Leaving aside the simpler case in which one or two of the four operators live on the single sites in DMRG, and assuming that they are all either in block S or E, this suggests that for L sites of the order of $O(L^4)$ operators have to be stored. As their form changes for each of the L possible block sizes, the total memory consumption would be $O(L^5 M^2)$ on disk for all blocks and $O(L^4 M^2)$ in RAM for the current block. At the same time, for each of the L steps of a sweep, calculation time
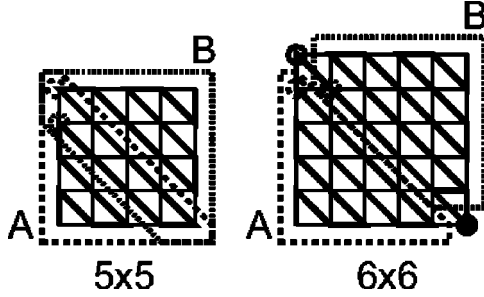
FIG. 21. Composition of blocks from a $(L-1)\times(L-1)$ system and two free sites into an $L\times L$ system as used by Xiang *et al.* (2001). The heavy solid line indicates the one-dimensional path through the lattice. The lattice subsets surrounded by the broken lines are blocks A and B; the last added sites are indicated by broken circles. Note that blocks overlap for the smaller lattice and are "pulled apart" for the big lattice. The $\bigcirc$ and $\bullet$ stand for the new sites added.

would be of order $O(L^4M^3)$, or $O(L^5M^3)$ for the entire calculation.

Memory consumption as well as the associated calculation time can, however, be reduced drastically (Xiang, 1996). Let us consider the three possible operator distributions on blocks S and E.

(a) Four operators in one block (4/0): Terms $V_{ijkl}c_i^\dagger c_j^\dagger c_k c_l$ are absorbed into a single-block Hamiltonian operator during block growth. Assuming i,j,k are in the previous block and site l is added to form the current block, a representation of $c_i^\dagger c_j^\dagger c_k$ in the previous block basis allows the formation of $V_{ijkl}\times c_i^\dagger c_j^\dagger c_k \times c_l$ in the block-plus-site product basis, which is then transformed into the basis of the current block and added into the single-block Hamiltonian operator. For L blocks, $O(L^3)$ representations each of $c_i^\dagger c_i^\dagger c_k$ are necessary. These in turn can be compounded into *complementary operators*,

$$O_l = \sum_{ijk} V_{ijkl}c_i^\dagger c_j^\dagger c_k, \tag{110}$$

so that

$$\sum_{ijkl} V_{ijkl}c_i^\dagger c_j^\dagger c_k c_l \rightarrow \sum_l O_l c_l. \tag{111}$$

The complementary operators can be constructed as discussed in Sec. II.G, assuming the knowledge of two-operator terms $c_i^\dagger c_j^\dagger$. For L blocks, $O(L^2)$ of those exist, leading to memory consumption $O(L^3M^2)$ on disk and $O(L^2M^2)$ in RAM.

(b) Three operators in a block (3/1): One applies the strategy of Eqs. (110) and (111), with O_l and c_l acting on different blocks.

(c) Two operators in a block (2/2): Again, the complementary-operator technique can be applied, with the modification that each complementary operator living on block S has now two matching operators in E. A further class of complementary operators

$$O_{kl} = \sum_{ij} V_{ijkl}c_i^\dagger c_j^\dagger \tag{112}$$

allows the simplification

$$\sum_{ijkl} V_{ijkl}c_i^\dagger c_j^\dagger c_k c_l \rightarrow \sum_{kl} O_{kl}c_k c_l. \tag{113}$$

Memory consumption for the second type of complementary operator is $O(L^3M^2)$ on disk and $O(L^2M^2)$ in RAM. Taking all operator combinations together, global memory consumption is to leading order $O(L^3M^2)$ on disk and $O(L^2M^2)$ in RAM, which is a reduction by L^2 compared to the naive estimate. In momentum space, due to momentum conservation, memory consumption is reduced by another factor of L to $O(L^2M^2)$ on disk and $O(LM^2)$ in RAM.

Using the complementary-operator technique, calculation times are dominated by the (2/2) terms. In analogy to the construction of (4/0) terms "on the fly" by generating the new terms of the sum, transforming them, and adding them into the operator, the O_{kl} can be constructed at a computational expense of $O(L^3M^2)$ for generating the L new terms to be added to each of the L^2 complementary operators with M^2 matrix elements each and $O(L^2M^3)$ for transforming the L^2 operators into the current basis. Using the multiplication technique of Sec. II.I, multiplying the Hamiltonian to the state vector costs $O(L^2M^3)$ time at each step or $O(L^3M^3)$ per sweep. Global calculation time per sweep is thus $O(L^3M^3)+O(L^4M^2)$, a reduction by L^2 for the dominant first term (typically, $M\gg L$ for the relevant DMRG applications).

(ii) *Setting up finite-system blocks*. The standard practice currently adopted in momentum space (Xiang, 1996; Nishimoto, Jeckelmann, *et al.*, 2002) is to use standard Wilsonian renormalization (Wilson, 1975, 1983): for the chosen sequence of momenta, blocks are grown linearly (as in infinite-system DMRG), but diagonalized without superblock embedding and the lowest-energy states retained, with the important modification that it should be ensured that at least one or two states are retained for each relevant Hilbert-space sector, i.e., all sectors within a certain spread about the average momentum, particle number, and magnetization. Otherwise DMRG may miss the right ground state, as certain sectors that make an important contribution to the ground state may not be constructed during the finite-system sweep. Left and right block sectors must be chosen such that all of them find a partner in the other block to combine to the desired total momentum, par-

ticle number, and magnetization. Moreover, it is advantageous to choose corresponding states in different sectors such that obvious symmetries are not broken, e.g., $S^z \leftrightarrow -S^z$ if the final state is known to be in the $S^z_{\text{tot}}=0$ sector; it has also been found that choosing initial block sizes too small may result in much slower convergence or trapping in wrong minima (Legeza *et al.*, 2003a).

(iii) *Determining the order of momentum sites*. Nishimoto, Jeckelmann, *et al.* (2002) report that what works best for short-ranged Hubbard models is ordering the levels according to increasing distance to the Fermi energy of the noninteracting limit, $|\epsilon(\mathbf{k}) - \epsilon_F|$, thus grouping levels that have strong scattering together, whereas for longer-ranged Hubbard models a simple ordering according to $\epsilon(\mathbf{k})$ works best. Similar results have been reported by Legeza *et al.* (2003a), who could demonstrate trapping in wrong minima for inadequate orderings; Legeza and Sólyom (2003) have provided a quantum-information-based method to avoid such orderings.

Nishimoto, Jeckelmann, *et al.* (2002) have carried out extensive convergence studies for Hubbard models in one dimension and two dimensions with various hoppings. Convergence seems to be dominated by the ratio of interaction to bandwidth, U/W rather than some U/t. The momentum-space DMRG algorithm becomes exact in the $U/W \rightarrow 0$ limit; convergence deteriorates drastically with U/W, but is acceptable for $U/W \lesssim 1$, which is $U \lesssim 8t$ for the 2D Hubbard model with nearest-neighbor hopping. Generally it seems that for momentum-space DMRG convergence depends only weakly on the range of hopping as opposed to real-space DMRG. Momentum-space DMRG is worst at half-filling and deteriorates somewhat with dimension (if calculations for the same physical scale U/W are compared). In two dimensions, for moderate U, momentum-space DMRG is more efficient than real-space DMRG.

As can be seen from the results of Nishimoto, Jeckelmann, *et al.* (2002), even for values of M as large as several 1000, convergence is not achieved. Due to the complex growth scheme, it cannot be taken for granted even after many sweeps that the environmental error has been eliminated; as in two-dimensional real-space DMRG, sudden drops in energy are observed. In their application, Nishimoto, Jeckelmann, *et al.* (2002) report that for fixed M a fit formula in $1/M$,

$$E_{\text{fit}}\left(\frac{1}{M}\right) = E_\infty + \frac{a_1}{M} + \frac{a_2}{M^2} + \cdots, \qquad (114)$$

works very well and improves results by over an order of magnitude even for final $M=2000$. Building on the proportionality between truncated weight and energy error for eliminated environ-

mental error, Legeza *et al.* (2003a) have proposed a "dynamical block selection scheme" to vary M to maintain a fixed truncated weight. They find that in this approach

$$\frac{E(\epsilon_\rho) - E_{\text{exact}}}{E_{\text{exact}}} = La\epsilon_\rho \qquad (115)$$

is very well satisfied for $a \approx 1$, where ϵ_ρ is the truncated weight. A further advantage of this approach is that the number of states needed for a certain precision varies widely in momentum-space DMRG, so that for many DMRG steps important savings in calculation time can be realized.

All in all, momentum-space DMRG seems a promising alternative to real-space DMRG, in particular for longer-ranged interactions (for short-ranged interactions in one dimension, real-space DMRG remains the method of choice). However, momentum-space DMRG presents additional complications (optimal ordering of levels, efficient encoding) that may not yet have been optimally solved.

B. Quantum chemistry

A field in which DMRG will make increasingly important contributions in the next few years is quantum chemistry. While the first quantum-chemical DMRG calculations on cyclic polyene by Fano *et al.* (1998) and polyacetylene by Bendazzoli *et al.* (1999) were still very much in the spirit of extended Hubbard models, more recent work has moved on to calculations in generic bases with arbitrary interactions. Let me situate this latter kind of DMRG application in the general context of quantum chemistry.

Within the framework of the Born-Oppenheimer approximation, i.e., fixed nuclear positions, two major ways of determining the electronic properties of molecules are given by Hartree-Fock (HF) and post-HF calculations and density-functional theory. Density-functional theory is computationally rather inexpensive and well-suited to quick and quite reliable studies of medium-sized molecules, but is not overly precise, in particular for small molecules. Here, Hartree-Fock calculations, incorporating Fermi statistics exactly and electron-electron interactions on a mean-field level, provide good (initial) results and a starting point for further refinement, so-called post-HF calculations. Quantum chemistry DMRG is one such calculation.

For both the HF and post-HF calculations, one starts from a first-quantized Schrödinger equation (in atomic units) for the full molecule with N electrons; second quantization is achieved by introducing some suitably chosen basis set $\{|\varphi_i\rangle\}$. In this way, a general two-body interaction Hamiltonian as in Eq. (108) can be derived.

A HF calculation now solves this Hamiltonian at mean-field level, and it can be reexpressed in terms of the HF orbitals. A closed-shell singlet ground state is then simply given by

$$|\text{HF}\rangle = c^\dagger_{\uparrow 1} c^\dagger_{\downarrow 1} \cdots c^\dagger_{\uparrow N/2} c^\dagger_{\downarrow N/2} |0\rangle. \qquad (116)$$

Within standard quantum chemistry post-HF calculations, one improves now on this ground state by a plethora of methods. Simple approaches consist in diagonalizing in the subspace of one- or two-particle excited states; others choose a certain subset of electrons and diagonalize the Hamiltonian fully in one subset of orbitals for those (complete active space). Taking all electrons (excitations) and all orbitals into account, one obtains, within the originally chosen basis set, the exact many-body solution, known as the full configuration-interaction solution. While the approximate schemes typically scale as N^5 to N^7 in the number of orbitals, full configuration-interaction solutions demand exponential effort and are available only for some very small molecules.

From the DMRG point of view, determining the ground state of the full second-quantized Hamiltonian is formally equivalent to an application of the momentum-space DMRG, with some additional complications. As momentum conservation does not hold for V_{ijkl}, there are $O(N)$ more operators. Moreover, the basis set must be chosen carefully from a quantum chemist's point of view. As in momentum-space DMRG, a good sequence of the strongly different orbitals has to be established for DMRG treatment so that convergence is optimized. Also, an initial setup of blocks must be provided, including operators.

Orbital ordering in quantum chemistry turns out to be crucial to the performance of the method; a badly chosen ordering may lead to much slower convergence or even trapping in some higher-energy local minimum. The simplest information available, the HF energy and occupation of the orbitals, has been exploited by White and Martin (1999), Daul, Ciofini, *et al.* (2000), and Mitrushenkov *et al.* (2001, 2003) to enforce various orderings of the orbitals.

Chan and Head-Gordon (2002) have proposed the use of the symmetric reverse Cuthill-McKee reordering (Cuthill and McKee, 1969; Liu and Sherman, 1975), in which orbitals are reordered such that T_{ij} matrix elements above a certain threshold are as band diagonal as possible. This reduces effective interaction range, leading to faster convergence in M and reduced sweep number, as confirmed by Legeza *et al.* (2003b), who optimized the position of the Fock term $T_{ij} + \Sigma_{k\ \text{occupied}}(4V_{ikkj} - 2V_{ikjk})$ and reported reductions in M by a third or so.

Another approach exploits the short range of chemical interactions which in the basis of typically delocalized HF orbitals leads to a large effective range of interactions detrimental to DMRG. This may be reduced by changing to more localized orbitals. Orbital-localization techniques were first studied by Daul, Ciofini, *et al.* (2000), who applied a localization procedure (Pipek and Mezey, 1989) to the unoccupied orbitals to avoid increases in the starting configuration energy, but they did not find remarkable improvement over orderings of the unmodified HF orbitals.

Quantum information techniques have been used by Legeza and Sólyom (2003) both for momentum-space and quantum chemistry DMRG to devise optimal orderings. Studying various *ad hoc* orderings, they find fastest and most stable convergence under sweeping for those orderings that maximize entanglement entropy [Eq. (22)] between orbitals and the rest of the chain for orbitals at the chain center; orderings are hence chosen such that strongly entangled orbitals are brought to the chain center (often those closest to the Fermi surface). This ordering can be constructed iteratively, starting from a first guess as obtained by the Cuthill-McKee ordering.

Once the orbital ordering has been selected, current applications follow a variety of warmup procedures to build all sizes of blocks and to ensure that block states contain as many states as possible relevant for the final result. This may be done by augmenting the block being built by a toy environment block with some low-energy states that provide an environment compatible with the block, i.e., leading to the desired total quantum numbers (Chan and Head-Gordon, 2002), doing infinite-system DMRG on left and right blocks while also targeting excited states (Mitrushenkov *et al.*, 2001), and defining a minimum number of states to be kept even if the non-zero eigenvalues of the density matrix do not provide enough states (Legeza *et al.*, 2003a). Block-state choice can also be guided by entanglement entropy calculations (Legeza and Sólyom, 2003).

Various molecules have by now been studied using DMRG, both for equilibrium and out-of-equilibrium configurations, ground states, and excitations. H_2O has been serving as a benchmark in many quantum chemistry calculations and has been studied within various finite one-particle bases, more recently in the so-called double ζ polarized (DZP) basis (Bauschlicher and Taylor, 1986) with 8 electrons in 25 orbitals (and 2 "frozen" electrons in the 1s oxygen orbital) and the larger triple ζ plus double polarization (TZ2P) basis (Widmark *et al.*, 1990) of 10 electrons in 41 orbitals. While the larger basis will generally yield lower energies, one can compare how close various approximations come to an exact diagonalization (full configuration interaction if at all possible) solution within one particular basis set. In the smaller DZP basis, the exact ground-state energy is at $-76.256\,634$ H (Hartree). While the Hartree-Fock solution is several hundred mH above, and the single and double configuration-interaction solution about ten mH too high, and various coupled-cluster approximations (Bartlett *et al.*, 1990) are reaching chemical accuracy of 1 mH with errors between 4.1 and 0.2 mH, DMRG results of various groups (White and Martin, 1999; Daul, Ciofini, *et al.*, 2000; Chan and Head-Gordon, 2002) are better than 0.2 mH at $M \sim 400$, reaching an error of about 0.004 mH at $M \sim 900$ (Chan and Head-Gordon, 2002; Legeza *et al.*, 2003a). Moving to the larger TZ2P basis (Chan and Head-Gordon, 2003), in which there is no exact solution, accuracies of all methods are ranking similarly, with DMRG outperforming the best coupled-cluster results with an error of 0.019 mH at $M \sim 3000$

and reaching an error of 0.005 mH at $M \sim 5000$, with the extrapolated result being $-76.314\,715$ H. The comparison is even more favorable if the nuclei are arranged away from their equilibrium configuration.

Excellent performance is also observed in the extraction of dissociation energy curves for N_2 (Mitrushenkov *et al.*, 2001) and water (Mitrushenkov *et al.*, 2003).

Low-lying excited states have been studied for HHeH (Daul, Ciofini, *et al.*, 2000), CH_2 (Legeza *et al.*, 2003a), and LiF (Legeza *et al.*, 2003b); the latter case has provided a test system to study how efficiently methods map out the ionic-neutral crossover of this alkali halogenide for increasing bond length. With relatively modest numerical effort (M not in excess of 500 even at the computationally most expensive avoided crossing) relative errors of 10^{-9}, 10^{-7}, and 10^{-3} for the ground-state energy, first-excited-state energy, and the dipole moment compared to the full configuration-interaction solution (Bauschlicher and Langhoff, 1988) have been obtained. The dipole-moment precision increases by orders of magnitude away from the avoided crossing.

To assess the further potential of quantum chemistry DMRG for larger molecules and N orbital bases, it should be kept in mind that the generic N^4 scaling of the algorithm—which does compare extremely favorably with competing methods that scale as N^5 to N^7—is modified by several factors. On the one hand, for a given desired error in energy, various authors report, as for conventional DMRG, that $\delta E \sim \epsilon_\rho$, the truncated weight, which scales (Sec. III.B) as $\epsilon_\rho = \exp(-k \ln^2 M)$. k, however, shrinks with size in a model-dependent fashion, the most favorable case being that orbitals have essentially chainlike interactions with only a few nearest-neighbor orbitals. It may be more realistic to think about molecular orbitals as arranged on a quasi-one-dimensional strip of some width L related to the number of locally interacting orbitals; in that case, for standard strip geometries, the constant has been found to scale as L^{-1}. So N^4 scaling is in my view overly optimistic. On the other hand, on larger molecules orbital-localization techniques may be more powerful than on the small molecules studied so far, so that orbital interactions become much more sparse and scaling may actually improve.

One other possible way of improving the scaling properties of quantum chemistry DMRG might be the *canonical diagonalization approach* proposed by White (2002), which attempts to transform away numerically by a sequence of canonical basis transformations as many as possible of the nondiagonal matrix elements of the second-quantized Hamiltonian $\hat{H}$ of Eq. (108). This is done so that entire orbitals can be removed from $\hat{H}$, resulting in a new, smaller quantum chemistry problem in a different basis set, which may then be attacked by some DMRG technique like those outlined above. The removed orbitals, which are no longer identical with the original ones, are typically strongly overlapping with the energetically very high-lying and low-lying orbitals of the original problem that are almost filled or empty. Of course, these transformations cannot be carried out for

the exponentially large number of Hilbert-space states. White (2002) moves to the HF basis and carries out a particle-hole transformation; the canonical transformations are then carried out in the much smaller space of states not annihilated by one of the V_{ijkl} and formed by the minimum of creation operators from the HF vacuum (ground state). For example, the term $V_{ijkl} d_i^\dagger d_j d_k d_l$, where the $d_i^\dagger, d_i$ are particle-hole transformed fermionic operators, implies the consideration of the "left" state $d_i^\dagger |0\rangle$ with HF energy E_l and the "right" state $d_j^\dagger d_k^\dagger d_l^\dagger |0\rangle$ with HF energy E_r. In this smaller state space, a sequence of canonical basis transformations may be implemented as a differential equation, as originally proposed by Wegner (1994) as the *flow-equation method:* and Glazek and Wilson (1994) as *similarity renormalization*. With A some anti-Hermitian operator, a formal time dependence is introduced to the unitary transformation $\hat{H}(t) = \exp(tA)\hat{H}(0)\exp(-tA)$, where $\hat{H}(0)$ is the original Hamiltonian of Eq. (108) expressed in the HF basis. The corresponding differential equation,

$$\frac{d\hat{H}(t)}{dt} = [A, \hat{H}(t)], \tag{117}$$

is modified by making A time dependent itself. One now expands

$$\hat{H}(t) = \sum_\alpha a_\alpha(t) h_\alpha \tag{118}$$

and

$$A(t) = \sum_\alpha s_\alpha a_\alpha(t) h_\alpha, \tag{119}$$

where each h_α is the product of creation and annihilation operators and each s_α some constant yet to be chosen under the constraint of the anti-Hermiticity of A. To avoid operator algebra, White introduces

$$[h_\alpha, h_\beta] = \sum_\gamma B_{\alpha\beta}^\gamma h_\gamma, \tag{120}$$

where additional contributions to the commutator that cannot be expressed by one of the operator terms in Eq. (118) are suppressed; this eliminates three-body interactions generically generated by the transformation and not present in the original Hamiltonian. Then Eq. (117), with A time dependent, reduces to a set of differential equations,

$$\frac{da_\gamma(t)}{dt} = \sum_{\alpha\beta} B_{\alpha\beta}^\gamma s_\alpha a_\alpha(t) a_\beta(t), \tag{121}$$

that can now be integrated numerically up to some time t. It can now be shown that the goal of diminishing $a_\alpha(t)$ for all nondiagonal contributions to $\hat{H}$ can be achieved efficiently by setting

$$s_\alpha = (E_l - E_r)^{-1}, \tag{122}$$

where E_l and E_r are the HF energies of the left and right HF orbitals in h_α. Stopping after some finite time t, one

can now remove orbitals (e.g., with the lowest occupancy, that is, almost full or empty before the particle-hole transformation) and use DMRG for the full many-body problem in the reduced orbital space. White (2002) finds this approach to yield very good results as compared to full configuration-interaction calculations for a stretched water molecule, but as of now the full potential of the method remains unexplored.

To conclude, in my opinion DMRG has been established as a competitive method with essentially the same quality as the full configuration-interaction method in quantum chemistry and should be taken seriously. However, efficient geometrical optimization techniques to determine lowest-energy molecular geometries are still lacking.

C. DMRG for small grains and nuclear physics

Let us reconsider the generic Hamiltonian of Eq. (108), where energy levels above and below the Fermi energy are ordered in ascending fashion and where a simple model interaction is chosen. This Hamiltonian can then be treated in the following so-called particle-hole reformulation of infinite-system real-space DMRG (Dukelsky and Sierra, 1999, 2000): Starting from two initial blocks from a small number of states, one (hole block) from the lowest unoccupied one-particle levels above the Fermi energy and the other (particle block) from the highest occupied one-particle levels below, we iteratively add further states to particle and hole blocks, moving away from the Fermi surface, determine the ground state, and in the usual DMRG procedure calculate density matrices and the reduced basis transformations by tracing out particle and hole states, respectively. This approach may work if there is a clear physical reason that states far away from the Fermi surface will hardly influence low-energy physics and if interactions show translational invariance in energy space; otherwise the infinite-system algorithm should fail. The advantage of such simple models is that much larger systems can be treated than in quantum chemistry.

A model Hamiltonian which happens to combine both features is the reduced BCS Hamiltonian

$$\hat{H}_{\text{BCS}} = \sum_{j\sigma} (\epsilon_j - \mu) c_{j\sigma}^\dagger c_{j\sigma} - \lambda d \sum_{ij} c_{i\uparrow}^\dagger c_{i\downarrow}^\dagger c_{j\downarrow} c_{j\uparrow}, \qquad (123)$$

where DMRG has been able to definitely settle long-standing questions (Dukelsky and Sierra, 1999, 2000; Dukelsky and Pittel, 2001) on the nature of the breakdown of BCS superconductivity in small grains, expected when the level spacing d in the finite system becomes of the order of the BCS gap Δ (Anderson, 1959). DMRG has conclusively shown that there is a smooth crossover between a normal and a superconducting regime in the pairing order parameter and other quantities, in contradiction to analytical approaches indicating a sharp crossover. This approach to DMRG has been extended to the study of the Josephson effect between superconducting nanograins with discrete energy levels (Gobert, Schollwöck, and von Delft, 2004) and to the

observation and calculation of well-defined quasiparticle excitations in small interacting disordered systems with high dimensionless conductance g (Gobert, Schechter, *et al.*, 2004).

Particle-hole DMRG has also been applied successfully in nuclear physics (Dukelsky and Pittel, 2001; Dimitrova *et al.*, 2002; Dukelsky *et al.*, 2002) in the framework of the nuclear shell model, in which a nucleus is modeled by core orbitals completely filled with neutrons and protons (a "doubly magic core") and valence orbitals partially filled with nucleons. The core is considered inert, and, starting from some Hartree-Fock-level orbital configuration for the valence nucleons, a two-body Hamiltonian for these nucleons is solved using the particle-hole method. This is conceptually very similar to the post-HF approaches of quantum chemistry, with model interactions for the nucleons as they are not so precisely known, such as pairing interactions, quadrupolar interactions, and the like.

This approach has been very successful for nucleons in very large angular momentum shells interacting through a pairing and a quadrupolar force in an oblate nucleus (Dukelsky and Pittel, 2001), with up to 20 particles of angular momentum $j=55/2$, obtaining energies converged up to 10^{-6} for $M=60$; for 40 nucleons of $j=99/2$, four-digit precision was possible; in this case, 38% of energy was contained in the correlations (Dukelsky *et al.*, 2002). For more realistic calculations of the nucleus ^{24}Mg, with four neutrons and four protons outside the doubly magic ^{16}O core, convergence in M was so slow that almost the complete Hilbert space had to be considered for good convergence (Dimitrova *et al.*, 2002). The fundamental drawback of the particle-hole approach is that it does not allow for an easy implementation of the finite-system algorithm (levels far away from the Fermi surface hardly couple to the system, giving little relevant information via the density matrix) and that angular momentum conservation is not exploited. Pittel *et al.* (2003) are currently aiming at implementing an algorithm for nuclei using angular momentum, circumventing these difficulties (see also Dukelsky and Pittel, 2004).

VIII. TRANSFER-MATRIX DMRG: CLASSICAL AND QUANTUM SYSTEMS

Conventional DMRG is essentially restricted to $T=0$ calculations, with some computationally expensive forays into the very-low-temperature regimes possible (Moukouri and Caron, 1996; Batista *et al.*, 1998; Hallberg *et al.*, 1999). Decisive progress was made by Nishino (1995), who realized that the DMRG idea could also be used for the decimation of transfer matrices, leading to the name of *transfer-matrix renormalization group* (TMRG). This opened the way to DMRG studies of classical statistical mechanics at finite temperature for systems on two-dimensional $L \times \infty$ strips. If one applies the generic mapping of d-dimensional quantum systems at finite temperature to $(d+1)$-dimensional classical sys-

tems, TMRG also permits study of thermodynamic properties of one-dimensional quantum systems at finite temperature.

A. Classical transfer-matrix DMRG in two dimensions: TMRG

Consider the textbook transfer-matrix method for a one-dimensional classical system with Hamiltonian $\hat{H}$ and N_{site} states $|\sigma_i\rangle$ on each site i, e.g., the Ising model. Assuming nearest-neighbor interactions, one performs a local decomposition of the Hamiltonian $\hat{H} = \Sigma \hat{h}_i$, where each $\hat{h}_i$ contains the interaction between sites i and $i+1$. Taking the partition function of a system of length N with periodic boundary conditions,

$$Z_L = \mathrm{Tr}\, e^{-\beta\mathcal{H}} = \mathrm{Tr}\, e^{-\Sigma_{i=1}^{N}\beta\hat{h}_i}, \tag{124}$$

and inserting identities $\Sigma_{\sigma_i}|\sigma_i\rangle\langle\sigma_i|$, one obtains for a translationally invariant system $Z_L = \mathrm{Tr}\,\mathcal{T}^N$, where the $N_{site} \times N_{site}$ transfer matrix $\mathcal{T}$ reads

$$\langle\sigma_i|\mathcal{T}|\sigma_{i+1}\rangle = \langle\sigma_i|e^{-\beta h_i}|\sigma_{i+1}\rangle.$$

From this, one deduces for $N\to\infty$ the free energy per site $f = -k_B T \ln \lambda_1[\mathcal{T}]$, where λ_1 is the largest eigenvalue of $\mathcal{T}$, from which all thermodynamic properties follow.

Moving now to a two-dimensional geometry, on a strip of dimension $L\times N$ with a short-ranged Hamiltonian, the transfer-matrix method may be applied in the limit $N\to\infty$ for some finite width $L\ll N$, treating a row of L sites as one big site; transfer-matrix size then grows as N_{site}^L, strongly limiting this approach in complete analogy to the exact diagonalization of quantum Hamiltonians. Hence (Fig. 22) the first dimension, with finite system length L, is attacked by DMRG applied to the transfer instead of the Hamiltonian matrix, to keep transfer-matrix size finite and sufficiently small by decimation, while retaining the most important information. Results are extrapolated to infinite size. The second dimension, with infinite system length, is accounted for by the one-dimensional transfer-matrix method.

To prove that this concept works, i.e., that an optimal decimation principle can be set up for transfer matrices in analogy to the case made for Hamiltonians, consider a short-ranged classical Hamiltonian at $T>0$ on a $L\times N$ strip, where $N\to\infty$. We now define an unnormalized density matrix $\hat{\rho}_u = e^{-\beta\hat{H}}$ (in reality an evolution operator) by

$$\langle\tilde{\boldsymbol{\sigma}}|\hat{\rho}_u|\boldsymbol{\sigma}\rangle = \langle\tilde{\boldsymbol{\sigma}}|[\mathcal{T}^{(L)}]^N|\boldsymbol{\sigma}\rangle, \tag{125}$$

where $\tilde{\boldsymbol{\sigma}}$ and $\boldsymbol{\sigma}$ label states of the L sites on top and bottom of the strip. $\mathcal{T}^{(L)}$ is the band transfer matrix of Fig. 22. The partition function $Z = \mathrm{Tr}\,\hat{\rho}_u$ is then given as

$$Z = \sum_{i=1}^{N_{site}^L} \lambda_i^N, \tag{126}$$

where $\lambda_1 > \lambda_2 \geqslant \cdots$ are the eigenvalues of $\mathcal{T}^{(L)}$; the largest being positive and nondegenerate for positive Boltzmann weights, partition function and unnormalized density matrix simplify in the thermodynamic limit $N\to\infty$ to

$$Z = \lambda_1^N \tag{127}$$

and

$$\hat{\rho}_u = \lambda_1^N|\lambda_1\rangle\langle\lambda_1|, \tag{128}$$

where $|\lambda_1\rangle$ is the normalized eigenvector of the largest transfer-matrix eigenvalue.

Consider now Fig. 23. The unnormalized density matrix has exactly the same form, up to the prefactor, of the pure-state projector of standard DMRG, with $|\lambda_1\rangle$ assuming the role of the target state there. Tracing out the right "environment" half, the left "system" unnormalized reduced density matrix is given by

$$\hat{\rho}_{uS} = \mathrm{Tr}_E \lambda_1^N|\lambda_1\rangle\langle\lambda_1| = \lambda_1^N \sum_{\alpha=1}^{N_{site}^{L/2}} w_\alpha|w_\alpha\rangle\langle w_\alpha|, \tag{129}$$

where w_α are the positive eigenvalues to the normalized eigenvectors $|w_\alpha\rangle$ of the reduced system density matrix; $\Sigma_\alpha w_\alpha = 1$. Completing the partial trace, one finds

$$Z = \mathrm{Tr}_S \hat{\rho}_{uS} = \lambda_1^N \sum_{\alpha=1}^{N_{site}^{L/2}} w_\alpha, \tag{130}$$

so that indeed the best approximation to Z is obtained by retaining in a reduced basis the eigenvectors to the largest eigenvalues w_α as in conventional DMRG.

Let us explain the DMRG transfer-matrix renormalization (Nishino, 1995) in more detail. Because the transfer matrix factorizes into local transfer matrices, some minor modifications of the standard DMRG approach are convenient. Assume as given an $M\times M$ transfer matrix of a system of length L,

$$\langle m\sigma|\mathcal{T}^{(L)}|\tilde{m}\tilde{\sigma}\rangle, \tag{131}$$

where the sites at the active (growth) end are kept explicitly as opposed to standard DMRG, and $|m\rangle, |\tilde{m}\rangle$ are block states (Fig. 24). Considering now the superblock of length $2L$, we see that the transfer matrix reads

$$\langle m^S\sigma^S\sigma^E m^E|\mathcal{T}^{(2L)}|\tilde{m}^S\tilde{\sigma}^S\tilde{\sigma}^E\tilde{m}^E\rangle$$
$$= \langle m^S\sigma^S|\mathcal{T}^{(L)}|\tilde{m}^S\tilde{\sigma}^S\rangle\langle\sigma^S\sigma^E|\mathcal{T}^{(2)}|\tilde{\sigma}^S\tilde{\sigma}^E\rangle$$
$$\times\langle m^E\sigma^E|\mathcal{T}^{(L)}|\tilde{m}^E\tilde{\sigma}^E\rangle. \tag{132}$$

Lanczos diagonalization yields the eigenvector of $\mathcal{T}^{(2L)}$ to the maximum eigenvalue λ_1. Again in some analogy to conventional DMRG, the fact that the transfer matrix is a product can be used to speed up calculations by decomposing $|\phi\rangle = \mathcal{T}^{(2L)}|\psi\rangle$ into three successive multiplications, $|\phi\rangle = \mathcal{T}^{(L)}[\mathcal{T}^{(2)}(\mathcal{T}^{(L)}|\psi\rangle)]$.

The obtained eigenvector now yields the reduced density matrices and the reduced basis transformations. The last step is to build the $MN_{\text{site}} \times MN_{\text{site}}$ transfer matrix for a system of length $L+1$ (Fig. 25):

$$\langle m\sigma | \mathcal{T}^{(L+1)} | \tilde{m}\tilde{\sigma} \rangle = \sum_{n\tilde{n}\tau\tilde{\tau}} \langle m | n\tau \rangle \langle n\tau | \mathcal{T}^{(L)} | \tilde{n}\tilde{\tau} \rangle \langle \tau\sigma | \mathcal{T}^{(2)} | \tilde{\tau}\tilde{\sigma} \rangle$$

$$\times \langle \tilde{n}\tilde{\tau} | \tilde{m} \rangle. \tag{133}$$

The TMRG procedure is repeated up to the desired final length, the free energy then obtained from λ_1; this allows the calculation of all thermodynamic quantities through numerical differentiation of the free energy. To avoid numerically unstable second derivatives for specific heat and susceptibility, it is convenient to consider the first-order derivative of the average energy extracted from expectation values such as $\langle \sigma_i \sigma_j \rangle = \langle \lambda_1 | \sigma_i \sigma_j | \lambda_1 \rangle$ obtained by replacements $e^{-\beta \hat{h}_i} \rightarrow \sigma_i e^{-\beta \hat{h}_i}$ in the above calculations. At the same time, correlation lengths may be extracted both from these expectation values or from the two leading transfer-matrix eigenvalues,

$$\xi = -1/\ln \operatorname{Re}(\lambda_2/\lambda_1). \tag{134}$$

To refine results, a finite-system calculation can be set up as in conventional DMRG. A main technical difference between conventional DMRG and classical transfer-matrix DMRG is the absence of good quantum numbers, which simplifies the algorithm but is hard on computational resources.

A large body of work has emerged that strongly relies on the finite strip width provided by the TMRG, studying competing bulk and surface effects in two-dimensional Ising models on a $L \times \infty$ strip. The confined Ising model has been used to model two coexisting phases in the presence of bulk and surface fields, as well as gravity, in order to model wetting and coexistence phenomena and the competition of bulk and surface effects in finite geometries. In the case of opposing surface fields favoring phase coexistence at zero bulk field up to some temperature that (unintuitively) goes to the wetting temperature for $L \rightarrow \infty$ (Parry and Evans, 1990), it could be shown that gravity along the finite-width direction suppresses fluctuations such that it restores the bulk critical temperature as limiting temperature for coexistence (Carlon and Drzewiński, 1997, 1998). These studies were extended to the competition of surface and bulk fields (Drzewiński *et al.*, 1998). Further studies elucidated finite-size corrections to the Kelvin equation at complete wetting for parallel surface and bulk fields (Carlon *et al.*, 1998), the nature of coexisting excited states (Drzewiński, 2000), the scaling of cumulant ratios (Drzewiński and Wojtkiewicz, 2000), and an analysis of the confined Ising model at and near criticality for competing surface and bulk fields (Maciołek, Drzewiński, and Ciach, 2001; Maciołek, Drzewiński, and Evans, 2001). In the case of the Potts model with $Q > 4$, where there is a first-order phase transition in the bulk (Baxter, 1982) but a second-order phase transition at the surface (Lipowsky, 1982), TMRG permitted the extraction of
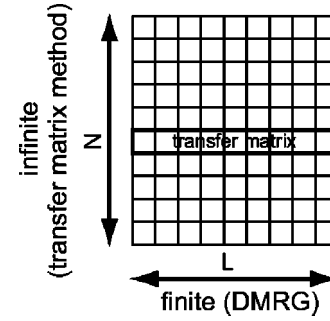

FIG. 22. Strategy for the DMRG treatment of two-dimensional classical systems.

surface critical exponents that demonstrate the Q independence of the universality class of the surface transition (Igloi and Carlon, 1999).

TMRG has also been used to study critical properties of truly two-dimensional classical systems (Honda and Horiguchi, 1997; Tsushima *et al.*, 1997; Carlon, Chatelain, and Berche, 1999; Sato and Sasaki, 2000), such as the spin-3/2 Ising model on a square lattice (Tsushima *et al.*, 1997), the Ising model with line defects (Chung *et al.*, 2000), the three-state chiral clock model as example of a commensurate-incommensurate phase transition (Sato and Sasaki, 2000), the 19-vertex model in two dimensions as a discrete version of the continuous *XY* model to study the Kosterlitz-Thouless phase transition (Honda and Horiguchi, 1997), and the random exchange-coupling classical Q-state Potts model which was demonstrated to have critical properties independent of Q (Carlon, Chatelain, and Berche, 1999). Lay and Rudnick (2002) have used the TMRG to study a continuous Ginzburg-Landau field-theory formulation of the two-dimensional Ising model by retaining the largest eigenvalue eigenfunctions of bond transfer matrices as state space.

Gendiar and Surda (2000) have extended the TMRG to periodic boundary conditions to obtain, at the expense of the expected lower DMRG precision much better thermodynamic-limit scaling behavior for $L \rightarrow \infty$. Critical temperature and thermal and magnetic critical exponents of the two-dimensional Ising model are all extracted with modest computational effort at a staggering six- to seven-digit precision compared to the Onsager solution.

B. Corner transfer-matrix DMRG: An alternative approach

Following Baxter (1982), one may conclude that the essential aspect of the reduced density-matrix is that it represents a half cut in the setup of Fig. 23 whose spatial extension is to be taken to the thermodynamic limit. The same setup can be obtained considering the geometry of Fig. 26, where four *corner transfer matrices* are defined as
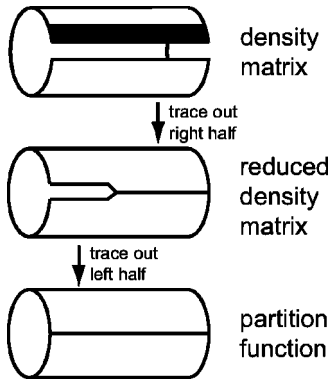
FIG. 23. Pictorial representation of the partition function, the (unnormalized) density matrix, and the reduced density matrix for a two-dimensional classical system on a strip geometry. The black stripe represents a band transfer matrix. Adapted from Nishino in Peschel, Hallberg, *et al.*, 1999.

$$\langle \boldsymbol{\sigma}' | C^{(L)} | \boldsymbol{\sigma} \rangle = \sum_{\boldsymbol{\sigma}_{\text{int}}} \prod_{\langle ijkl \rangle} \langle \sigma_i \sigma_j | \mathcal{T}^{(2)} | \sigma_k \sigma_l \rangle, \tag{135}$$

where the product runs over all site plaquettes and the sum over all internal site configurations, i.e., the states on the sites linking to neighboring corner transfer matrices are kept fixed. The corner-site state is invariant under application of the these matrices. The unnormalized reduced density matrix is then given by

$$\langle \boldsymbol{\sigma}^{(5)} | \hat{\rho}_u | \boldsymbol{\sigma}^{(1)} \rangle = \sum_{\boldsymbol{\sigma}^{(4)} \boldsymbol{\sigma}^{(3)} \boldsymbol{\sigma}^{(2)}} \langle \boldsymbol{\sigma}^{(5)} | C^{(L)} | \boldsymbol{\sigma}^{(4)} \rangle \langle \boldsymbol{\sigma}^{(4)} | C^{(L)} | \boldsymbol{\sigma}^{(3)} \rangle$$
$$\times \langle \boldsymbol{\sigma}^{(3)} | C^{(L)} | \boldsymbol{\sigma}^{(2)} \rangle \langle \boldsymbol{\sigma}^{(2)} | C^{(L)} | \boldsymbol{\sigma}^{(1)} \rangle \tag{136}$$

with the center site fixed. Diagonalizing $C^{(L)}$, and obtaining eigenvalues λ_i and eigenvectors $|\lambda_i\rangle$, we see that the reduced density matrix $\hat{\rho}_u(L)$ then reads

$$\hat{\rho}_u(L) = \sum_i \lambda_i^4 |\lambda_i\rangle\langle\lambda_i| \tag{137}$$

and the partition function, obtained by tracing out the reduced density matrix, is

$$Z(L) \sum_i \lambda_i^4. \tag{138}$$

Following the argument for classical TMRG, Nishino and Okunishi (1996) have introduced the *corner transfer-matrix renormalization group*. A sequence of increasingly large corner transfer matrices is built (Fig. 27) as

$$\langle m\sigma\sigma^C | C^{(L+1)} | \tilde{m}\tilde{\sigma}\sigma^C \rangle = \sum_{n\tilde{n}\tau^C} \langle \sigma\sigma^C | \mathcal{T}^{(2)} | \tau^C \tilde{\sigma} \rangle$$
$$\times \langle n\tau^C | C^{(L)} | \tilde{n}\tau^C \rangle$$
$$\times \langle m\sigma | \mathcal{T}^{(L)} | n\tau^C \rangle$$
$$\times \langle \tilde{n}\tau^C | \mathcal{T}^{(L)} | \tilde{m}\tilde{\sigma} \rangle, \tag{139}$$

where previous reduced basis transformations are supposed to have taken place for $C^{(L)}$ and $\mathcal{T}^{(L)}$. Similarly, $\mathcal{T}^{(L+1)}$ is built as in classical TMRG. Diagonalizing $C^{(L+1)}$ yields eigenvalues λ_i and associated eigenvectors, the M
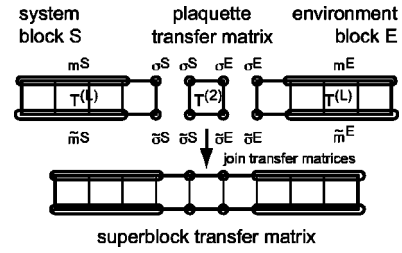
FIG. 24. Transfer-matrix DMRG step.

most important of which define the reduced basis transformation. This reduced basis transformation is then carried out on $\mathcal{T}^{(L+1)}$ and $C^{(L+1)}$, completing one corner TMRG step. The crucial advantage of this algorithm is that it completely avoids the diagonalization of some large sparse matrix.

The corner TMRG allows us to calculate quantities similar to TMRG, all thermodynamic variables as some derivative of the free energy or using local expectation values. For the two-dimensional Ising model, Nishino and Okunishi (1997) obtained Ising critical exponents at four-digit precision, using systems of up to $L=20\,000$. For the $Q=5$ two-dimensional Potts model, which has a very weak first-order transition, they could determine the latent heat $\mathcal{L} \approx 0.027$ compared to an exact $\mathcal{L} =0.0265$ (Baxter, 1982), which is hard to see in Monte Carlo simulations due to metastability problems. Other applications have considered the spin-3/2 Ising model (Tsushima and Horiguchi, 1998) and a vertex model with seven vertex configurations, modeling an order-disorder transition (Takasaki *et al.*, 2001). More recent extensions study self-avoiding-walk models in two dimensions (Foster and Pinettes, 2003a, 2003b).

One may also generalize the corner TMRG to three-dimensional classical models (Nishino and Okunishi, 1998). While the implementation is cumbersome, the idea is simple: the semi-infinite cut line in the plane leading to four corner matrices gives way to a semi-infinite cut plane in some volume leading to eight corner tensors, two of which have an open side. Growing these corner tensors involves concurrent growing of corner matrices, band transfer matrices, and plaquette transfer
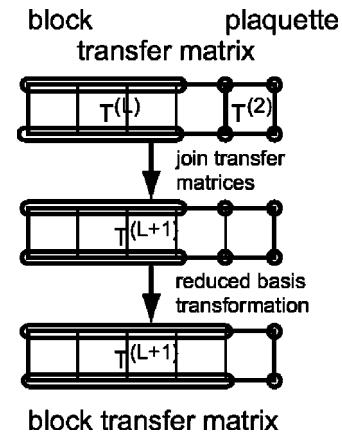

FIG. 25. Construction of the enlarged transfer matrix.

matrices. Numerical results, however, indicate clear practical limitations of the concept.

C. Quantum statistical mechanics in one dimension: Quantum TMRG

It is now straightforward—at least in principle—to extend classical TMRG to the calculation of the thermodynamics of one-dimensional quantum systems due to the general relationship between d-dimensional quantum and $(d+1)$-dimensional classical problems. This approach was first used by Bursill *et al.* (1996) and fully developed by Wang and Xiang (1997) as well as by Shibata (1997). To appreciate the following, it is best to visualize quantum TMRG as an extension of the quantum transfer-matrix method (Betsuyaku, 1984, 1985) in the same way conventional DMRG extends exact diagonalization.

Consider the mapping of one-dimensional quantum systems to two-dimensional classical systems, as used in the quantum transfer-matrix and quantum Monte Carlo (Suzuki, 1976) methods: Assume a Hamiltonian that contains nearest-neighbor interactions only and is invariant under translations by an even number of sites. We now introduce the well-known checkerboard decomposition (Suzuki, 1976) $\hat{H} = \hat{H}_1 + \hat{H}_2$. $\hat{H}_1 = \sum_{i=1}^{N/2} \hat{h}_{2i-1}$ and $\hat{H}_2 = \sum_{i=1}^{N/2} \hat{h}_{2i}$. Here $\hat{h}_i$ is the local Hamiltonian linking sites i and $i+1$; neighboring local Hamiltonians will in general not commute, hence $[\hat{H}_1, \hat{H}_2] \neq 0$. However, all terms in $\hat{H}_1$ or $\hat{H}_2$ commute. N is the system size in real space (which we shall take to infinity).

Following Trotter (1959), we consider a sequence of approximate partition functions

$$Z_L := \mathrm{Tr}(e^{-\beta H_1/L} e^{-\beta H_2/L})^L, \tag{140}$$

with Trotter number L. Then

$$Z = \lim_{L \to \infty} Z_L \tag{141}$$

holds: quantum effects are suppressed as neglected commutators between local Hamiltonians scale as $(\beta/L)^2$.

One now expands $\hat{H}_1$ and $\hat{H}_2$ in the exponentials of Z_L in Eq. (140) into the sums of local Hamiltonians and inserts $2L+1$ times the identity decomposition

$$\mathbb{1} = \prod_{i=1}^{N} \left(\sum_{\sigma_i} |\sigma_i\rangle\langle\sigma_i| \right), \tag{142}$$

sandwiching each exponential. Introducing an additional label j for the identity decompositions, we find $(2L+1) \times N$ sites, of which each site carries two labels, corresponding to two dimensions, the real-space coordinate (subscript) i and the Trotter-space (imaginary-time) coordinate (superscript) j. Thinking of both coordinates as spatial, one obtains a two-dimensional lattice of dimension $(2L+1) \times N$, for which the approximate partition function Z_L reads
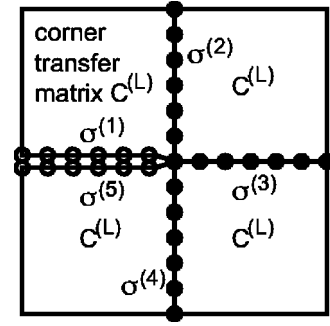

FIG. 26. Corner transfer-matrix setup for the calculation of reduced density matrices and partition functions in two-dimensional classical models.

$$Z_L = \mathrm{Tr} \prod_{i=1}^{N/2} \prod_{j=1}^{L} \langle \sigma_{2i-1}^{2j+1} \sigma_{2i}^{2j+1} | e^{-\beta h_{2i-1}/L} | \sigma_{2i-1}^{2j} \sigma_{2i}^{2j} \rangle$$
$$\times \langle \sigma_{2i}^{2j} \sigma_{2i+1}^{2j} | e^{-\beta h_{2i}/L} | \sigma_{2i}^{2j-1} \sigma_{2i+1}^{2j-1} \rangle.$$

Figure 28 shows that as in a checkerboard only every second plaquette of the two-dimensional lattice is active (i.e., black). To evaluate Z_L the trace is taken over all local states of the $(2L+1) \times N$ sites, while noting that the trace in Eq. (140) enforces periodic boundary conditions along the imaginary-time direction, $|\sigma_i^1\rangle = |\sigma_i^{2L+1}\rangle$. Nothing specific needs to be assumed about boundary conditions along the real-space direction. Note that the orientation of the transfer matrix has changed compared to Fig. 22.

Working backward from the partition function Z_L, we can now identify transfer and density matrices. Introducing a local transfer matrix as $\hat{\tau}_k = \exp(-\beta h_k/L)$, and exploiting the assumed restricted translational invariance, we find that the global transfer matrices

$$\langle \sigma^1 \cdots \sigma^{2L+1} | \mathcal{T}_1^{(2L+1)} | \nu^1 \cdots \nu^{2L+1} \rangle$$
$$= \prod_{j=1}^{L} \langle \sigma^{2j+1} \nu^{2j+1} | \hat{\tau}_1 | \sigma^{2j} \nu^{2j} \rangle,$$

$$\langle \nu^1 \cdots \nu^{2L+1} | \mathcal{T}_2^{(2L+1)} | \tau^1 \cdots \tau^{2L+1} \rangle$$
$$= \prod_{j=1}^{L} \langle \nu^{2j} \tau^{2j} | \hat{\tau}_2 | \nu^{2j-1} \tau^{2j-1} \rangle$$

can be defined (see Fig. 28), representing odd and even bonds on the chain because of the alternating checkerboard decomposition. The local transfer matrices are linking the states of two sites at different Trotter times and are evaluated using the Trotter-time-independent eigenbasis of the local Hamiltonian, $\hat{h}|i\rangle = E_i|i\rangle$:

$$e^{-\beta\hat{h}/L} = \sum_i e^{-\beta E_i/L} |i\rangle\langle i|. \tag{143}$$

Summing over all internal degrees of freedom $|\nu^j\rangle$, we obtain matrix elements
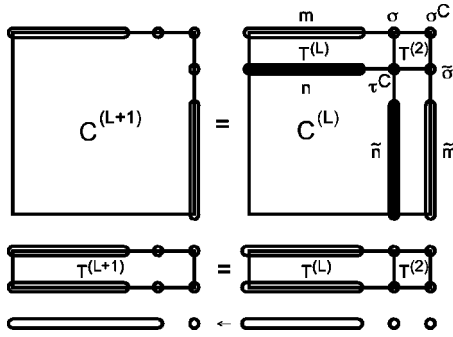
FIG. 27. Corner transfer-matrix growth using band and plaquette transfer matrices. Solid states are summed over.

$$\langle \sigma^1 \cdots \sigma^{2L+1} | \mathcal{T}_1 \mathcal{T}_2 | \tau^1 \cdots \tau^{2L+1} \rangle. \tag{144}$$

Using the global transfer matrices, the unnormalized density matrix reads

$$\hat{\rho}_{uL} = [\mathcal{T}_1 \mathcal{T}_2]^{N/2} \tag{145}$$

and

$$Z_L = \mathrm{Tr}[\mathcal{T}_1 \mathcal{T}_2]^{N/2}, \tag{146}$$

somewhat modified from the classical TMRG expression.

As $Z_L = \lambda_1^{N/2} + \lambda_2^{N/2} + \cdots$, where λ_i are the eigenvalues of $\mathcal{T}_1 \mathcal{T}_2$, the largest eigenvalue λ_1 of $\mathcal{T}_1 \mathcal{T}_2$ dominates in the thermodynamic limit $N \to \infty$. The density matrix simplifies to

$$\hat{\rho}_{uL} = \lambda_1^{N/2} |\psi_R\rangle\langle\psi_L|, \tag{147}$$

where $\langle\psi_L|$ and $|\psi_R\rangle$ are the left and right eigenvectors to eigenvalue λ_1. Due to the checkerboard decomposition, the transfer matrix $\mathcal{T}_1 \mathcal{T}_2$ is nonsymmetric, so that left and right eigenvectors are not identical. Normalization to $\langle\psi_L|\psi_R\rangle = 1$ is assumed. The free energy per site is given as

$$f_L = -\frac{1}{2} k_B T \ln \lambda_1. \tag{148}$$

If Z_L (i.e., the eigenvalue λ_1) is calculated exactly, computational effort scales exponentially with L as in exact diagonalization. As the errors scale as $(\beta/L)^2$, reliable calculations are restricted to small β, and the interesting low-temperature limit is inaccessible. Instead, one can adopt the classical TMRG on the checkerboard transfer matrix to access large L, hence low temperatures.

Conceptually, the main steps of the algorithm are unchanged from the classical case and the argument for the optimality of the decimation procedure is unchanged. Explicit construction and decimation formulas are, however, slightly changed from the classical case and are much more complicated notationally because of the checkerboard decomposition (see Wang and Xiang, 1997 and Shibata, 1997, 2003).

At the start, the transfer matrix $\mathcal{T}^{(3)}$ of two plaquettes is given by (Fig. 29)

$$\mathcal{T}^{(3)}(\sigma_1^3\sigma_2^3; \sigma_1^2\sigma_3^2; \sigma_2^1\sigma_3^1)$$
$$= \sum_{\sigma_2^2} \langle \sigma_1^3\sigma_2^3 | \hat{\tau}_1 | \sigma_1^2\sigma_2^2 \rangle \langle \sigma_2^2\sigma_3^3 | \hat{\tau}_2 | \sigma_2^1\sigma_3^1 \rangle. \tag{149}$$

The addition of plaquettes follows a zigzag pattern. Let us consider just the case in which the transfer matrix grows to comprise an even number of plaquettes. This number is L. Then the growth formula reads (Fig. 29)

$$\mathcal{T}^{(L+1)}(\sigma_1^{L+1}\sigma_2^{L+1}; m_1\sigma_1^L m_3\sigma_3^L; \sigma_2^1\sigma_3^1)$$
$$= \sum_{\sigma_2^L} \langle \sigma_1^{L+1}\sigma_2^{L+1} | \hat{\tau}_1 | \sigma_1^L\sigma_2^L \rangle \mathcal{T}^{(L)}(\sigma_2^L\sigma_3^L; m_1 m_3; \sigma_2^1\sigma_3^1).$$

I distinguish between inner and outer states, the outer states being those of the first and last row of the transfer matrix. For the inner states, the compound notation m_1 and m_3 indicates that they may have been subject to a reduced basis transformation beforehand. If the number of states $m_1\sigma_1^L$ and $m_3\sigma_3^L$ is in excess of the number of states to be kept, a reduced basis transformation is carried out, $m_1\sigma_1^L \to \tilde{m}_1$ and $m_3\sigma_3^L \to \tilde{m}_3$, using the reduced basis transformation as obtained in the previous superblock diagonalization.

The superblock transfer matrix of $2L$ plaquettes is now formed from the product of two such $\mathcal{T}^{(L+1)}$, summing over states $\sigma_2^1 \equiv \sigma_2^{2L+1}$ and σ_2^{L+1} (Fig. 30). This superblock transfer matrix is diagonalized using some large sparse eigensolver to get the maximum eigenvalue λ_1 and the right and left eigenvectors $\langle\psi_L|$ and $|\psi_R\rangle$, which may be chosen mutually biorthonormal; $\langle\psi_L|\psi_R\rangle = 1$. In view of the possible need for a reduced basis transformation in the next step, nonsymmetric reduced density matrices are formed,

$$\hat{\rho} = \mathrm{Tr}|\psi_R\rangle\langle\psi_L|, \tag{150}$$

where the trace is over all states in columns 1 and 3 except $\tilde{m}^1$, $\tilde{m}^3$, σ_1^{L+1}, and σ_3^{L+1}, as they are the states subject to a subsequent reduced basis transformation. Row and column matrices of the M left and right eigenvectors with highest eigenvalue weight yield the transformation matrices for left and right basis states, i.e., in columns 1 and 3. This construction implies that basis vectors $\langle m_1|$ and $|m_3\rangle$ will also be biorthonormal. The procedure is repeated until the system has reached the desired final size of $2L_{\max}$ plaquettes.

Several technical issues have to be discussed for quantum TMRG. An important reduction of the computational load comes from the existence of modified good quantum numbers derived from conservation laws of the underlying Hamiltonian. Their existence was already observed in the quantum transfer-matrix method (Nomura and Yamada, 1991): The action of a local magnetization-conserving Hamiltonian in Trotter direction between imaginary times j and $j+1$ obeys $[S_1^{j+1}]^z + [S_2^{j+1}]^z = [S_1^j]^z + [S_2^j]^z$ or $[S_1^{j+1}]^z - [S_1^j]^z = -[S_2^{j+1}]^z + [S_2^j]^z$. This generalizes to $\Sigma_j(-1)^j[S_1^j]^z = -\Sigma_j(-1)^j[S_2^j]^z$. Thus the staggered magnetization, summed in the Trotter direction, is a conserved quantity, i.e., constant along the real-space axis:
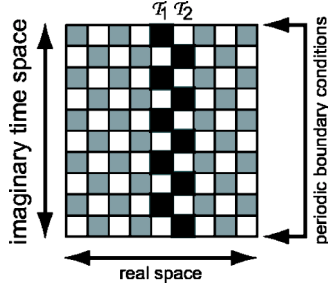
FIG. 28. Checkerboard decomposition: active vs inactive plaquettes of the two-dimensional effective classical model.

$$Q = \sum_{j=1}^{2L} (-1)^{i+j} [S_i^j]^z = \text{cst.} \tag{151}$$

In fermionic systems, particle number conservation implies that $P = \Sigma_{j=1}^{2L} (-1)^{i+j} n_i^j$ is an additional good quantum number (Shibata and Tsunetsugu, 1999a). As in $T=0$ DMRG, the good quantum numbers are conserved by the DMRG decimation process. Moreover, the eigenstate with the maximum eigenvalue is always in the subspace $Q=0$ (or $P=0$, respectively): Thermodynamic quantities are independent of boundary conditions in high-temperature phases, which are found for all finite temperatures in one dimension. For open boundary conditions in real space, the lack of an update at the open ends at every second Trotter time step implies the subtraction of equal quantities when forming Q, leading to $Q=0$.

An important technical complication occurs because the transfer matrices to be diagonalized are asymmetric due to the checkerboard decomposition. We therefore have to distinguish between left and right eigenvectors $\langle \psi_L |$ and $|\psi_R\rangle$. Non-Hermitian diagonalization routines lack the stabilizing variational principle of the Hermitian case and have to be monitored extremely carefully. The simplest choice, very slow but stable, is the power method applied to the transfer matrix and its transpose. Faster algorithms that have been used to obtain stable results are the Arnoldi and unsymmetric Lanczos methods (Golub and van Loan, 1996), combined with rebiorthogonalization. Once the eigenvectors have been obtained, the unsymmetric density matrix [Eq. (150)] has to be fully diagonalized. Here, two numerical problems typically occur: the appearance of complex-conjugate eigenvalue pairs with spurious imaginary parts and the loss of biorthonormality. The former is dealt with by discarding the spurious imaginary parts and by taking the real and imaginary part of one of the eigenvectors as two real-valued eigenvectors. The latter, less frequent problem is dealt with by iterative reorthogonalization (Ammon *et al.*, 1999).

Both left and right eigenvectors $\langle \psi_L |$ and $|\psi_R\rangle$ are needed to construct the density matrix as in Eq. (150). Having both eigenvectors, a symmetric choice [with $\langle \psi_R | = (|\psi_R\rangle)^\dagger$]

$$\hat{\rho}_{\text{symm}} = \text{Tr} \frac{1}{2} [|\psi_R\rangle\langle\psi_R| + |\psi_L\rangle\langle\psi_L|] \tag{152}$$

for the density matrix is also conceivable, if one argues that this amounts to trying to optimally represent both the left and right eigenvectors at the same time. This choice is much more stable numerically, as no complex eigenvalue problem appears and diagonalization routines are much more stable, and it somehow also accounts for the information carried by both eigenvectors. A detailed study by Nishino and Shibata (1999) clearly favors the asymmetric choice. They showed that if the asymmetric density matrix has real eigenvalues, it is for M retained states as precise as the symmetric choice for $2M$ states; if they are complex, there is no such advantage.

For the extraction of physical quantities it is now advantageous not to fix the inverse temperature β and vary the Trotter number L, but to replace β/L by a fixed initial inverse temperature $\beta_0 \ll 1$ in Eq. (140). Quantum TMRG growth then reaches for $2L$ plaquettes all inverse temperatures $\beta_0, 2\beta_0, \ldots, L\beta_0$. At each step we obtain the free energy per site $f(T)$ and thus all thermodynamic quantities, such as the internal energy u, magnetization m, specific heat at constant volume c_v, and magnetic susceptibility χ by numerical differentiation. Temperatures less than a hundredth of the main energy scale of the Hamiltonian can be reached. Convergence must be checked both in $M \to \infty$ and in $\beta_0 \to 0$; the latter convergence is in β_0^2. For a fixed number of plaquettes, finite-system DMRG runs can be carried out.

Severe numerical problems may occur for the second-order derivatives c_v and χ. A *direct calculation* of u and m, which are expectation values, reduces the number of differentiations to one.

To do this, consider the internal energy $\langle u \rangle = Z^{-1} \text{Tr}[\hat{h}_1 e^{-\beta\hat{H}}]$. In the Trotter decomposition $\mathcal{T}_1$ changes to

$$\langle \sigma^1 \cdots \sigma^{2L+1} | \mathcal{T}_u^{(2L+1)} | \nu^1 \cdots \nu^{2L+1} \rangle$$
$$= \langle \sigma^3 \nu^3 | \hat{h}_1 e^{-\beta\hat{h}_1} | \sigma^2 \nu^2 \rangle \prod_{j=2}^{L} \langle \sigma^{2j+1} \nu^{2j+1} | \hat{\tau}_1 | \sigma^{2j} \nu^{2j} \rangle \tag{153}$$

and therefore [$\langle \psi_L |$ and $|\psi_R\rangle$ are the left (right) eigenvectors of λ_1]

$$\langle u \rangle = \frac{\text{Tr}[\hat{h}_1 e^{-\beta\hat{H}}]}{\text{Tr}[e^{-\beta\hat{H}}]} = \frac{\langle \Psi_L | \mathcal{T}_u \mathcal{T}_2 | \Psi_R \rangle}{\lambda_1}. \tag{154}$$

A direct calculation of c_v from energy fluctuations is less accurate. The susceptibility can be obtained from calculating the magnetization m at two infinitesimally different fields.

In the beginning, applications of the quantum TMRG focused on the thermodynamics of simple Heisenberg spin chains (Shibata, 1997; Wang and Xiang, 1997; Xiang, 1998); but modified (e.g., frustrated and dimerized) spin chains are also easily accessible (Maisinger and Schollwöck, 1998; Klümper *et al.*, 1999, 2000;
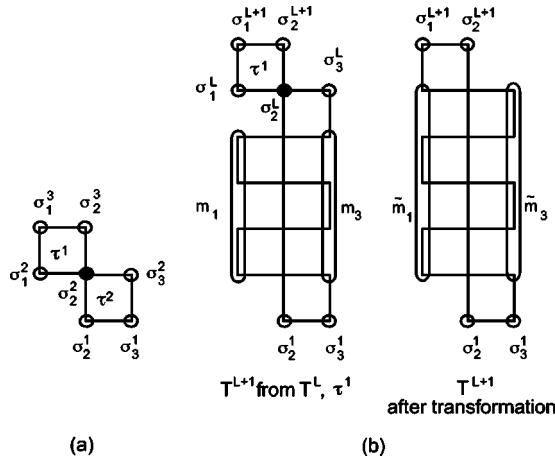
FIG. 29. Two-plaquette transfer matrix $\mathcal{T}^{(3)}$ and transfer-matrix growth. ● are summed over.

Johnston *et al.*, 2000; Maeshima and Okunishi, 2000; Wang *et al.*, 2000; Karadamoglou *et al.*, 2001; Shibata and Ueda, 2001); for frustrated chains, effective sites of two original sites are formed to ensure nearest-neighbor interactions and applicability. Quantum TMRG studies of ferrimagnetic spin chains have revealed an interesting combination of thermodynamics typical of ferromagnets and antiferromagnets (Maisinger *et al.*, 1998; Yamamoto *et al.*, 1998; Kolezhuk *et al.*, 1999). In fact, the results are remarkably similar to those obtained for spin ladders (Hagiwara *et al.*, 2000; Wang and Yu, 2000).

Electronic degrees of freedom have been studied for the *t-J* model by Ammon *et al.* (1999), and Sirker and Klümper (2002a, 2002b) and for the Kondo lattice (Shibata *et al.*, 1998; Shibata and Tsunetsugu, 1999b). Lately, quantum TMRG has also been applied to the algorithmically very similar spin-orbit chain by Sirker and Khaliullin (2003).

Rommer and Eggert (1999) studied one localized impurity linking two spin chains in the thermodynamic limit; there has also been strong interest in the case of
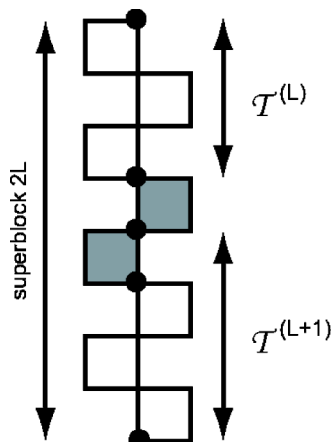

FIG. 30. Quantum transfer-matrix DMRG step. ● are summed over; note the periodic boundary conditions.

multiple mobile impurities (Ammon and Imada, 2000a, 2000b, 2001).

Dynamic properties at finite temperature are among the most frequently available experimental data. Quantum TMRG offers, in close analogy to quantum Monte Carlo calculations, a way to calculate these properties, albeit with far less than the usual precision. It has been applied to anisotropic spin chains (Naef *et al.*, 1999) and the one-dimensional Kondo chain (Mutou *et al.*, 1998b, 1999; Shibata and Tsunetsugu, 1999a) and has been used to calculate nuclear relaxation rates (Naef and Wang, 2000). One starts by calculating imaginary-time correlations $G(\tau)$ and inserting two operators at different imaginary times and time distance τ into the transfer matrix analogous to Eq. (153). The spectral function $A(\omega)$ can now be extracted from the well-known relationship to $G(\tau)$,

$$G(\tau) = \frac{1}{2\pi} \int_0^\infty d\omega K(\tau, \omega) A(\omega), \tag{155}$$

where the kernel $K(\tau, \omega)$ is

$$K(\tau, \omega) = e^{-\tau\omega} + e^{-\beta\omega + \tau\omega} \tag{156}$$

and the extension to negative frequencies obtained through $A(-\omega) = e^{-\beta\omega} A(\omega)$. This decomposition is not unique; other authors also use related expressions (Naef *et al.*, 1999), but the essential difficulty in using these expressions is invariant: If we introduce a finite number of discrete imaginary times τ_i and frequencies ω_j, and a set $K_{ij} = K(\tau_i, \omega_j)$, $G_i = G(\tau_i)$, $A_j = A(\omega_j)$, the spectral function $A(\omega)$ is in principle obtained from inverting (by carrying out a singular-value decomposition of K_{ij})

$$G_i = \sum_j K_{ij} A_j, \tag{157}$$

which, as has been known to practitioners of quantum Monte Carlo for a long time, is a numerically unstable procedure, because K_{ij} is very badly conditioned. The ratio of its largest eigenvalues to its smallest eigenvalues is normally so big that it is not encoded properly in computer number representations. Naef *et al.* (1999) have argued, as is done in quantum Monte Carlo, that given the algorithm-based imprecisions in the imaginary-time data, one may merely try to find the spectral function that is (in a probabilistic sense) most compatible with the raw data. This *maximum-entropy procedure* leads to finding the set $\{A(\omega_j)\}$ that maximizes

$$\alpha S[A] - \frac{1}{2}\chi^2[A], \tag{158}$$

where $S[A]$ is the relative entropy

$$S[A] = \sum_j [A_j - m_j - A_j \ln(A_j/m_j)](1 + e^{-\beta\omega}) \tag{159}$$

and $\chi^2[A]$ accommodates the noisiness of the raw data,

$$\chi^2[A] = \sum_i \left(G_i - \sum_j K_{ij} A_j \right)^2 \bigg/ \sigma_i^2. \qquad (160)$$

In the relative entropy, m_j is some spectral function that embodies previous knowledge relative to which information of $A(\omega_j)$ is measured. It may simply be assumed to be flat. The factor $1 + e^{-\beta\omega}$ ensures that contributions for $\omega < 0$ are considered correctly. σ_i^2 measures the estimated error of the raw data and is in TMRG of the order of 10^{-6}. It is found by looking for that order of magnitude of σ_i^2 where results change least by varying it. α is determined self-consistently such that, of all solutions that can be generated for various α, the one most probable in the light of the input data is chosen (Jarrell and Gubernatis, 1996).

Another way of calculating $A(\omega)$ is given by Fourier-transforming the raw imaginary-time data to Matsubara frequencies on the imaginary axis, $\omega_n = (2n+1)/\pi$ for fermions and $\omega_n = 2n/\pi$ for bosons, using $\tau_i = i\beta/L$ and

$$G(i\omega_n) = \frac{\beta}{L} \sum_{i=0}^{L} e^{i\omega_n \tau_i} G(\tau_i). \qquad (161)$$

$G(i\omega_n)$ is written in some Padé approximation and then analytically continued from $i\omega_n$ to infinitesimally above the real frequency axis, $\omega + i\eta, \eta = 0^+$.

The precision of quantum TMRG dynamics is far lower than that of $T=0$ dynamics. Essential spectral features are captured, but results are not very reliable quantitatively. A serious alternative is currently emerging in time-dependent DMRG methods at finite temperature (Sec. IX.C), but their potential in this field has not yet been demonstrated.

IX. SYSTEMS OUT OF EQUILIBRIUM: NON-HERMITIAN AND TIME-DEPENDENT DMRG

The study of strongly correlated electronic systems, from which DMRG originated, is dominated by attempts to understand equilibrium properties of these systems. Hence the theoretical framework underlying all previous considerations has been that of equilibrium statistical mechanics, which has been extremely well established for a long time. Much less understanding and in particular no unifying framework is available so far for nonequilibrium physical systems, the main difficulty being the absence of a canonical (Gibbs-Boltzmann) ensemble. Physical questions to be studied range from transport through quantum dots with strong voltage bias in the leads far from linear response, to reaction-diffusion processes in chemistry, to ion transport in biological systems, to traffic flow on multilane systems. Quite generically these situations may be described by time-evolution rules that, if cast in some operator language, lead to non-Hermitian operators (Glauber, 1963).

The application of DMRG to such problems in one spatial dimension was pioneered by Hieida (1998), who studied, using a transfer-matrix approach, the discrete-time asymmetric exclusion process, a biased hopping of hard-core particles on a chain with injection and re-

moval of particles at both ends (Derrida *et al.*, 1993). Excellent agreement with exact solutions for particular parameter sets (which correspond to matrix-product *Ansätze*) and with other numerics was found. Kaulke and Peschel (1998) studied the q-symmetric Heisenberg model out of equilibrium.

A. Transition matrices

In the field of nonequilibrium statistical mechanics there has been special interest in those one-dimensional systems with transitions from active to absorbing steady states under a change of parameters. Active steady states show internal particle dynamics, whereas absorbing steady states are truly frozen (e.g., a vacuum state). These transitions are characterized by universal critical exponents, quite analogously to equilibrium phase transitions (see Hinrichsen, 2000 for a review). Carlon, Henkel, and Schollwöck (1999) have shown that DMRG is able to provide reliable estimates of critical exponents for nonequilibrium phase transitions in one-dimensional reaction-diffusion models. To this end they applied DMRG to a (non-Hermitian) master equation of a pseudo-Schrödinger form. This approach has been at the basis of most later DMRG work on out-of-equilibrium phenomena. Considering a chain of length L, in which each site is either occupied by a particle (A) or empty ($\varnothing$), the time evolution of the system is given in terms of microscopic rules involving only neighboring sites. Typical rules of evolution are site-to-site hopping (diffusion) $A\varnothing \leftrightarrow \varnothing A$ or the annihilation of neighboring particles $AA \rightarrow \varnothing\varnothing$, all with some fixed rates. Nonequilibrium phase transitions in the steady state may arise for competing reactions, such as $AA \rightarrow \varnothing\varnothing$ and $A\varnothing, \varnothing A \rightarrow AA$ simultaneously present. The last model is referred to as the contact process. Its steady-state transition between steady states of finite and vanishing density in the thermodynamic limit is in the universality class of directed percolation.

Once the reaction rates are given, the stochastic evolution follows from a master equation, which can be written as

$$\frac{d|P(t)\rangle}{dt} = -\hat{H}|P(t)\rangle, \qquad (162)$$

where $|P(t)\rangle$ is the state vector containing the probabilities of all configurations, as opposed to the true quantum case, in which the coefficients are probability amplitudes. The elements of the "Hamiltonian" $\hat{H}$ (which is actually a transition matrix) are given by

$$\langle \sigma | \hat{H} | \tau \rangle = -w(\tau \rightarrow \sigma); \ \sigma \neq \tau,$$

$$\langle \sigma | \hat{H} | \sigma \rangle = \sum_{\tau \neq \sigma} w(\sigma \rightarrow \tau), \qquad (163)$$

where $|\sigma\rangle, |\tau\rangle$ are the state vectors of two particle configurations and $w(\tau \rightarrow \sigma)$ denotes the transition rates between the two states and is constructed from the rates of

the elementary processes. $\hat{H}$ will in general be non-Hermitian. Since $\hat{H}$ is a stochastic matrix, its columns add to zero. The left ground state $\langle\psi_L|$ is hence given by

$$\langle\psi_L| = \sum_\sigma \langle\sigma|, \qquad (164)$$

with ground-state energy $E_0=0$, since $\langle\psi_L|\hat{H}=0$; the right ground state $|\psi_R\rangle$ is problem-dependent. All other eigenvalues E_i of $\hat{H}$ have a non-negative real part $\mathrm{Re}\,E_i\geq 0$ (Alcaraz *et al.*, 1994; van Kampen, 1997).

Since the formal solution of Eq. (162) is

$$|P(t)\rangle = e^{-\hat{H}t}|P(0)\rangle, \qquad (165)$$

the system evolves towards its steady state $|P(\infty)\rangle$. Let $\Gamma := \inf_i \mathrm{Re}\,E_i$ for $i\neq 0$. If $\Gamma>0$, the approach towards the steady state is characterized by a finite relaxation time $\tau=1/\Gamma$, but if $\Gamma=0$, that approach is algebraic. This situation is quite analogous to noncritical phases ($\tau\neq 0$) and critical points ($\tau=\infty$), respectively, which may arise in equilibrium quantum Hamiltonians. The big advantage of DMRG is that the steady-state behavior is addressed directly and that all initial configurations are inherently averaged over in this approach; the price to be paid is restriction to relatively small system sizes, currently $L\sim 100$, due to inherent numerical instabilities in non-Hermitian large sparse eigenvalue solvers.

Standard DMRG as in one-dimensional $T=0$ quantum problems is now used to calculate both left and right lowest eigenstates. Steady-state expectation values such as density profiles or steady-state two-point correlations are given by expressions

$$\langle n_i\rangle = \langle\psi_L|n_i|\psi_R\rangle/\langle\psi_L|\psi_R\rangle, \qquad (166)$$

where the subscripts L,R serve to remind us that two distinct left and right ground states are employed in the calculation. The gap allows the extraction of the relaxation time on a finite lattice and the use of standard finite-size scaling theory. The Bulirsch-Stoer-transformation extrapolation scheme (Henkel and Schütz, 1988) has been found very useful in extracting critical exponents from the finite-size scaling functions for density profiles and gaps. In this way Carlon, Henkel, and Schollwöck (1999) determined both bulk and surface critical exponents of the contact process and found their values to be compatible with the directed-percolation class, as expected.

In cases where the right ground state is also trivially known (e.g., the empty state), DMRG calculations can be made more stable by shifting this trivially known eigenstate pair to some high energy in Hilbert space by adding a term $E_{\mathrm{shift}}|\psi_R\rangle\langle\psi_L|$ to the Hamiltonian, turning the nontrivial first excitation into the more easily accessible ground state.

For a correct choice of the density matrix it is always crucial to target the ground state, even if it has shifted away; otherwise it will reappear due to numerical inaccuracies in the representation of the shift operator (Carlon, Henkel, and Schollwöck, 2001). Moreover, the

trivial left ground state must be targeted, although it contains no information, to get a good representation of the right eigenstates that are joined in a biorthonormality relation (Carlon, Henkel, and Schollwöck, 1999). For non-Hermitian Hamiltonians, there is also a choice between symmetric and nonsymmetric density matrices. It was found empirically (Carlon, Henkel, and Schollwöck, 1999) that the symmetric choice

$$\hat{\rho} = \mathrm{Tr}_E \frac{1}{2}(|\psi_R\rangle\langle\psi_R| + |\psi_L\rangle\langle\psi_L|) \qquad (167)$$

was most efficient, as opposed to quantum TMRG, in which the nonsymmetric choice is to be preferred. This is probably due to numerical stability: a nonsymmetric density matrix makes this numerically subtle DMRG variant even less stable. The same observation was made by Senthil *et al.* (1999) in the context of SUSY chains.

The method has been applied to the asymmetric exclusion model by Nagy *et al.* (2002). A series of papers has been able to show impressive results on reptating polymers exposed to the drag of an external field such as in electrophoresis in the framework of the Rubinstein-Duke model (Carlon, Drzewinski, and van Leeuwen, 2001, 2002; Paeßens and Schütz, 2002; Barkema and Carlon, 2003; Paeßens, 2003). DMRG has been able to show for the renewal time (longest relaxation time) τ a crossover from an (experimentally observed) behavior $\tau\sim N^{3.3\pm 0.1}$ for short polymers to the theoretically predicted $\tau\sim N^3$ for long polymers.

Another field of application that is under active debate is determination of the properties of the one-dimensional pair-contact process with single-particle diffusion (PCPD), which is characterized by the reactions $AA\rightarrow\varnothing\varnothing$, $\varnothing AA, AA\varnothing\rightarrow AAA$. While early field-theoretic studies (Howard and Täuber, 1997) showed that its steady-state transition was not in the directed-percolation class, the first quantitative data came from a DMRG study (Carlon, Henkel, and Schollwöck, 2001) and suggested again a universality class different from directed percolation. At present, despite further extensive DMRG studies (Henkel and Schollwöck, 2001; Barkema and Carlon, 2003) and additional simulational and analytical studies, no consensus on the critical behavior of the one-dimensional PCPD has been reached yet. It may be safely stated that DMRG has sparked a major debate in this field. While the raw data as such are not disputed, the extrapolations to the infinite-size limit are highly controversial. The answer to this issue is beyond the scope of this review.

B. Stochastic transfer matrices

Kemper *et al.* (2001) have made use of the pseudo-Hamiltonian formulation of stochastic systems as outlined above to apply the formalism of quantum TMRG. The time evolution of Eq. (165) and the Boltzmann operator $e^{-\beta\hat{H}}$ are formally identical, such that in both cases the transfer-matrix construction outlined in Sec. VIII.C can be carried out. In the thermodynamic limit $N\rightarrow\infty$ all

physical information is encoded in the left and right eigenvectors to the largest eigenvalue, which are approximately represented using the TMRG machinery.

In the stochastic TMRG the local transfer matrices are direct evolutions in a time interval Δt obtained from the discretized time evolution,

$$|P(t + \Delta t)\rangle = e^{-\hat{H}\Delta t}|P(t)\rangle. \tag{168}$$

Otherwise, the formalism outlined in Sec. VIII.C carries over identically, with some minor but important modifications. Boundary conditions in time are open, since periodic boundary conditions would set the future equal to the past. Moreover, stochastic TMRG only works with a symmetric density matrix constructed from left and right eigenvectors: Enss and Schollwöck (2001) have shown that the open boundary conditions imply that the unsymmetric choice of the density matrix, $\hat{\rho} = \mathrm{Tr}_E |\psi_R\rangle\langle\psi_L|$, which was superior in quantum TMRG, has no meaningful information because it has only one nonzero eigenvalue. Moreover, for stochastic TMRG the use of the symmetric choice, $\hat{\rho} = (1/2)\mathrm{Tr}_E[|\psi_L\rangle\langle\psi_L| + |\psi_R\rangle\langle\psi_R|]$, is mandatory.

The advantages of the stochastic TMRG are that it works in the thermodynamic limit and that, although it can only deal with comparatively short time scales of some hundred time steps, it automatically averages over all initial conditions and is hence bias-free. It can be seen as complementary to the method of the last section. Unfortunately, it has also been shown by Enss and Schollwöck (2001) that there is a critical loss of precision strongly limiting the number L of possible time steps; it is a property of probability-conserving stochastic transfer matrices that the norm of the left and right eigenvectors to the largest eigenvalue diverges exponentially in L, while biorthonormality $\langle\psi_L|\psi_R\rangle = 1$ should hold exactly as well, which cannot be ensured by finite computer precision.

Building on the observation by Enss and Schollwöck (2001) that the local physics at some place and at time t is determined by past events in a finite-sized light cone, Kemper *et al.* (2003) have applied a variant of the corner transfer-matrix algorithm to the light cone (Fig. 31), reporting that the numerical loss-of-precision problem now occurs at times several orders of magnitude larger, greatly enhancing the applicability of stochastic TMRG. This method has been applied by Enss *et al.* (2004) to study scaling functions for aging phenomena in systems without detailed balance.

C. Time-dependent DMRG

So far, all physical properties discussed in this review and obtained via DMRG have been either true equilibrium quantities, static or dynamic, or steady-state quantities. However, time-dependent phenomena in strongly correlated systems are increasingly coming to the forefront of interest. On the one hand, in technological applications such as are envisaged in nanoelectronics, it will be of great interest to fully understand the time-dependent response of quantum many-body systems to external time-dependent perturbations and to calculate transport far from equilibrium. On the other hand, the recent mastery of storing ultracold bosonic atoms in a magnetic trap superimposed by an optical lattice has allowed us to drive, at will, by time-dependent variations of the optical lattice strength, quantum phase transitions from the superfluid (metallic) to the Mott insulating regime, which is one of the key phase transitions in strongly correlated electron systems (Greiner *et al.*, 2002).

The fundamental difficulty can be seen when considering the time evolution of a quantum state $|\psi(t=0)\rangle$ under the action of some time-independent Hamiltonian $\hat{H}|\psi_n\rangle = E_n|\psi_n\rangle$. If the eigenstates $|\psi_n\rangle$ are known, expanding $|\psi(t=0)\rangle = \Sigma_n c_n|\psi_n\rangle$ leads to the well-known time evolution

$$|\psi(t)\rangle = \sum_n c_n \exp(-iE_n t)|\psi_n\rangle, \tag{169}$$

where the modulus of the expansion coefficients of $|\psi(t)\rangle$ is time independent. A sensible Hilbert-space truncation is then given by a projection onto the large-modulus eigenstates. In strongly correlated systems, however, we usually have no good knowledge of the eigenstates. Instead, one uses some orthonormal basis with unknown eigenbasis expansion, $|m\rangle = \Sigma_n a_{mn}|\psi_n\rangle$. The time evolution of the state $|\psi(t=0)\rangle = \Sigma_m d_m(0)|m\rangle$ then reads

$$|\psi(t)\rangle = \sum_m \left(\sum_n d_m(0)a_{mn}e^{-iE_n t} \right)|m\rangle \equiv \sum_m d_m(t)|m\rangle, \tag{170}$$

where the modulus of the expansion coefficients is time dependent. For a general orthonormal basis, Hilbert-space truncation at one fixed time (i.e., $t=0$) will therefore not ensure a reliable approximation of the time evolution. Also, energy differences matter in time evolution. The sometimes justified hope that DMRG yields a good approximation to the low-energy Hamiltonian is hence of limited use.

All time-evolution schemes for DMRG so far follow one of two different strategies. Static Hilbert-space DMRG methods try to enlarge the truncated Hilbert space optimally to approximate $|\psi(t=0)\rangle$ so that it is big enough to accommodate (i.e., maintain large overlap with the exact result) $|\psi(t)\rangle$ for a sufficiently long time to a very good approximation. More recently, adaptive Hilbert-space DMRG methods keep the size of the truncated Hilbert space fixed, but try to change it as time evolves so that it also accommodates $|\psi(t)\rangle$ to a very good approximation.

1. Static time-dependent DMRG

Cazalilla and Marston (2002) were the first to exploit DMRG to systematically calculate quantum many-body effects out of equilibrium. After applying a standard DMRG calculation to the Hamiltonian $\hat{H}(t=0)$, the time-dependent Schrödinger equation is numerically in-

tegrated forward in time, building an effective $\hat{H}_{\mathrm{eff}}(t)$ $=\hat{H}_{\mathrm{eff}}(0)+\hat{V}_{\mathrm{eff}}(t)$, where $\hat{H}_{\mathrm{eff}}(0)$ is taken as the last superblock Hamiltonian approximating $\hat{H}(0)$. $\hat{V}_{\mathrm{eff}}(t)$ as an approximation to $\hat{V}$ is built using the representations of operators in the final block bases:

$$i\frac{\partial}{\partial t}|\psi(t)\rangle = [\hat{H}_{\mathrm{eff}} - E_0 + \hat{V}_{\mathrm{eff}}(t)]|\psi(t)\rangle. \qquad (171)$$

The initial condition is obviously to take $|\psi(0)\rangle = |\psi_0\rangle$ obtained by the preliminary DMRG run. Forward integration can be carried out by step-size adaptive methods such as Runge-Kutta integration based on the infinitesimal time-evolution operator

$$|\psi(t+\Delta t)\rangle = (1 - i\hat{H}(t)\Delta t)|\psi(t)\rangle. \qquad (172)$$

As an application, Cazalilla and Marston have considered a quantum dot weakly coupled to noninteracting leads of spinless fermions, where time dependency is introduced through a time-dependent chemical potential coupling to the number of particles left and right of the dot,

$$\hat{V}(t) = -\delta\mu_R(t)\hat{N}_R - \delta\mu_L(t)\hat{N}_L, \qquad (173)$$

which is switched on smoothly at $t=0$. Setting $\delta\mu_L = -\delta\mu_R$, one may gauge-transform this chemical potential away into a time-dependent complex hopping from and to the dot,

$$t_q(t) = t_q\exp\left[i\int_{-\infty}^{t} dt'\,\delta\mu_L(t')\right]. \qquad (174)$$

The current is then given by evaluating the imaginary part of the local hopping expectation value. Obviously, in a finite system currents will not stay at some steady-state value but go to zero on a time scale of the inverse system size when lead depletion has occurred.

In this approach the hope is that an effective Hamiltonian obtained by targeting the ground state of the $t=0$ Hamiltonian will be capable of catching the states that will be visited by the time-dependent Hamiltonian during time evolution. Cazalilla and Marston argue that on short time scales the perturbation can only access a few excited states, which are well represented in the effective Hamiltonian. With one exception (Luo et al., 2003) this seems borne out in their main application, transport through a quantum dot; in many other applications, this approach is not sufficient.

As one way out of this problem, it has been demonstrated (Luo et al., 2003) that using a density matrix that is given by a superposition of states $|\psi(t_i)\rangle$ at various times of the evolution, $\hat{\rho} = \sum_{i=0}^{N_t} \alpha_i |\psi(t_i)\rangle\langle\psi(t_i)|$ with $\Sigma\alpha_i = 1$ for the determination of the reduced Hilbert space is much more precise, whereas simply increasing M is not sufficient. Of course, these states are not known initially; it was proposed to start from a small DMRG system, evolve it in time, take these state vectors, use them in the density matrix to determine the reduced Hilbert
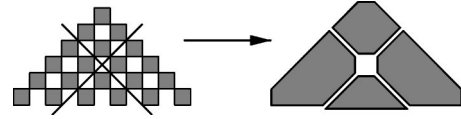

FIG. 31. Transfer-matrix renormalization group (TMRG) applied to the causal light cone of a stochastic Hamiltonian evolving in real time: four corner transfer matrices make up the light cone. From Kemper et al., 2003. Reprinted with permission.

space, and then to move on to the next-larger DMRG system where the procedure is repeated, which is very time consuming.

It is important to note that the simple Runge-Kutta approach is not even unitary and should be improved by using, e.g., the unitary Crank-Nicholson time evolution (Daley et al., 2004).

Instead of considering time evolution as a differential equation, one may also consider the time-evolution operator $\exp(-i\hat{H}t)$, which avoids the numerical delicacies of the Schrödinger equation. Schmitteckert (2004) computes the transport through a small interacting nanostructure using this approach. To this end, he splits the problem into two parts: By obtaining a relatively large number of low-lying eigenstates exactly (within time-independent DMRG precision), he can calculate their time evolution exactly. For the subspace orthogonal to these eigenstates, he uses an efficient implementation of the matrix exponential $|\psi(t+\Delta t)\rangle = \exp(-i\hat{H}\Delta t)|\psi(t)\rangle$ using a Krylov subspace approximation; the reduced Hilbert space is determined by finite-system sweeps, concurrently targeting all $|\psi(t_i)\rangle$ at fixed times t_i up to the time presently reached in the calculation. The limitation to this algorithm comes from the fact that to target more and more states as time evolves, the effective Hilbert space chosen has to be increasingly large.

2. Adaptive time-dependent DMRG

Time-dependent DMRG using adaptive Hilbert spaces was first proposed in essentially identical form by Daley et al. (2004) and White and Feiguin (2004). Both approaches are efficient implementations of an algorithm for the classical simulation of the time evolution of weakly entangled quantum states invented by Vidal (2003, 2004) [known as the time-evolving block-decimation (TEBD) algorithm]. This algorithm was originally formulated in the matrix-product-state language. For simplicity, I shall explain the algorithm in its DMRG context. A detailed discussion of the very strong connection between adaptive time-dependent DMRG and the original simulation algorithm is given by Daley et al. (2004). It turns out that DMRG naturally attaches good quantum numbers to state spaces used by the TEBD algorithm, allowing for drastic increases in performance due to the use of good quantum numbers.

Time evolution in the adaptive time-dependent DMRG is generated using a Trotter-Suzuki decomposition as discussed for quantum TMRG (Sec. VIII.C). As-

suming only nearest-neighbor interactions, the decomposition reads $\hat{H} = \hat{H}_1 + \hat{H}_2$. $\hat{H}_1 = \Sigma_{i=1}^{N/2} \hat{h}_{2i-1}$ and $\hat{H}_2 = \Sigma_{i=1}^{N/2} \hat{h}_{2i}$. Here $\hat{h}_i$ is the local Hamiltonian linking sites i and $i+1$; neighboring local Hamiltonians will in general not commute, hence $[\hat{H}_1, \hat{H}_2] \neq 0$. However, all terms in $\hat{H}_1$ or $\hat{H}_2$ commute. The first-order Trotter decomposition of the infinitesimal time-evolution operator then reads

$$\exp(-i\hat{H}\Delta t) = \exp(-i\hat{H}_1\Delta t)\exp(-i\hat{H}_2\Delta t) + O(\Delta t^2). \tag{175}$$

Expanding $\hat{H}_1$ and $\hat{H}_2$ into the local Hamiltonians, one infinitesimal time step $t \to t + \Delta t$ may be carried out by performing the local time-evolution on (say) all even bonds first and then all odd bonds. In DMRG, a bond can be time evolved exactly if it is formed by the two explicit sites typically occurring in DMRG states. We may therefore carry out an exact time evolution by performing one finite-system sweep forward and backward through an entire one-dimensional chain, with time evolutions on all even bonds on the forward sweep and all odd bonds on the backward sweep, at the price of the Trotter error of $O(\Delta t^2)$. This procedure necessitates that $|\psi(t)\rangle$ be available in the right block bases, which is ensured by carrying out the reduced basis transformations on $|\psi(t)\rangle$ that in standard DMRG form the basis of White's prediction method (White, 1996b). The decisive idea of Vidal (2003, 2004) was now to carry out a new Schmidt decomposition and make a new choice of the most relevant block basis states for $|\psi(t)\rangle$ after each local bond update. Therefore, as the quantum state changes in time, so do the block bases such that an optimal representation of the time-evolving state is ensured. Choosing new block bases changes the effective Hilbert space, hence the name *adaptive* time-dependent DMRG.

An appealing feature of this algorithm is that it can be very easily implemented in existing finite-system DMRG. One uses standard finite-system DMRG to generate a high-precision initial state $|\psi(0)\rangle$ and continues to run finite-system sweeps, one for each infinitesimal time step, merely replacing the large sparse-matrix diagonalization at each step of the sweep by local bond updates for the odd and even bonds, respectively.

Errors are reduced by using the second-order Trotter decomposition

$$e^{-i\hat{H}\Delta t} = e^{-i\hat{H}_1\Delta t/2}e^{-i\hat{H}_2\Delta t}e^{-i\hat{H}_1\Delta t/2} + O(\Delta t^3). \tag{176}$$

As Δt^{-1} steps are needed to reach a fixed time t, the overall error is then of order $O(\Delta t^2)$. One efficient way of implementing this is to group the half time steps of two subsequent infinitesimal evolution steps together, i.e., carry out the standard first-order procedure, but calculate expectation values as averages of expectation values measured before and after an $\exp(-i\hat{H}_2\Delta t)$ step.

Further errors are produced by the reduced basis transformations and the sequential update of the representation of block states in the Schmidt decomposition after each bond update during an infinitesimal time step. Applications of adaptive time-dependent DMRG so far for the time-dependent Bose-Hubbard model (Daley *et al.*, 2004) and spin-1 Heisenberg chains (White and Feiguin, 2004) have demonstrated that it allows access to large time scales very reliably. The errors mentioned can be well controlled by increasing M and can show significant accumulation only after relatively long times.

3. Time-dependent correlations

Time-dependent DMRG also yields an alternative approach to time-dependent correlations which have been evaluated in frequency space in Sec. IV. Alternatively, one may calculate expressions as

$$\langle \psi | c_i^\dagger(t) c_j(0) | \psi \rangle = \langle \psi | e^{+i\hat{H}t} c_i^\dagger e^{-i\hat{H}t} c_j | \psi \rangle \tag{177}$$

constructing both $|\psi\rangle$ and $|\phi\rangle = c_j|\psi\rangle$ using standard DMRG (targeting both), and calculating both $|\psi(t)\rangle$ and $|\phi(t)\rangle$ using time-dependent DMRG. The desired correlator is then simply given as

$$\langle \psi(t) | c_i^\dagger | \phi(t) \rangle \tag{178}$$

and can be calculated for all i and t as time proceeds. Frequency-momentum space is reached by Fourier transformation. Finite system sizes and edge effects impose physical constraints on the largest times and distances $|i-j|$ or minimal frequencies and wave vectors accessible, but unlike dynamical DMRG, one run of the time-dependent algorithm is sufficient to cover the entire accessible frequency-momentum range. White and Feiguin (2004) report a very successful calculation of the one-magnon dispersion relation in an $S=1$ Heisenberg antiferromagnetic chain using adaptive time-dependent DMRG, but similar calculations are in principle feasible in all time-dependent methods.

D. Finite temperature revisited: Time evolution and dissipation at $T > 0$

While our discussion so far has been restricted to time evolution at $T=0$, it is possible to generalize to the (possibly dissipative) time evolution at $T > 0$ (Verstraete, Garcia-Ripoll, and Cirac, 2004; Zwolak and Vidal, 2004). Both proposals are in the spirit of adaptive Hilbert-space methods. One prepares a $T=\infty$ completely mixed state $\hat{\rho}_\infty$, essentially the identity operator, from which a finite-temperature mixed state $\exp(-\beta\hat{H})$ at $\beta^{-1} = T > 0$ is created by imaginary-time evolution, i.e.,

$$\exp(-\beta\hat{H}) = (e^{-\tau\hat{H}})^N \hat{\rho}_\infty (e^{-\tau\hat{H}})^N, \tag{179}$$

where $\beta = 2N\tau$ and $\tau \to 0$. The infinitesimal-time evolution operator $e^{-\tau\hat{H}}$ is Trotter decomposed into locally acting bond evolution operators. The finite-temperature state is then evolved in real time using Hamiltonian or Lindbladian dynamics. The differences reside essentially in the representation of mixed states and the truncation procedure.

Verstraete, Garcia-Ripoll, and Cirac (2004) consider the $T=0$ matrix-product state of Eq. (47), where the $A_i[\sigma_i]$ are interpreted (see Sec. III.A) as maps from the tensor product of two auxiliary states (dimension M^2) to a physical state space of dimension N_{site}. This can be generalized to finite-temperature *matrix-product density operators*,

$$\hat{\rho} = \sum_{\{\boldsymbol{\sigma}\}\{\boldsymbol{\sigma}'\}} \text{Tr}\left[\prod_{i=1}^{L} \hat{M}_i[\sigma_i \sigma_i']\right] |\boldsymbol{\sigma}\rangle\langle\boldsymbol{\sigma}'|. \tag{180}$$

Here, the $\hat{M}[\sigma_i \sigma_i']$ are now maps from the tensor product of four auxiliary state spaces (two left, two right of the physical site) of dimension M^4 to the N_{site}^2-dimensional local density-operator state space. The most general case allowed by quantum mechanics is for $\hat{M}$ to be a completely positive map. The dimension of $\hat{M}$ seems to be prohibitive, but it can be decomposed into a sum of d tensor products of A maps as

$$\hat{M}_i[\sigma_i \sigma_i'] = \sum_{a_i=1}^{d} A_i[\sigma_i a_i] \otimes A_i^*[\sigma_i' a_i]. \tag{181}$$

In general, $d \leqslant N_{\text{site}} M^2$, but it will be important to realize that for thermal states $d = N_{\text{site}}$ only. At $T=0$, one recovers the standard matrix-product state, i.e., $d=1$. In order to actually simulate $\hat{\rho}$, Verstraete, Garcia-Ripoll, and Cirac (2004) consider the purification

$$|\psi_{MPDO}\rangle = \sum_{\{\boldsymbol{\sigma}\}\{\mathbf{a}\}} \text{Tr}\left[\prod_{i=1}^{L} \hat{A}_i[\sigma_i a_i]\right] |\boldsymbol{\sigma}\mathbf{a}\rangle, \tag{182}$$

such that $\hat{\rho} = \text{Tr}_{\mathbf{a}} |\psi_{MPDO}\rangle\langle\psi_{MPDO}|$. Here, ancilla state spaces $\{|a_i\rangle\}$ of dimension d have been introduced.

In this form, a completely mixed state is obtained from matrices $A_i[\sigma_i a_i] \propto \mathbb{I} \cdot \delta_{\sigma_i, a_i}$, in which M may be 1 and normalization has been ignored. This shows $d = N_{\text{site}}$. This state is now subjected to infinitesimal evolution in imaginary time, $e^{-\tau \hat{H}}$. As it acts on σ only, the dimension of the ancilla state spaces need not be increased. Of course, for $T=0$ the state may be efficiently prepared using standard methods.

The imaginary-time evolution is carried out after a Trotter decomposition into infinitesimal time steps on bonds. The local bond evolution operator $\hat{U}_{i,i+1}$ is conveniently decomposed into a sum of d_U tensor products of on-site evolution operators,

$$\hat{U}_{i,i+1} = \sum_{k=1}^{d_U} \hat{u}_i^k \otimes \hat{u}_{i+1}^k. \tag{183}$$

d_U is typically small, say 2 to 4. Applying now the time evolution at, say, all odd bonds exactly, the auxiliary state spaces are enlarged from dimension M to $M d_U$. One now has to find the optimal approximation $|\tilde{\psi}(t+\Delta t)\rangle$ to $|\psi(t+\Delta t)\rangle$ using auxiliary state spaces of dimension M only. Hence the state spaces of dimension $M d_U$ must be truncated optimally to minimize $\||\tilde{\psi}(t+\Delta t)\rangle$

$- |\psi(t+\Delta t)\rangle\|$. If one uses the matrices composing the state at t as initial guesses and keeps all but one A matrix fixed, one obtains a linear equation system for this A; sweeping through all A matrices several times is sufficient to reach the fixed point that is the variational optimum. As temperature is lowered, M will be increased to maintain a desired precision. Once the thermal state is constructed, real-time evolutions governed by Hamiltonians can be calculated similarly. In the case of Lindbladian time evolutions, they are carried out directly on states of the form of Eq. (180), which is formally equivalent to a matrix-product state on a local N_{site}^2-dimensional state space.

The approach of Zwolak and Vidal (2004) is based on the observation that local (density) operators $\Sigma \rho_{\sigma\sigma'} |\sigma\rangle\langle\sigma'|$ can be represented as $N_{\text{site}} \times N_{\text{site}}$ Hermitian matrices. They now reinterpret the matrix coefficients as the coefficients of a local "superket" defined on a N_{site}^2-dimensional local state space. Any globally acting (density) operator is now a global superket expanded as a linear combination of tensor products of local superkets,

$$\hat{\rho} = \sum_{\bar{\sigma}_1=1}^{N_{\text{site}}^2} \cdots \sum_{\bar{\sigma}_L=1}^{N_{\text{site}}^2} c_{\bar{\sigma}_1 \cdots \bar{\sigma}_L} |\bar{\sigma}_1 \cdots \bar{\sigma}_L\rangle. \tag{184}$$

Here, $|\bar{\sigma}_i\rangle = |\sigma_i\rangle|\sigma_i'\rangle$, the state space of the local superket. We have now reached complete formal equivalence between the description of a pure state and a mixed state, such that the time-evolving block decimation algorithm (Vidal, 2003, 2004) or its DMRG incarnation (Daley *et al.*, 2004; White and Feiguin, 2004) can be applied to the time evolution of this state.

Choosing the local totally mixed state as one basis state of the local superket state space, say $\bar{\sigma}_i = 1$, we find that the global totally mixed state has only one nonzero expansion coefficient, $c_{1\cdots 1} = 1$ upon suitable normalization. This shows that the $T=\infty$ state, as in the previous algorithm, takes a particularly simple form in this expansion; it can also be brought very easily to some matrix-product form corresponding to a DMRG system consisting of two blocks and two sites. The time-evolution operators, whether of Hamiltonian or Lindbladian origin, now map from operators to operators and are hence referred to as *superoperators*. If one represents operators as superkets, these superoperators are formally equivalent to standard operators. As in the $T=0$ case therefore they are now Trotter decomposed, applied in infinitesimal time steps to all bonds sequentially, with Schmidt decompositions being carried out to determine block (super)state spaces. The number of states kept is determined from the acceptable truncation error. Imaginary-time evolutions starting from the totally mixed state generate thermal states of a given temperature that may then be subjected to some evolution in real time. It turns out again that the number of states to be kept grows with inverse temperature.

For the simulation of dissipative systems, both approaches are effectively identical except for the optimal

approximation of Verstraete, Garcia-Ripoll, and Cirac (2004) replacing the somewhat less precise truncation of the approach of Zwolak and Vidal (2004; see the discussion of the precision achievable for various DMRG setups in Sec. III.A).

X. OUTLOOK

What lies ahead for DMRG? On the one hand, DMRG is quickly becoming a standard tool, to be routinely applied to the study of all low-energy properties of strongly correlated one-dimensional quantum systems, most often probably using black-box DMRG codes. On the other hand, there are several axes of DMRG research that I expect to be quite fruitful in the future: DMRG might emerge as a very powerful tool in quantum chemistry in the near future; its potential for time-dependent problems is far from being understood. Last but not least I feel that two-dimensional model Hamiltonians will be increasingly within reach of DMRG methods, at least for moderate system sizes that are still beyond the possibilities of exact diagonalization and quantum Monte Carlo.

The strong link of DMRG to quantum information theory has only recently begun to be exploited—DMRG variants to carry out complex calculations of interest in quantum information theory might emerge, while DMRG itself could be applied in a more focused manner using the new insights about its intrinsic rationale. In that sense, DMRG would be at the forefront of a growing entanglement between condensed-matter physics and quantum computation.

ACKNOWLEDGMENTS

REFERENCES

Aebischer, C., D. Baeriswyl, and R. M. Noack, 2001, Phys. Rev. Lett. **86**, 468.

Affleck, I., T. Kennedy, E. H. Lieb, and H. Tasaki, 1987, Phys. Rev. Lett. **59**, 799.

Affleck, I., T. Kennedy, E. H. Lieb, and H. Tasaki, 1988, Commun. Math. Phys. **115**, 477.

Akutsu, N., and Y. Akutsu, 1998, Phys. Rev. B **57**, R4233.

Akutsu, N., Y. Akutsu, and T. Yamamoto, 2001a, Phys. Rev. B **64**, 085415.

Akutsu, N., Y. Akutsu, and T. Yamamoto, 2001b, Surf. Sci. **493**, 475.

Alcaraz, F. C., M. Droz, M. Henkel, and V. Rittenberg, 1994, Ann. Phys. (N.Y.) **230**, 250.

Aligia, A. A., K. Hallberg, C. D. Batista, and G. Ortiz, 2000, Phys. Rev. B **61**, 7883.

Ammon, B., and M. Imada, 2000a, J. Phys. Soc. Jpn. **69**, 1946.

Ammon, B., and M. Imada, 2000b, Phys. Rev. Lett. **85**, 1056.

Ammon, B., and M. Imada, 2001, J. Phys. Soc. Jpn. **70**, 547.

Ammon, B., M. Troyer, T. M. Rice, and N. Shibata, 1999, Phys. Rev. Lett. **82**, 3855.

Anderson, P. W., 1959, J. Phys. Chem. Solids **11**, 28.

Andersson, M., M. Boman, and S. Östlund, 1999, Phys. Rev. B **59**, 10 493.

Anusooya, Y., S. K. Pati, and S. Ramasesha, 1997, J. Chem. Phys. **106**, 10230.

Anussoya, Y., S. K. Pati, and S. Ramasesha, 1999, J. Phys.: Condens. Matter **11**, 2395.

Aschauer, H., and U. Schollwöck, 1998, Phys. Rev. B **58**, 359.

Barford, W., and R. J. Bursill, 2001, Synth. Met. **119**, 251.

Barford, W., R. J. Bursill, and M. Y. Lavrentiev, 1998, J. Phys.: Condens. Matter **10**, 6429.

Barford, W., R. J. Bursill, and M. Y. Lavrentiev, 2001, Phys. Rev. B **63**, 195108.

Barford, W., R. J. Bursill, and M. Y. Lavrentiev, 2002, Phys. Rev. B **65**, 075107.

Barford, W., R. J. Bursill, and R. W. Smith, 2002, Phys. Rev. B **66**, 115205.

Barkema, G. T., and E. Carlon, 2003, Phys. Rev. E **68**, 036113.

Bartlett, R., J. Watts, S. Kucharski, and J. Noga, 1990, Chem. Phys. Lett. **165**, 513.

Batista, C. D., K. Hallberg, and A. A. Aligia, 1998, Phys. Rev. B **58**, 9248.

Batista, C. D., K. Hallberg, and A. A. Aligia, 1999, Phys. Rev. B **60**, R12 553.

Bauschlicher, C. W., and S. Langhoff, 1988, J. Chem. Phys. **89**, 4246.

Bauschlicher, C. W., and P. R. Taylor, 1986, J. Chem. Phys. **85**, 2779.

Baxter, R. J., 1982, *Exactly Solved Models in Statistical Mechanics* (Academic, London).

Bedürftig, G., B. Brendel, H. Frahm, and R. M. Noack, 1998, Phys. Rev. B **58**, 10 225.

Bendazzoli, G. L., S. Evangelisti, G. Fano, F. Ortolani, and L. Ziosi, 1999, J. Chem. Phys. **110**, 1277.

Benthien, H., F. Gebhard, and E. Jeckelmann, 2004, Phys. Rev. Lett. **92**, 256401.

Bergholtz, E. J., and A. Karlhede, 2003, "Density matrix renormalization group study of a lowest Landau level electron gas on a thin cylinder," cond-mat/0304517.

Betsuyaku, H., 1984, Phys. Rev. Lett. **53**, 629.

Betsuyaku, H., 1985, Prog. Theor. Phys. **73**, 319.

Boman, M., and R. J. Bursill, 1998, Phys. Rev. B **57**, 15 167.

Bonca, J., J. E. Gubernatis, M. Guerrero, E. Jeckelmann, and S. R. White, 2000, Phys. Rev. B **61**, 3251.

Boos, H. E., V. E. Korepin, Y. Nishiyama, and M. Shiroishi, 2002, J. Phys. A **35**, 4443.

Bursill, R. J., 1999, Phys. Rev. B **60**, 1643.

Bursill, R. J., and W. Barford, 1999, Phys. Rev. Lett. **82**, 1514.

Bursill, R. J., and W. Barford, 2002, Phys. Rev. B **66**, 205112.

Bursill, R. J., G. A. Gehring, D. J. J. Farnell, J. B. Parkinson, T. Xiang, and C. Zeng, 1995, J. Phys.: Condens. Matter **7**, 8605.

Bursill, R. J., R. H. McKenzie, and C. J. Hamer, 1998, Phys. Rev. Lett. **80**, 5607.

Bursill, R. J., R. H. McKenzie, and C. J. Hamer, 1999, Phys. Rev. Lett. **83**, 408.

Bursill, R. J., T. Xiang, and G. A. Gehring, 1994, J. Phys. A **28**, 2109.

Bursill, R. J., T. Xiang, and G. A. Gehring, 1996, J. Phys.: Condens. Matter **8**, L583.

Byrnes, T. M. R., R. J. Bursill, H. P. Eckle, C. J. Hamer, and A. W. Sandvik, 2002, Phys. Rev. B **66**, 195313.

Callan, C., and F. Wilczek, 1994, Phys. Lett. B **333**, 55.

Capone, M., and S. Caprara, 2001, Phys. Rev. B **64**, 184418.

Caprara, S., and A. Rosengren, 1997, Europhys. Lett. **39**, 55.

Carlon, E., C. Chatelain, and B. Berche, 1999, Phys. Rev. B **60**, 12 974.

Carlon, E., and A. Drzewiński, 1997, Phys. Rev. Lett. **79**, 1591.

Carlon, E., and A. Drzewiński, 1998, Phys. Rev. E **57**, 2626.

Carlon, E., A. Drzewiński, and J. Rogiers, 1998, Phys. Rev. B **58**, 5070.

Carlon, E., A. Drzewiński, and J. M. J. van Leeuwen, 2001, Phys. Rev. E **64**, 010801.

Carlon, E., A. Drzewiński, and J. M. J. van Leeuwen, 2002, J. Chem. Phys. **117**, 2425.

Carlon, E., M. Henkel, and U. Schollwöck, 1999, Eur. Phys. J. B **12**, 99.

Carlon, E., M. Henkel, and U. Schollwöck, 2001, Phys. Rev. E **63**, 036101.

Caron, L. G., and S. Moukouri, 1996, Phys. Rev. Lett. **76**, 4050.

Caron, L. G., and S. Moukouri, 1997, Phys. Rev. B **56**, R8471.

Carruzo, H. M., and C. C. Yu, 1996, Phys. Rev. B **53**, 15 377.

Cazalilla, M. A., and J. B. Marston, 2002, Phys. Rev. Lett. **88**, 256403.

Chan, G. K. L., P. W. Ayers, and I. E. S. Croot, 2002, J. Stat. Phys. **109**, 289.

Chan, G. K. L., and M. Head-Gordon, 2002, J. Chem. Phys. **116**, 4462.

Chan, G. K. L., and M. Head-Gordon, 2003, J. Chem. Phys. **118**, 8551.

Chen, L., and S. Moukouri, 1996, Phys. Rev. B **53**, 1866.

Chernychev, A. L., S. R. White, and A. H. Castro-Neto, 2003, Phys. Rev. B **65**, 214527.

Chung, M. C., M. Kaulke, I. Peschel, M. Pleimling, and W. Selke, 2000, Eur. Phys. J. B **18**, 655.

Chung, M. C., and I. Peschel, 2000, Phys. Rev. B **62**, 4191.

Chung, M. C., and I. Peschel, 2001, Phys. Rev. B **64**, 064412.

Citro, R., E. Orignac, N. Andrei, C. Itoi, and S. Qin, 2000, J. Phys.: Condens. Matter **12**, 3041.

Cullum, J., and R. A. Willoughby, 1985, *Lanczos Algorithms for Large Symmetric Eigenvalue Computations*, Vols. I and II (Birkhäuser, Boston).

Cuthill, E., and J. McKee, 1969, *Proceedings of the 24th National Conference of the Association for Computing Machinery*, *ACM Publication P-69*, Association for Computing Machinery, New York.

Daley, A. J., C. Kollath, U. Schollwöck, and G. Vidal, 2004, .J. Stat. Mech. P04005.

Daul, S., 2000, Eur. Phys. J. B **14**, 649.

Daul, S., I. Ciofini, C. Daul, and S. R. White, 2000, Int. J. Quantum Chem. **79**, 331.

Daul, S., and R. M. Noack, 1997, Z. Phys. B: Condens. Matter **103**, 293.

Daul, S., and R. M. Noack, 1998, Phys. Rev. B **58**, 2635.

Daul, S., and R. M. Noack, 2000, Phys. Rev. B **61**, 1646.

Daul, S., and D. J. Scalapino, 2000, Phys. Rev. B **62**, 8658.

Daul, S., D. J. Scalapino, and S. R. White, 2000, Phys. Rev. B **61**, 15 526.

Derrida, B., M. R. Evans, V. Hakim, and V. Pasquier, 1993, J. Phys. A **26**, 1493.

Dimitrova, S. S., S. Pittel, J. Dukelsky, and M. V. Stoitsov, 2002, in *Proceedings of the 21st Workshop on Nuclear Theory 2002*, edited by V. Nikolaev (Heron, Sofia).

Doublet, M. L., and M. B. Lepetit, 1999, J. Chem. Phys. **110**, 1767.

Drzewiński, A., 2000, Phys. Rev. E **62**, 4378.

Drzewiński, A., A. Ciach, and A. Maciolek, 1998, Eur. Phys. J. B **5**, 825.

Drzewiński, A., and J. Wojtkiewicz, 2000, Phys. Rev. E **62**, 4397.

du Croo de Jongh, M. S. L., and J. M. J. van Leeuwen, 1998, Phys. Rev. B **57**, 8494.

Dukelsky, J., M. A. Martín-Delgado, T. Nishino, and G. Sierra, 1998, Europhys. Lett. **43**, 457.

Dukelsky, J., and S. Pittel, 2001, Phys. Rev. C **63**, 061303.

Dukelsky, J., and S. Pittel, 2004, Rep. Prog. Phys. **67**, 513.

Dukelsky, J., S. Pittel, S. S. Dimitrova, and M. V. Stoitsov, 2002, Phys. Rev. C **65**, 054319.

Dukelsky, J., and G. Sierra, 1999, Phys. Rev. Lett. **83**, 172.

Dukelsky, J., and G. Sierra, 2000, Phys. Rev. B **61**, 12 302.

Enss, T., M. Henkel, A. Picone, and U. Schollwöck, 2004, J. Phys. A **37**, 10 479.

Enss, T., and U. Schollwöck, 2001, J. Phys. A **34**, 7769.

Ercolessi, E., G. Morandi, P. Pieri, and M. Roncaglia, 2000, Europhys. Lett. **52**, 434.

Essler, F. H. L., F. Gebhard, and E. Jeckelmann, 2001, Phys. Rev. B **64**, 125119.

Exler, M., and J. Schnack, 2003, Phys. Rev. B **67**, 094440.

Fannes, M., B. Nachtergaele, and R. F. Werner, 1989, Europhys. Lett. **10**, 633.

Fano, G., F. Ortolani, and L. Ziosi, 1998, J. Chem. Phys. **108**, 9246.

Farnell, D. J. J., 2003, Phys. Rev. B **68**, 134419.

Fáth, G., Ö. Legeza, and J. Sólyom, 2001, Phys. Rev. B **63**, 134403.

Fehske, H., 2000, Phys. Rev. B **62**, R747.

Foster, D. P., and C. Pinettes, 2003a, J. Phys. A **36**, 10 279.

Foster, D. P., and C. Pinettes, 2003b, Phys. Rev. E **67**, 045105.

Friedman, B., 2000, Phys. Rev. B **61**, 6701.

Gagliano, E. R., and C. A. Balseiro, 1987, Phys. Rev. Lett. **59**, 2999.

Gaite, J., 2001, Mod. Phys. Lett. A **16**, 1109.

Gaite, J., 2003, "Entanglement entropy and the density matrix renormalization group," quant-ph/0301120.

Galindo, A., and M. A. Martín-Delgado, 2002, Rev. Mod. Phys. **74**, 347.

Garcia, D. J., K. Hallberg, C. D. Batista, M. Avignon, and B. Alascio, 2000, Phys. Rev. Lett. **85**, 3720.

Garcia, D. J., K. Hallberg, C. D. Batista, S. Capponi, D. Poilblanc, M. Avignon, and B. Alascio, 2002, Phys. Rev. B **65**, 134444.

Garcia, D. J., K. Hallberg, and M. J. Rozenberg, 2004, Phys. Rev. Lett. **93**, 246403.

Gendiar, A., N. Maeshima, and T. Nishino, 2003, Prog. Theor. Phys. **110**, 691.

Gendiar, A., and T. Nishino, 2002, Phys. Rev. E **65**, 046702.

Gendiar, A., and A. Surda, 2000, Phys. Rev. B **62**, 3960.

Georges, A., G. Kotliar, W. Krauth, and M. J. Rozenberg, 1996, Rev. Mod. Phys. **68**, 13.

Glauber, R., 1963, J. Math. Phys. **4**, 294.

Glazek, S. D., and K. G. Wilson, 1994, Phys. Rev. D **49**, 4214.

Gobert, D., M. Schechter, U. Schollwöck, and J. von Delft, 2004, Phys. Rev. Lett. **93**, 186402.

Gobert, D., U. Schollwöck, and J. von Delft, 2004, Eur. Phys. J. B **38**, 501.

Golub, G., and C. F. van Loan, 1996, *Matrix Computations* (Johns Hopkins University, Baltimore, MD).

Greiner, M., O. Mandel, T. Esslinger, T. W. Hänsch, and I. Bloch, 2002, Nature (London) **415**, 39.

Guerrero, M., and R. M. Noack, 1996, Phys. Rev. B **53**, 3707.

Guerrero, M., and R. M. Noack, 2001, Phys. Rev. B **63**, 144423.

Guerrero, M., and C. C. Yu, 1995, Phys. Rev. B **51**, 10 301.

Hagiwara, M., H. A. Katori, U. Schollwöck, and H. J. Mikeska, 2000, Phys. Rev. B **62**, 1051.

Hallberg, K., 1995, Phys. Rev. B **52**, R9827.

Hallberg, K., 2003, in, *Theoretical Methods for Strongly Correlated Electrons*, edited by D. Senechal, A-.M. Tremblay, and C. Bourbonnais, CRM Series in Mathematical Physics (Springer, New York).

Hallberg, K., C. D. Batista, and A. A. Aligia, 1999, Physica B **261**, 1017.

Hallberg, K., P. Horsch, and G. Martinez, 1995, Phys. Rev. B **52**, R719.

Hallberg, K. A., X. Q. Wang, P. Horsch, and A. Moreo, 1996, Phys. Rev. Lett. **76**, 4955.

Hamacher, K., C. Gros, and W. Wenzel, 2002, Phys. Rev. Lett. **88**, 217203.

Haywood, C. A., D. Poilblanc, R. M. Noack, D. J. Scalapino, and W. Hanke, 1995, Phys. Rev. Lett. **75**, 926.

Henelius, P., 1999, Phys. Rev. B **60**, 9561.

Henkel, M., and U. Schollwöck, 2001, J. Phys. A **34**, 3333.

Henkel, M., and G. Schütz, 1988, J. Phys. A **21**, 2617.

Hida, K., 1996, J. Phys. Soc. Jpn. **65**, 895.

Hida, K., 1997a, J. Phys. Soc. Jpn. **66**, 3237.

Hida, K., 1997b, J. Phys. Soc. Jpn. **66**, 330.

Hida, K., 1999a, Phys. Rev. Lett. **83**, 3297.

Hida, K., 1999b, J. Phys. Soc. Jpn. **68**, 3177.

Hida, K., 2000, J. Phys. Soc. Jpn. **69**, 311.

Hida, K., 2003, J. Phys. Soc. Jpn. **72**, 911.

Hieida, Y., 1998, J. Phys. Soc. Jpn. **67**, 369.

Hieida, Y., K. Okunishi, and Y. Akutsu, 1997, Phys. Lett. A **233**, 464.

Hieida, Y., K. Okunishi, and Y. Akutsu, 1999, New J. Phys. **1**, 7.

Hieida, Y., K. Okunishi, and Y. Akutsu, 2001, Phys. Rev. B **64**, 224422.

Hikihara, T., 2001, Can. J. Phys. **79**, 1593.

Hikihara, T., 2002, J. Phys. Soc. Jpn. **71**, 319.

Hikihara, T., and A. Furusaki, 1998, Phys. Rev. B **58**, R583.

Hikihara, T., and A. Furusaki, 2001, Phys. Rev. B **63**, 134438.

Hikihara, T., A. Furusaki, and M. Sigrist, 1999, Phys. Rev. B **60**, 12 116.

Hikihara, T., M. Kaburagi, H. Kamura, and T. Tonegawa, 2000, J. Phys. Soc. Jpn. **69**, 259.

Hikihara, T., M. Kaburagi, and H. Kawamura, 2001a, Can. J. Phys. **79**, 1587.

Hikihara, T., M. Kaburagi, and H. Kawamura, 2001b, Phys. Rev. B **63**, 174430.

Hikihara, T., T. Momoi, and X. Hu, 2003, Phys. Rev. Lett. **90**, 087204.

Hikihara, T., T. Tonegawa, M. Kaburagi, T. Nishino, S. Miyashita, and H. J. Mikeska, 2000, J. Phys. Soc. Jpn. **69**, 1207.

Hinrichsen, H., 2000, Adv. Phys. **49**, 815.

Hofstetter, W., I. Affleck, D. Nelson, and U. Schollwöck, 2004, Europhys. Lett. **66**, 178.

Honda, Y., and T. Horiguchi, 1997, Phys. Rev. E **56**, 3920.

Honda, Y., and T. Horiguchi, 2001, "Quantum phase transition by cyclic four-spin exchange interaction for $S=1/2$ two-leg spin ladder," cond-mat/0106426.

Howard, M. J., and U. Täuber, 1997, J. Phys. A **30**, 7721.

Hubbard, J., 1963, Proc. R. Soc. London, Ser. A **276**, 238.

Hubbard, J., 1964, Proc. R. Soc. London, Ser. A **281**, 401.

Igloi, F., and E. Carlon, 1999, Phys. Rev. B **59**, 3783.

Itoi, C., and S. J. Qin, 2001, Phys. Rev. B **63**, 224423.

Itoi, C., S. J. Qin, and I. Affleck, 2000, Phys. Rev. B **61**, 6747.

Jannod, E., C. Payen, K. Schoumacker, C. D. Batista, K. Hallberg, and A. A. Aligia, 2000, Phys. Rev. B **62**, 2998.

Jarrell, M., and J. E. Gubernatis, 1996, Phys. Rep. **269**, 133.

Jeckelmann, E., 1998, Phys. Rev. B **57**, 11 838.

Jeckelmann, E., 2002a, Phys. Rev. B **66**, 045114.

Jeckelmann, E., 2002b, Phys. Rev. Lett. **89**, 236401.

Jeckelmann, E., 2003a, Phys. Rev. B **67**, 075106.

Jeckelmann, E., 2003b, Phys. Rev. Lett. **91**, 089702.

Jeckelmann, E., F. Gebhard, and F. H. L. Essler, 2000, Phys. Rev. Lett. **85**, 3910.

Jeckelmann, E., D. J. Scalapino, and S. R. White, 1998, Phys. Rev. B **58**, 9492.

Jeckelmann, E., and S. R. White, 1998, Phys. Rev. B **57**, 6376.

Jeckelmann, E., C. L. Zhang, and S. R. White, 1999, Phys. Rev. B **60**, 7950.

Johnston, D. C., R. K. Kremer, M. Troyer, X. Q. Wang, A. Klümper, S. L. Budko, A. F. Panchula, and P. C. Canfield, 2000, Phys. Rev. B **61**, 9558.

Juozapavicius, A., L. Urba, S. Caprara, and A. Rosengren, 1999, Phys. Rev. B **60**, 14 771.

Kaburagi, M., H. Kawamura, and T. Hikihara, 1999, J. Phys. Soc. Jpn. **68**, 3185.

Kampf, A. P., S. R. White, and D. J. Scalapino, 2001, Phys. Rev. B **64**, 052509.

Karadamoglou, J., N. Papanicolaou, X. Wang, and X. Zotos, 2001, Phys. Rev. B **63**, 224406.

Kaulke, M., and I. Peschel, 1998, Eur. Phys. J. B **5**, 727.

Kawaguchi, A., A. Koga, K. Okunishi, and N. Kawakami, 2003, J. Phys. Soc. Jpn. **72**, 405.

Kawaguchi, A., A. Koga, K. Okunishi, and N. Kawakami, 2002, Phys. Rev. B **65**, 214405.

Kemper, A., A. Gendiar, T. Nishino, A. Schadschneider, and J. Zittartz, 2003, J. Phys. A **36**, 29.

Kemper, A., A. Schadschneider, and J. Zittartz, 2001, J. Phys. A **34**, L279.

Kim, Y.-J., J. P. Hill, H. Benthien, F. H. L. Essler, E. Jeckelmann, H. S. Choi, T. W. Noh, N. Motoyama, K. M. Kojima, S. Uchida, D. Casa, and T. Gog, 2004, Phys. Rev. Lett. **92**, 137402.

Klümper, A., R. Raupach, and F. Schönfeld, 1999, Phys. Rev. B **59**, 3612.

Klümper, A., R. Raupach, and F. Schönfeld, 2000, Eur. Phys. J. B **17**, 51.

Klümper, A., A. Schadschneider, and J. Zittartz, 1993, Europhys. Lett. **24**, 293.

Kolezhuk, A., R. Roth, and U. Schollwöck, 1996, Phys. Rev. Lett. **77**, 5142.

Kolezhuk, A., R. Roth, and U. Schollwöck, 1997, Phys. Rev. B **55**, 8928.

Kolezhuk, A. K., H. J. Mikeska, K. Maisinger, and U. Schollwöck, 1999, Phys. Rev. B **59**, 13 565.

Kolezhuk, A. K., and U. Schollwöck, 2002, Phys. Rev. B **65**, 100401.

Kollath, C., U. Schollwöck, J. von Delft, and W. Zwerger, 2004, Phys. Rev. A **69**, 031601(R).

Kühner, T. D., and H. Monien, 1998, Phys. Rev. B **58**, R14 741.

Kühner, T. D., and S. R. White, 1999, Phys. Rev. B **60**, 335.

Kühner, T. D., S. R. White, and H. Monien, 2000, Phys. Rev. B **61**, 12 474.

Kuwabara, M., Y. Shimoi, and S. Abe, 1998, J. Phys. Soc. Jpn. **67**, 1521.

Landau, D. P., K. K. Mon, and H. B. Schüttler, 1994, Eds., *Computer Simulations in Condensed Matter Physics*, Vol. 7 (Springer, New York).

Langari, A., M. Abolfath, and M. A. Martín-Delgado, 2000, Phys. Rev. B **61**, 343.

Latorre, J. I., E. Rico, and G. Vidal, 2004, Quantum Inf. Comput. **4**, 48.

Läuchli, A., G. Schmid, and M. Troyer, 2003, Phys. Rev. B **67**, 100409.

Laukamp, M., G. B. Martins, C. Gazza, A. L. Malvezzi, E. Dagotto, P. M. Hansen, A. C. Lopez, and J. Riera, 1998, Phys. Rev. B **57**, 10 755.

Lay, W., and J. Rudnick, 2002, Phys. Rev. Lett. **88**, 057203.

Legeza, Ö., and G. Fáth, 1996, Phys. Rev. B **53**, 14 349.

Legeza, Ö., J. Röder, and B. Hess, 2003a, Phys. Rev. B **67**, 125114.

Legeza, Ö., J. Röder, and B. Hess, 2003b, Mol. Phys. **101**, 2019.

Legeza, Ö., and J. Sólyom, 1997, Phys. Rev. B **56**, 14 449.

Legeza, Ö., and J. Sólyom, 2003, Phys. Rev. B **68**, 195116.

Legeza, Ö., and J. Sólyom, 2004, Phys. Rev. B **70**, 205118.

Lepetit, M. B., M. Cousy, and G. M. Pastor, 2000, Eur. Phys. J. B **13**, 421.

Lepetit, M. B., and G. M. Pastor, 1997, Phys. Rev. B **56**, 4447.

Liang, S., and H. Pang, 1994, Phys. Rev. B **49**, 9214.

Lipowsky, R., 1982, Phys. Rev. Lett. **49**, 1575.

Liu, J., and A. Sherman, 1975, SIAM (Soc. Ind. Appl. Math.) J. Numer. Anal. **13**, 198.

Lou, J., X. Dai, S. Qin, Z. Su, and L. Yu, 1999, Phys. Rev. B **60**, 52.

Lou, J. Z., S. J. Qin, and C. F. Chen, 2003, Phys. Rev. Lett. **91**, 087204.

Lou, J. Z., S. J. Qin, T. K. Ng, Z. Su, and I. Affleck, 2000, Phys. Rev. B **62**, 3786.

Lou, J. Z., S. J. Qin, T. K. Ng, and Z. B. Su, 2002, Phys. Rev. B **65**, 104401.

Lou, J. Z., S. J. Qin, and Z. B. Su, 2000, Phys. Rev. B **62**, 13 832.

Lou, J. Z., S. J. Qin, Z. B. Su, and L. Yu, 1998, Phys. Rev. B **58**, 12 672.

Luo, H. G., T. Xiang, and X. Q. Wang, 2003, Phys. Rev. Lett. **91**, 049701.

Maciolek, A., A. Drzewiński, and A. Ciach, 2001, Phys. Rev. E **64**, 026123.

Maciolek, A., A. Drzewiński, and R. Evans, 2001, Phys. Rev. E **64**, 056137.

Maeshima, N., Y. Hieida, Y. Akutsu, T. Nishino, and K. Okunishi, 2001, Phys. Rev. E **64**, 016705.

Maeshima, N., and K. Okunishi, 2000, Phys. Rev. B **62**, 934.

Maisinger, K., and U. Schollwöck, 1998, Phys. Rev. Lett. **81**, 445.

Maisinger, K., U. Schollwöck, S. Brehmer, J. Mikeska, and S. Yamamoto, 1998, Phys. Rev. B **58**, R5908.

Marston, J. B., J. O. Fjaerestad, and A. Sudbo, 2002, Phys. Rev. Lett. **89**, 056404.

Marston, J. B., and S. W. Tsai, 1999, Phys. Rev. Lett. **82**, 4906.

Martín-Delgado, M. A., J. Rodriguez-Laguna, and G. Sierra, 2001, Nucl. Phys. B **601**, 569.

Martín-Delgado, M. A., and G. Sierra, 1996, Int. J. Mod. Phys. A **11**, 3145.

Martín-Delgado, M. A., and G. Sierra, 1999, Phys. Rev. Lett. **83**, 1514.

Martín-Delgado, M. A., G. Sierra, and R. M. Noack, 1999, J. Phys. A **32**, 6079.

Martins, G. B., M. Laukamp, J. Riera, and E. Dagotto, 1997, Phys. Rev. Lett. **78**, 3563.

Maurel, P., and M. B. Lepetit, 2000, Phys. Rev. B **62**, 10 744.

Maurel, P., M. B. Lepetit, and D. Poilblanc, 2001, Eur. Phys. J. B **21**, 481.

McCulloch, I. P., A. R. Bishop, and M. Gulacsi, 2001, Philos. Mag. B **81**, 1603.

McCulloch, I. P., and M. Gulacsi, 2000, Aust. J. Phys. **53**, 597.

McCulloch, I. P., and M. Gulacsi, 2001, Philos. Mag. Lett. **81**, 447.

McCulloch, I. P., and M. Gulacsi, 2002, Europhys. Lett. **57**, 852.

McCulloch, I. P., M. Gulacsi, S. Caprara, A. Jazavaou, and A. Rosengren, 1999, J. Low Temp. Phys. **117**, 323.

Meden, V., and U. Schollwöck, 2003a, Phys. Rev. B **67**, 035106.

Meden, V., and U. Schollwöck, 2003b, Phys. Rev. B **67**, 193303.

Metzner, W., and D. Vollhardt, 1989, Phys. Rev. Lett. **62**, 324.

Mikeska, H. J., U. Neugebauer, and U. Schollwöck, 1997, Phys. Rev. B **55**, 2955.

Mitrushenkov, A. O., G. Fano, F. Ortolani, R. Linguerri, and P. Palmieri, 2001, J. Chem. Phys. **115**, 6815.

Mitrushenkov, A. O., R. Linguerri, P. Palmieri, and G. Fano, 2003, J. Chem. Phys. **119**, 4148.

Molina, R. A., D. Weinmann, R. A. Jalabert, G.-L. Ingold, and J.-L. Pichard, 2003, Phys. Rev. B **67**, 235306.

Moreno, J., S. J. Qin, P. Coleman, and L. Yu, 2001, Phys. Rev. B **64**, 085116.

Moukouri, S., 2004, Phys. Rev. B **70**, 014403.

Moukouri, S., and L. G. Caron, 1996, Phys. Rev. Lett. **77**, 4640.

Moukouri, S., and L. G. Caron, 2003, Phys. Rev. B **67**, 092405.

Mutou, T., N. Shibata, and K. Ueda, 1998a, Phys. Rev. B **57**, 13 702.

Mutou, T., N. Shibata, and K. Ueda, 1998b, Phys. Rev. Lett. **81**, 4939.

Mutou, T., N. Shibata, and K. Ueda, 1999, Phys. Rev. Lett. **82**, 3727.

Naef, F., and X. Q. Wang, 2000, Phys. Rev. Lett. **84**, 1320.

Naef, F., X. Q. Wang, X. Zotos, and W. von der Linden, 1999, Phys. Rev. B **60**, 359.

Nagy, Z., C. Appert, and L. Santen, 2002, J. Stat. Phys. **109**, 623.

Ng, T. K., J. Z. Lou, and Z. B. Su, 2000, Phys. Rev. B **61**, 11 487.

Nielsen, M. A., and I. L. Chuang, 2000, *Quantum Computation and Quantum Information* (Cambridge University, Cambridge, England).

Nishimoto, S., F. Gebhard, and E. Jeckelmann, 2004, J. Phys.: Condens. Matter **16**, 7063.

Nishimoto, S., and E. Jeckelmann, 2004, J. Phys.: Condens. Matter **16**, 613.

Nishimoto, S., E. Jeckelmann, F. Gebhard, and R. Noack, 2002, Phys. Rev. B **65**, 165114.

Nishimoto, S., E. Jeckelmann, and D. J. Scalapino, 2002, Phys. Rev. B **66**, 245109.

Nishimoto, S., M. Takahashi, and Y. Oiita, 2000, J. Phys. Soc. Jpn. **69**, 1594.

Nishino, T., 1995, J. Phys. Soc. Jpn. **64**, 3598.

Nishino, T., Y. Hieida, K. Okunishi, N. Maeshima, Y. Akutsu,

and A. Gendiar, 2001, Prog. Theor. Phys. **105**, 409.

Nishino, T., and K. Okunishi, 1995, J. Phys. Soc. Jpn. **64**, 4084.

Nishino, T., and K. Okunishi, 1996, J. Phys. Soc. Jpn. **65**, 891.

Nishino, T., and K. Okunishi, 1997, J. Phys. Soc. Jpn. **66**, 3040.

Nishino, T., and K. Okunishi, 1998, J. Phys. Soc. Jpn. **67**, 3066.

Nishino, T., K. Okunishi, Y. Hieida, N. Maeshima, and Y. Akutsu, 2000, Nucl. Phys. B **575**, 504.

Nishino, T., and N. Shibata, 1999, J. Phys. Soc. Jpn. **68**, 3501.

Nishiyama, Y., 1999, Eur. Phys. J. B **12**, 547.

Nishiyama, Y., 2001, Phys. Rev. B **64**, 064510.

Nishiyama, Y., 2002a, Phys. Rev. B **66**, 184501.

Nishiyama, Y., 2002b, Phys. Rev. E **66**, 061907.

Nishiyama, Y., 2003, Phys. Rev. E **68**, 031901.

Noack, R. M., N. Bulut, D. J. Scalapino, and M. G. Zacher, 1997, Phys. Rev. B **56**, 7162.

Noack, R. M., S. R. White, and D. J. Scalapino, 1994, Phys. Rev. Lett. **73**, 882.

Noack, R. M., S. R. White, and D. J. Scalapino, 1995a, J. Low Temp. Phys. **99**, 593.

Noack, R. M., S. R. White, and D. J. Scalapino, 1995b, Europhys. Lett. **30**, 163.

Nomura, K., and K. Okamoto, 1994, J. Phys. A **27**, 5773.

Nomura, K., and M. Yamada, 1991, Phys. Rev. B **43**, 8217.

Normand, B., X. Q. Wang, X. Xotos, and D. Loss, 2001, Phys. Rev. B **63**, 184409.

Nunner, T., P. Brune, T. Kopp, M. Windt, and M. Grüninger, 2002, Phys. Rev. B **66**, 180404.

Okamoto, K., and K. Nomura, 1992, Phys. Lett. A **169**, 433.

Okunishi, K., Y. Akutsu, N. Akutsu, and T. Yamamoto, 2001, Phys. Rev. B **64**, 104432.

Okunishi, K., Y. Hieida, and Y. Akutsu, 1999a, Phys. Rev. B **60**, R6953.

Okunishi, K., Y. Hieida, and Y. Akutsu, 1999b, Phys. Rev. E **59**, R6227.

Osborne, T. J., and M. A. Nielsen, 2002, Quantum Inf. Process. **1**, 45.

Östlund, S., and S. Rommer, 1995, Phys. Rev. Lett. **75**, 3537.

Otsuka, H., 1998, Phys. Rev. B **57**, 14 658.

Paeßens, M., 2003, J. Chem. Phys. **118**, 10 287.

Paeßens, M., and G. M. Schütz, 2002, Phys. Rev. E **66**, 021806.

Pang, H. B., and S. Liang, 1995, Phys. Rev. B **51**, 10 287.

Pariser, R., and R. G. Parr, 1953, J. Chem. Phys. **21**, 466.

Parry, A. O., and R. Evans, 1990, Phys. Rev. Lett. **64**, 439.

Pati, S. K., R. Chitra, D. Sen, H. R. Krishnamurthy, and S. Ramasesha, 1996, Europhys. Lett. **33**, 707.

Pati, S. K., R. Chitra, D. Sen, S. Ramasesha, and H. R. Krishnamurthy, 1997, J. Phys.: Condens. Matter **9**, 219.

Pati, S. K., S. Ramasesha, and D. Sen, 1997a, J. Phys.: Condens. Matter **9**, 8707.

Pati, S. K., S. Ramasesha, and D. Sen, 1997b, Phys. Rev. B **55**, 8894.

Pati, S. K., S. Ramasesha, Z. Shuai, and J. Brédas, 1999, Phys. Rev. B **59**, 14 827.

Pati, S. K., and R. R. P. Singh, 1999, Phys. Rev. B **60**, 7695.

Pati, S. K., and R. R. P. Singh, 2000, Phys. Rev. B **61**, 5868.

Pati, S. K., R. R. P. Singh, and D. I. Khomskii, 1998, Phys. Rev. Lett. **81**, 5406.

Peschel, I., K. Hallberg, X. Wang, and M. Kaulke, 1999, Eds., *Density Matrix Renormalization: a New Numerical Method*, Lecture Notes in Physics No. 528 (Springer, New York).

Peschel, I., M. Kaulke, and Ö. Legeza, 1999, Ann. Phys. **8**, 153.

Pipek, J., and P. G. Mezey, 1989, J. Chem. Phys. **90**, 4916.

Pittel, S., J. Dukelsky, S. Dimitrova, and M. Stoitsov, 2003,

Rev. Mex. Fis. **49S4**, 82.

Polizzi, E., F. Mila, and E. S. Sørensen, 1998, Phys. Rev. B **58**, 2407.

Pople, J. A., 1953, Trans. Faraday Soc. **49**, 1375.

Qin, S. J., M. Fabrizio, and L. Yu, 1996, Phys. Rev. B **54**, R9643.

Qin, S. J., M. Fabrizio, L. Yu, M. Oshikawa, and I. Affleck, 1997, Phys. Rev. B **56**, 9766.

Qin, S. J., and J. Z. Lou, 2001, Commun. Theor. Phys. **36**, 635.

Qin, S. J., J. Z. Lou, L. Q. Sun, and C. F. Chen, 2003, Phys. Rev. Lett. **90**, 067202.

Qin, S. J., X. Q. Wang, and L. Yu, 1997, Phys. Rev. B **56**, R14 251.

Raas, C., G. S. Uhrig, and F. B. Anders, 2004, Phys. Rev. B **69**, 041102.

Race, A., W. Barford, and R. J. Bursill, 2001, Phys. Rev. B **64**, 035208.

Race, A., W. Barford, and R. J. Bursill, 2003, Phys. Rev. B **67**, 245202.

Raghu, C., Y. A. Pati, and S. Ramasesha, 2002, Phys. Rev. B **65**, 155204.

Ramasesha, S., S. K. Pati, H. R. Krishnamurthy, Z. Shuai, and J. L. Brédas, 1997, Synth. Met. **85**, 1019.

Ramasesha, S., S. K. Pati, Z. Shuai, and J. L. Brédas, 2000, Adv. Quantum Chem. **38**, 121.

Rapsch, S., U. Schollwöck, and W. Zwerger, 1999, Europhys. Lett. **46**, 559.

Rommer, S., and S. Eggert, 1999, Phys. Rev. B **59**, 6301.

Rommer, S., and S. Östlund, 1997, Phys. Rev. B **55**, 2164.

Rommer, S., S. R. White, and D. J. Scalapino, 2000, Phys. Rev. B **61**, 13 424.

Sakai, T., and Y. Hasegawa, 1999, Phys. Rev. B **60**, 48.

Sakamoto, H., and K. Kubo, 1996, J. Phys. Soc. Jpn. **65**, 3732.

Sandvik, A. W., 1997, Phys. Rev. B **56**, 11 678.

Sandvik, A. W., L. Balents, and D. K. Campbell, 2004, Phys. Rev. Lett. **92**, 236401.

Sandvik, A. W., P. Sengupta, and D. K. Campbell, 2003, Phys. Rev. Lett. **91**, 089701.

Sato, H., and K. Sasaki, 2000, J. Phys. Soc. Jpn. **69**, 1050.

Sato, R., 1998, Mod. Phys. Lett. B **11**, 1295.

Sato, R., and Y. Akutsu, 1996, J. Phys. Soc. Jpn. **65**, 1885.

Scalapino, D. J., S. R. White, and I. Affleck, 2002, Phys. Rev. B **67**, 094440.

Schmitteckert, P., 2004, Phys. Rev. B **70**, 121302.

Schmitteckert, P., and U. Eckern, 1996, Phys. Rev. B **53**, 15 397.

Schmitteckert, P., T. Schulze, C. Schuster, P. Schwab, and U. Eckern, 1998, Phys. Rev. Lett. **80**, 560.

Schollwöck, U., 1998, Phys. Rev. B **58**, 8194.

Schollwöck, U., S. Chakravarty, J. O. Fjaerestad, J. Marston, and M. Troyer, 2003, Phys. Rev. Lett. **90**, 186401.

Schollwöck, U., O. Golinelli, and T. Jolicœur, 1996, Phys. Rev. B **54**, 4038.

Schollwöck, U., and T. Jolicœur, 1995, Europhys. Lett. **30**, 494.

Schollwöck, U., and T. Jolicœur, 1996, Phys. Rev. Lett. **77**, 2844.

Schollwöck, U., T. Jolicœur, and T. Garel, 1996, Phys. Rev. B **53**, 3304.

Schönhammer, K., V. Meden, W. Metzner, U. Schollwöck, and O. Gunnarsson, 2000, Phys. Rev. B **61**, 4393.

Senthil, T., J. B. Marston, and M. P. A. Fisher, 1999, Phys. Rev. B **60**, 4245.

Shibata, N., 1997, J. Phys. Soc. Jpn. **66**, 2221.

Shibata, N., 2003, J. Phys. A **36**, 381.

Shibata, N., B. Ammon, M. Troyer, M. Sigrist, and K. Ueda, 1998, J. Phys. Soc. Jpn. **67**, 1086.

Shibata, N., T. Nishino, K. Ueda, and C. Ishii, 1996, Phys. Rev. B **53**, R8828.

Shibata, N., M. Sigrist, and E. Heeb, 1997, Phys. Rev. B **56**, 11 084.

Shibata, N., and H. Tsunetsugu, 1999a, J. Phys. Soc. Jpn. **68**, 3138.

Shibata, N., and H. Tsunetsugu, 1999b, J. Phys. Soc. Jpn. **68**, 744.

Shibata, N., A. Tsvelik, and K. Ueda, 1997, Phys. Rev. B **56**, 330.

Shibata, N., and K. Ueda, 2001, J. Phys. Soc. Jpn. **70**, 3690.

Shibata, N., K. Ueda, T. Nishino, and C. Ishii, 1996, Phys. Rev. B **54**, 13 495.

Shibata, N., K. Ueda, T. Nishino, and C. Ishii, 1997, Physica B **230**, 1024.

Shibata, N., and D. Yoshioka, 2001, Phys. Rev. Lett. **86**, 5755.

Shibata, N., and D. Yoshioka, 2003, J. Phys. Soc. Jpn. **72**, 664.

Shiroishi, M., M. Takahashi, and Y. Nishiyama, 2001, J. Phys. Soc. Jpn. **70**, 3535.

Shuai, Z., J. L. Brédas, S. K. Pati, and S. Ramasesha, 1997, Phys. Rev. B **56**, 9298.

Shuai, Z., J. L. Brédas, S. K. Pati, and S. Ramasesha, 1998, Phys. Rev. B **58**, 15 329.

Shuai, Z., S. K. Pati, J. L. Brédas, and S. Ramasesha, 1997, Synth. Met. **85**, 1011.

Shuai, Z., S. K. Pati, W. P. Su, J. L. Brédas, and S. Ramasesha, 1997, Phys. Rev. B **55**, 15 368.

Sieling, M., U. Löw, B. Wolf, S. Schmidt, S. Zvyagin, and B. Lüthi, 2000, Phys. Rev. B **61**, 88.

Sierra, G., and T. Nishino, 1997, Nucl. Phys. B **495**, 505.

Sikkema, A. E., I. Affleck, and S. R. White, 1997, Phys. Rev. Lett. **79**, 929.

Siller, T., M. Troyer, T. M. Rice, and S. R. White, 2001, Phys. Rev. B **63**, 195106.

Siller, T., M. Troyer, T. M. Rice, and S. R. White, 2002, Phys. Rev. B **65**, 205109.

Silva-Valencia, J., and E. Miranda, 2002, Phys. Rev. B **65**, 024443.

Sirker, J., and G. Khaliullin, 2003, Phys. Rev. B **67**, 100408.

Sirker, J., and A. Klümper, 2002a, Europhys. Lett. **60**, 262.

Sirker, J., and A. Klümper, 2002b, Phys. Rev. B **66**, 245102.

Sleijpen, G. L. G., and H. A. van der Vorst, 1996, SIAM J. Matrix Anal. Appl. **17**, 401.

Soos, Z. G., and S. Ramasesha, 1989, J. Chem. Phys. **90**, 1067.

Sørensen, E., and I. Affleck, 1993, Phys. Rev. Lett. **71**, 1633.

Sørensen, E., and I. Affleck, 1994a, Phys. Rev. B **49**, 15 771.

Sørensen, E., and I. Affleck, 1994b, Phys. Rev. B **49**, 13 235.

Sugihara, T., 2004, J. High Energy Phys. **05**, 007.

Sun, L. Q., J. Zhang, S. J. Qin, and Y. Lei, 2002, Phys. Rev. B **65**, 132412.

Suzuki, M., 1976, Prog. Theor. Phys. **56**, 1454.

Takasaki, H., T. Hikihara, and T. Nishino, 1999, J. Phys. Soc. Jpn. **68**, 1537.

Takasaki, H., T. Nishino, and Y. Hieida, 2001, J. Phys. Soc. Jpn. **70**, 1429.

Tandon, K., S. Lal, S. K. Pati, S. Ramasesha, and D. Sen, 1999, Phys. Rev. B **59**, 396.

Tonegawa, T., T. Hikihara, M. Kaburagi, T. Nishino, S. Miyashita, and H. J. Mikeska, 1998, J. Phys. Soc. Jpn. **67**, 1000.

Trotter, H. F., 1959, Proc. Am. Math. Soc. **10**, 545.

Trumper, A. E., and C. Gazza, 2001, Phys. Rev. B **64**, 134408.

Tsai, S. W., and J. B. Marston, 2000, Phys. Rev. B **62**, 5546.

Tsushima, N., Y. Honda, and T. Horiguchi, 1997, J. Phys. Soc. Jpn. **66**, 3053.

Tsushima, N., and T. Horiguchi, 1998, J. Phys. Soc. Jpn. **67**, 1574.

Uhrig, G. S., F. Schönfeld, J. P. Boucher, and M. Horvatic, 1999, Phys. Rev. B **60**, 9468.

Uhrig, G. S., F. Schönfeld, M. Laukamp, and E. Dagotto, 1999, Eur. Phys. J. B **7**, 67.

Urba, L., and A. Rosengren, 2003, Phys. Rev. B **67**, 104406.

van Kampen, N. G., 1997, *Stochastic Processes in Physics and Chemistry* (Springer, New York).

Verstraete, F., and J. I. Cirac, 2004, "Renormalization algorithms for quantum many-body systems in two and higher dimensions," cond-mat/0407066.

Verstraete, F., J. J. Garcia-Ripoll, and J. I. Cirac, 2004, Phys. Rev. Lett. **93**, 207204.

Verstraete, F., D. Porras, and J. I. Cirac, 2004, Phys. Rev. Lett. **93**, 227204.

Vidal, G., 2003, Phys. Rev. Lett. **91**, 147902.

Vidal, G., 2004, Phys. Rev. Lett. **93**, 040502.

Vojta, M., R. E. Hetzel, and R. M. Noack, 1999, Phys. Rev. B **60**, R8417.

Vojta, M., A. Hübsch, and R. M. Noack, 2001, Phys. Rev. B **63**, 045105.

Wada, T., 2000, Phys. Rev. E **61**, 3199.

Waldtmann, C., H. Kreutzmann, U. Schollwöck, K. Maisinger, and H. U. Everts, 2000, Phys. Rev. B **62**, 9472.

Wang, X. Q., 1998, Mod. Phys. Lett. B **12**, 667.

Wang, X. Q., 2000, Mod. Phys. Lett. B **14**, 327.

Wang, X. Q., and S. Mallwitz, 1996, Phys. Rev. B **53**, R492.

Wang, X. Q., S. J. Qin, and L. Yu, 1999, Phys. Rev. B **60**, 14 529.

Wang, X. Q., and T. Xiang, 1997, Phys. Rev. B **56**, 5061.

Wang, X. Q., and L. Yu, 2000, Phys. Rev. Lett. **84**, 5399.

Wang, X. Q., N. S. Zhu, and C. F. Chen, 2002, Phys. Rev. B **66**, 172405.

Wang, X. Q., X. Zotos, J. Karadamoglou, and N. Papanicolaou, 2000, Phys. Rev. B **61**, 14 303.

Watanabe, S., Y. Kuramoto, T. Nishino, and N. Shibata, 1999, J. Phys. Soc. Jpn. **68**, 159.

Wegner, F., 1994, Ann. Phys. (Leipzig) **3**, 77.

Weihong, Z., J. Oitmaa, C. J. Hamer, and R. J. Bursill, 2001, J. Phys.: Condens. Matter **13**, 433.

White, S. R., 1992, Phys. Rev. Lett. **69**, 2863.

White, S. R., 1993, Phys. Rev. B **48**, 10 345.

White, S. R., 1996a, Phys. Rev. B **53**, 52.

White, S. R., 1996b, Phys. Rev. Lett. **77**, 3633.

White, S. R., 1998, Phys. Rep. **301**, 187.

White, S. R., 2002, J. Chem. Phys. **117**, 7472.

White, S. R., and I. Affleck, 1996, Phys. Rev. B **54**, 9862.

White, S. R., I. Affleck, and D. J. Scalapino, 2002, Phys. Rev. B **65**, 165122.

White, S. R., and A. E. Feiguin, 2004, Phys. Rev. Lett. **93**, 076401.

White, S. R., and D. Huse, 1993, Phys. Rev. B **48**, 3844.

White, S. R., and R. L. Martin, 1999, J. Chem. Phys. **110**, 4127.

White, S. R., and R. M. Noack, 1992, Phys. Rev. Lett. **68**, 3487.

White, S. R., R. M. Noack, and D. J. Scalapino, 1994, Phys. Rev. Lett. **73**, 886.

White, S. R., and D. J. Scalapino, 1997a, Phys. Rev. B **55**, R14 701.

White, S. R., and D. J. Scalapino, 1997b, Phys. Rev. B **55**, 6504.

White, S. R., and D. J. Scalapino, 1998a, Phys. Rev. Lett. **80**, 1272.

White, S. R., and D. J. Scalapino, 1998b, Phys. Rev. Lett. **81**, 3227.

White, S. R., and D. J. Scalapino, 1998c, Phys. Rev. B **57**, 3031.

White, S. R., and D. J. Scalapino, 2000, Phys. Rev. B **61**, 6320.

White, S. R., and D. J. Scalapino, 2003, Phys. Rev. Lett. **91**, 136403.

White, S. R., and R. R. P. Singh, 2000, Phys. Rev. Lett. **85**, 3330.

Widmark, P. O., P. A. Malmqvist, and B. Roos, 1990, Theor. Chim. Acta **77**, 291.

Wilson, K. G., 1975, Rev. Mod. Phys. **47**, 773.

Wilson, K. G., 1983, Rev. Mod. Phys. **55**, 583.

Xiang, T., 1996, Phys. Rev. B **53**, R10 445.

Xiang, T., 1998, Phys. Rev. B **58**, 9142.

Xiang, T., J. Z. Lou, and Z. B. Su, 2001, Phys. Rev. B **64**, 104414.

Yamamoto, S., T. Fukui, K. Maisinger, and U. Schollwöck, 1998, J. Phys.: Condens. Matter **10**, 11033.

Yamamoto, T., M. Asano, and C. Ishii, 2000, J. Phys. Soc. Jpn. **69**, 2965.

Yamashita, Y., N. Shibata, and K. Ueda, 1998, Phys. Rev. B **58**, 9114.

Yamashita, K., N. Shibata, and K. Ueda, 2000a, J. Phys. Soc. Jpn. **69**, 242.

Yamashita, Y., N. Shibata, and K. Ueda, 2000b, Phys. Rev. B **61**, 4012.

Yang, C. N., and S. C. Zhang, 1990, Mod. Phys. Lett. B **4**, 759.

Yaron, D., E. E. Moore, Z. Shuai, and J. L. Brédas, 1998, J. Chem. Phys. **108**, 7451.

Yu, C. C., and S. R. White, 1993, Phys. Rev. Lett. **71**, 3866.

Yu, W. Q., and S. Haas, 2000, Phys. Rev. B **63**, 024423.

Zhang, C. L., E. Jeckelmann, and S. R. White, 1998, Phys. Rev. Lett. **80**, 2661.

Zhang, C. L., E. Jeckelmann, and S. R. White, 1999, Phys. Rev. B **60**, 14 092.

Zhang, G. P., 1997, Phys. Rev. B **56**, 9189.

Zhang, G. P., and T. F. George, 2001, Phys. Rev. B **63**, 113107.

Zhang, W., J. Igarashi, and P. Fulde, 1997, Phys. Rev. B **56**, 654.

Zhang, W., J. Igarashi, and P. Fulde, 1998, J. Phys. Soc. Jpn. **67**, 1537.

Zhang, Y. Z., 2004, Phys. Rev. Lett. **92**, 246404.

Zhao, J. Z., X. Q. Wang, T. Xiang, Z. B. Su, and L. Yu, 2003, Phys. Rev. Lett. **90**, 207204.

Zhu, N. S., X. Q. Wang, and C. F. Chen, 2001, Phys. Rev. B **63**, 012401.

Zwolak, M., and G. Vidal, 2004, Phys. Rev. Lett. **93**, 207205.